REFRACTIVE INDICES OF LIQUID CRYSTALS AND PURE FLUIDS NEAR PHASE TRANSITIONS

by

PETER PALFFY-MUHORAY

B.A. Sc., University of British Columbia, 1966

M.A. Sc., University of British Columbia, 1969

A THESIS SUBMITTED IN PARTIAL FULFILLMENT OF

THE REQUIREMENTS FOR THE DEGREE OF

DOCTOR OF PHILOSOPHY

in

THE FACULTY OF GRADUATE STUDIES

THE DEPARTMENT OF PHYSICS

We accept this thesis as conforming

to the required standard

THE UNIVERSITY OF BRITISH COLUMBIA

August, 1977

In presenting this thesis in partial fulfilment of the requirements for an advanced degree at the University of British Columbia, I agree that the Library shall make it freely available for reference and study. I further agree that permission for extensive copying of this thesis for scholarly purposes may be granted by the Head of my Department or by his representatives. It is understood that copying or publication of this thesis for financial gain shall not be allowed without my written permission.

Department of Physics

The University of British Columbia
2075 Wesbrook Place
Vancouver, Canada
V6T 1W5

Date October 5, 1977

ABSTRACT

Interferometric measurements to determine the refractive indices of the nematic liquid crystals EBBA and BEPC as a function of temperature are described utilizing modified Rayleigh and conoscopic interferometers. Theory is presented relating the refractive indices and density to the orientational order, local field parameter and molecular properties. The results of simple thermal expansivity measurements are also given for EBBA.

The Lorentz-Lorenz coefficient for SF_6 and GeH_4 has been determined from refractive index and density measurements. The method utilizes a prism shaped high pressure cell which can be removed from a temperature controlled holder and weighed on a precision balance. The results indicate a variation of 0.5% for SF_6 and 0.8% for GeH_4 over the density range covered.

TABLE OF CONTENTS

LIST OF TABLES

LIST OF FIGURES

PREFACE

In an attempt to make this thesis more easily readable by maintaining continuity of thought throughout, we have derived, from basic principles, certain well known theoretical results. Although the methods of derivation are often somewhat different from those in the literature, we have attempted to indicate in the text whenever the results are not original. In order to clearly define the original contributions presented in this thesis, however, we wish to make note of the following. The results of Sec. 1.2 regarding the propagation of plane waves in anisotropic media are well known; similarly, the results obtained from applying the Landau theory of phase transitions to liquid crystals, presented in Sec. 2.4, are not original. Finally, the topics discussed in Secs. 6.2 and 6.3 appear in liquid crystal literature as mentioned in the text, although our formalism is different.

Our original contributions may be summarized as follows. We have generalized the Clausius-Mossotti relation so as to make it applicable to certain anistropic molecular fluids. We have attempted to include the effects of an anisotropic hard-core repulsive term in the intermolecular interaction potential in the mean-field theory of nematic liquid crystals. Experimentally, we have measured directly the Lorentz-Lorenz coefficient of pure fluids, and, using a new and sensitive interferometric technique, measured the refractive indices of nematic liquid crystals. The theory enables the orientational order parameter and the local field anisotropy parameter to be calculated from experimental results.

ACKNOWLEDGMENTS

I should like to express my sincere appreciation to Professor D.A. Balzarini for his guidance and assistance throughout this work.

I am especially indebted to the late Professor R.E. Burgess for his interest in and encouragement of this research, and also for his patience and tolerance during our chess games.

I should also like to thank Professor L. Sobrino for his help with the theoretical aspects of this work, and Professor W. Unruh who helped me avert the polarization catastrophe.

To A. Rosenberg, M. Burton and J. Shelton I extend my thanks for their participation in this research.

I am indebted to the technical staff of the Physics department for their assistance in manufacturing the experimental apparatus.

I wish to thank Professors F.W. Dalby, A.V. Gold, W.N. Hardy, W. Opechowski, B.G. Turrell, B.L. White for interesting and illuminating discussions. I should like to thank Darlene Crowe for typing the manuscript, and Mikey Burton for his help with the illustrations.

Finally, I am grateful to Eunice for putting up with it all.

CHAPTER 1

REFRACTIVE INDICES IN ANISOTROPIC MEDIA

1.1 Introduction

Dielectric properties of materials reflect the changes in molecular order that occur at phase transitions. Refractive index measurements provide a simple and sensitive method of studying these changes.

In addition to the liquid-vapor transition, certain fluids exhibit phase changes that correspond to loss of orientational order of the molecules; these liquid crystals have been the source of considerable interest recently. In this thesis, we wish to report a new and sensitive interferometric method of measuring the refractive indices of nematic liquid crystals, and in addition, a simple direct method of measuring the refractive index together with the density of pure fluids. In order to relate these measurements to molecular properties, we have derived a general relation between the dielectric permittivity and molecular polarizability for a broad class of ordered fluids. Using this relation, experimental results may be interpreted in terms of simple statistical mechanical models.

1.2 The Propagation of Plane Waves

Refractive indices of materials may be defined formally in terms of the phase velocities of plane waves propagating in them. Maxwell's equations, in Gaussian units, are

$$\nabla \times \vec{H} = \frac{1}{c} \frac{\partial \vec{D}}{\partial t} \tag{1.1}$$

and

$$\nabla \times \vec{E} = - \frac{1}{c} \frac{\partial \vec{B}}{\partial t} \tag{1.2}$$

for a region that does not contain currents. If $\vec{B} = \vec{H}$, elimination of $\vec{H}$ from Eq.'s (1.1) and (1.2) yields

$$\frac{1}{c^2} \frac{\partial^2 \vec{D}}{\partial t^2} = -\nabla \times (\nabla \times \vec{E}). \tag{1.3}$$

The dielectric permittivity tensor $\varepsilon_{\alpha\beta}$ is defined by

$$D_\alpha = \varepsilon_{\alpha\beta} E_\beta \ , \tag{1.4}$$

where $\alpha = x,y,z$ and summation is implied over repeated greek indices. It is well known (1) that $\varepsilon_{\alpha\beta}$ is diagonal in a system of coordinate axes coincident with the principal dielectric axes of the material. A monochromatic plane wave of frequency $\nu = \omega/2\pi$ propagating in the $\vec{k}$-direction

in the material will have a time and space variation proportional to $\exp[i(\omega t-\vec{k}\cdot\vec{r})]$; then Eq. (1.3) becomes

$$-\frac{\omega^2}{c^2}\vec{D} = -\vec{k}\times(\vec{k}\times\vec{E}) = \vec{k}(\vec{k}\cdot\vec{E})-\vec{E}k^2 \tag{1.5}$$

or

$$\vec{D} = \frac{k^2c^2}{\omega^2}\vec{E}_{\perp} \tag{1.6}$$

where $\vec{E}_{\perp}$ denotes the component of $\vec{E}$ perpendicular to $\vec{k}$. Clearly, $\vec{D}$, $\vec{E}$, and $\vec{k}$ are coplanar, and $\vec{D}$ is perpendicular to $\vec{k}$. The phase velocity v_p of the wave is given by $v_p = \omega/k$, and the refractive index n is defined by

$$n = \frac{c}{v_p} = \frac{kc}{\omega} \tag{1.7}$$

Eq. (1.6) may be re-written in the following form:

$$\vec{D} = n^2\,\frac{(\vec{E}\cdot\vec{D})\vec{D}}{D^2} \tag{1.8}$$

or

$$n^2 = \frac{D^2}{(\vec{E}\cdot\vec{D})} \tag{1.9}$$

If the components of $\vec{D}$ in the principal axis system are denoted by $D_i = Dd_i$ where i = x,y,z and the d_i are the components of a unit vector along $\vec{D}$, then

$$E_i = \frac{Dd_i}{\varepsilon_{ii}} \tag{1.10}$$

and

$$\frac{1}{n^2} = \frac{d_x^2}{\varepsilon_{xx}} + \frac{d_y^2}{\varepsilon_{yy}} + \frac{d_z^2}{\varepsilon_{zz}} \quad . \tag{1.11}$$

It is shown in Appendix A, that, for a given $\vec{k}$, the allowed values of d_i are those for which n is an extremum. It follows immediately that for $\vec{k}$ along one of the principal axes, say the z-axis, the allowed directions of $\vec{D}$ are along the x-axis, with $n = \sqrt{\varepsilon_{xx}}$, and along the y-axis, with $n = \sqrt{\varepsilon_{yy}}$. In general, for a given direction of propagation, two allowed perpendicular directions for $\vec{D}$ exist, with corresponding refractive indices. Materials in which all three principal dielectric constants have different values are termed biaxial, since two different directions of propagation exist in which the phase velocity is independent of the direction of $\vec{D}$. If two of the principal dielectric constants are equal, say $\varepsilon_{xx} = \varepsilon_{yy} = \varepsilon_{\perp}$, then the phase velocity for wave propagation along the z-axis is independent of the direction of $\vec{D}$, and $n = n_{\perp} = \sqrt{\varepsilon_{\perp}}$.

For propagation perpendicular to the z-axis, say in the x-direction, extremal values of n are $n = n_{\perp} = \sqrt{\varepsilon_{\perp}}$ if $\vec{D}$ is along the y-axis, and $n = n_{\parallel} = \sqrt{\varepsilon_{zz}} = \sqrt{\varepsilon_{\parallel}}$ if $\vec{D}$ is along the z-axis. Such materials

are termed uniaxial; all liquid crystals considered in this thesis belong to this category. For historical reasons, $n_\perp$ is often called the ordinary index, denoted by n_0, while $n_\parallel$ is called the extraordinary index, denoted by n_e; the subscripts $\parallel$ and $\perp$ denote directions perpendicular and parallel to the optic axis. Finally, if all the dielectric constants are equal, $n = \sqrt{\varepsilon}$ regardless of the direction of $\vec{D}$, and the material is isotropic.

1.3 The Local Field Anisotropy Tensor

In order to relate the dielectric tensor of fluids to molecular properties, it is necessary to know the relation between an applied field $\vec{E}$ and the local electric field $\vec{F}$ experienced by a molecule in the medium. In cubic crystals, the local field has been evaluated by Lorentz, and is given by $\vec{F} = (\epsilon+2)\vec{E}/3$, where ϵ is the isotropic dielectric permittivity. This result has been extended to isotropic fluids by Hirschfelder et al. (2). A more complicated expression for the local field in certain anisotropic crystals has been derived by Ewald (3) and Born (4); and more recently by Neugebauer (5) and Dunmur (6). For anisotropic fluids, the relation between $\vec{E}$ and $\vec{F}$ is not known. For fluids whose pair-correlation function can be made isotropic by scaling in radial directions after averaging over molecular orientations, the local field can be easily evaluated in terms of the scaling transformation.

We assume that a fluid polarized by an applied electric field may be represented as an assembly of identical dipoles $\vec{\mu}$ whose relative spatial distribution is characterized by a pair-correlation function $g(\vec{r})$, normalized such that the $\lim_{r\to\infty} g(r\hat{r}) = 1$ where $\vec{r} = r\hat{r}$ is a position vector originating from a dipole in the fluid. Let $r' = r/f(\hat{r})$ be the radial scaling transformation under which $g(\vec{r})$ becomes isotropic; that is, $g(r\hat{r}) = g(r'f(\hat{r})\hat{r}) = g_0(r')$. Let U be the surface given by $r = cf(\hat{r})$ where c is some positive constant; evidently $g(\vec{r}) = g_0(c)$, a constant everywhere on U.

The electric field $\vec{F}_1$ at the origin due to all dipoles within a sphere $r = R$ is given in cartesian tensor notation by

$$F_{1\alpha} = \int\int_0^R \rho g(r\hat{r}) \frac{(3r_\alpha r_\beta \mu_\beta - \mu_\alpha) r^2}{r^3} \, dr d\Omega \tag{1.12}$$

where r_α and μ_α are the components of $\hat{r}$ and $\vec{\mu}$ respectively, ρ is the average number density of molecules in the fluid, and $d\Omega$ is the element of solid angle. Letting $r' = r/f(\hat{r})$ and $P_\alpha = \rho\mu_\alpha$ where P_α is the polarization,

$$F_{1\alpha} = 4\pi\eta_{\alpha\beta}P_\beta \tag{1.13}$$

and

$$\eta_{\alpha\beta} = \frac{1}{4\pi}\int\int_0^{R/f(\hat{r})} \frac{g_0(r')dr'}{r'} (3r_\alpha r_\beta - \delta_{\alpha\beta}) d\Omega \tag{1.14}$$

The integration is performed over two regions; over the volume bounded by the sphere $r' = c$, and over the volume between the sphere $r' = c$ and the surface $r' = R/f(\hat{r})$. The regions of integration are shown in Fig. 1. The constant c is chosen such that $0<c<R/f(\hat{r})$ for all $\hat{r}$. Then

$$\eta_{\alpha\beta} = \frac{1}{4\pi}\int_0^c \frac{g_0(r')dr'}{r'} \int (3r_\alpha r_\beta - \delta_{\alpha\beta}) d\Omega$$

$$+ \frac{1}{4\pi}\int\int_c^{R/f(\hat{r})} \frac{g_0(r')dr'}{r'} (3r_\alpha r_\beta - \delta_{\alpha\beta}) d\Omega \, . \tag{1.15}$$

Fig. 1a Regions of integration in the local field calculation, showing the arbitrary surface U.

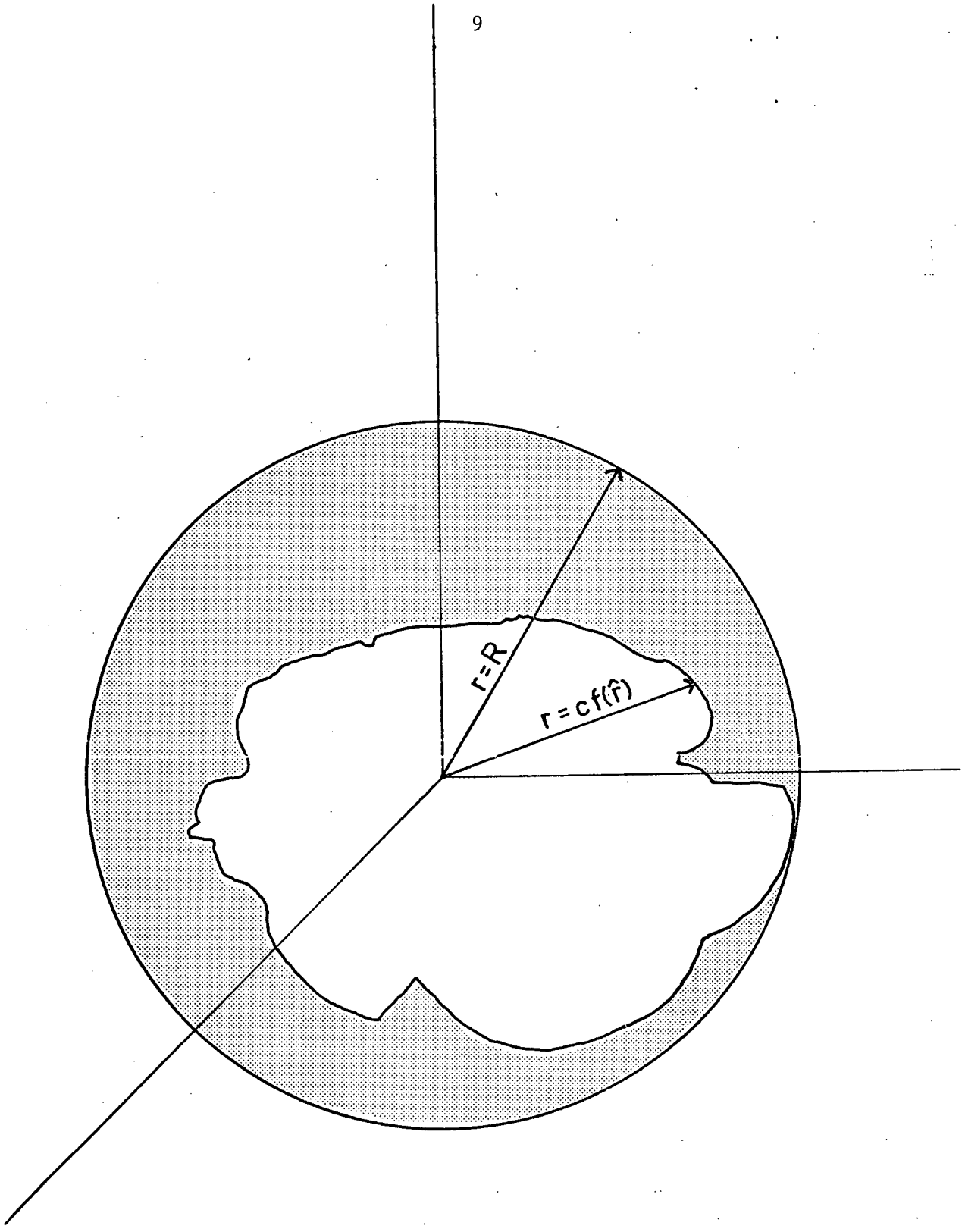
r=R
r = cf(r̂)

Fig. 1b The transformed surfaces.

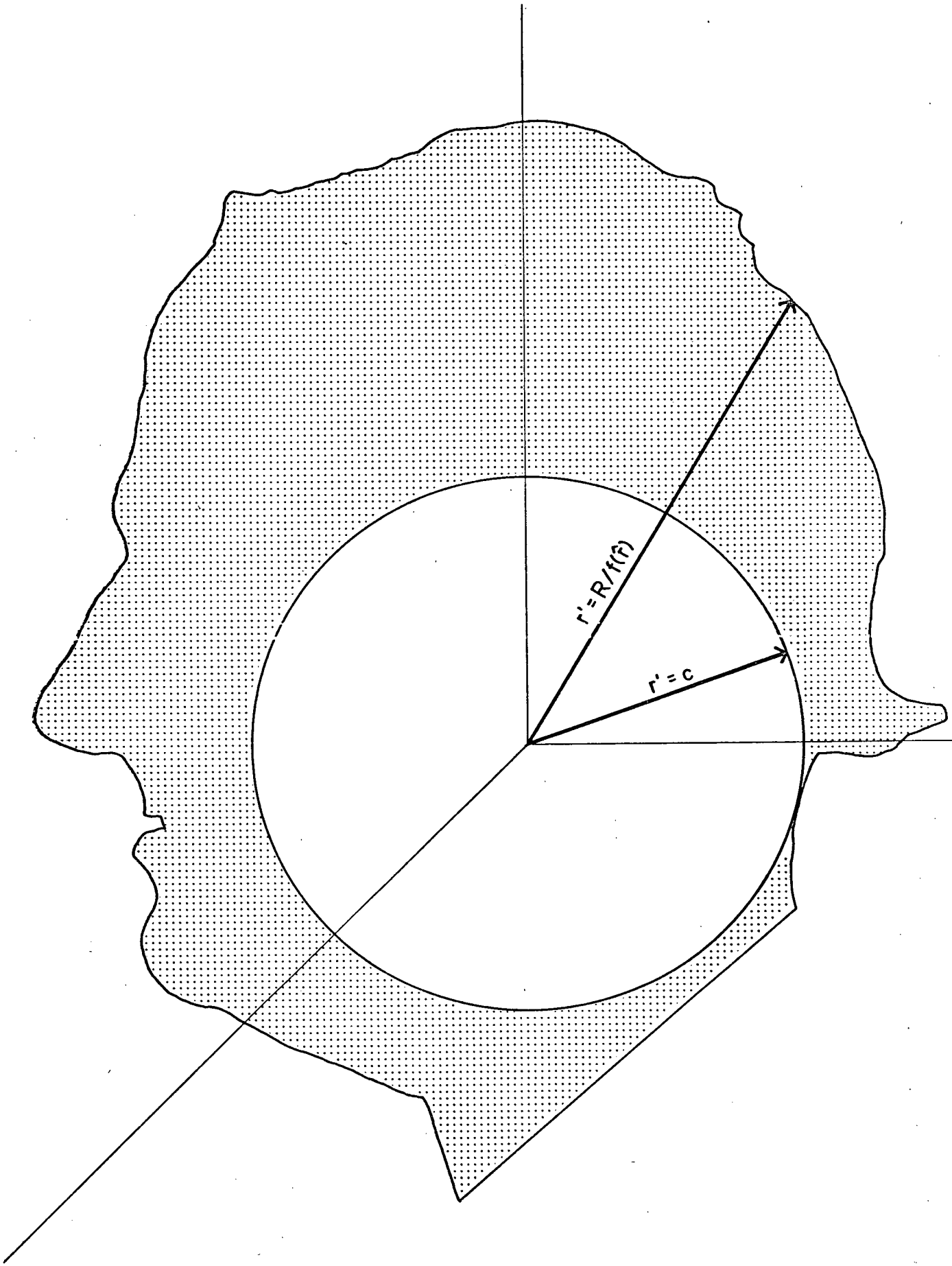
r' = R/f(r̂)
r' = c

The first term corresponds to the contribution of dipoles within U to the local field; it vanishes for all c since the integral over the solid angle is zero. The second term, corresponding to the contribution of dipoles between the surface U and the sphere r = R to the local field, can be integrated over r' if c is sufficiently large that $g_0(r') \tilde{=} 1$ for $r' \geq c$. Then

$$\eta_{\alpha\beta} = \frac{1}{4\pi}\int (\ln\frac{1}{f(\hat{r})})(3r_\alpha r_\beta - \delta_{\alpha\beta})\,d\Omega \tag{1.16}$$

independent of R, c and the detailed structure of $g(\vec{r})$. The symmetric zero-trace tensor $\eta_{\alpha\beta}$, defined by Eq. (1.16), yields a measure of the anisotropy of $f(\hat{r})$, or equivalently of U. The off-diagonal elements of $\eta_{\alpha\beta}$ can be made to vanish if $f(\hat{r})$ is a quadratic form, and $\eta_{\alpha\beta} = 0$ if $f(\hat{r})$ is spherically symmetric.

The simplest case of anisotropy occurs when the pair-correlation function $g(\vec{r})$ can be made isotropic by a scaling in one direction only. The surface U upon which $g(\vec{r})$ is a constant is, in this case, a spheroid; and the scaling transformation which renders $g(\vec{r})$ isotropic is given by $r' = r/f(\hat{r}) = r(r_\alpha A_{\alpha\beta} r_\beta)^{\frac{1}{2}}$. If the spheroid is prolate,

$$A_{\alpha\beta} = \begin{bmatrix} 1 & 0 & 0 \\ 0 & 1 & 0 \\ 0 & 0 & 1-e_g^2 \end{bmatrix} \tag{1.17}$$

where e_g is the eccentricity of the pair correlation function. The diagonal elements of the anisotropy tensor $\eta_{\alpha\beta}$ are given by

$$\eta_{zz} = \frac{1}{4\pi}\int_0^{2\pi}\int_0^{\pi} (\ln(1-e_g^2\cos^2\theta)^{\frac{1}{2}})(3\cos^2\theta-1)\sin\theta d\theta d\phi; \qquad (1.18)$$

$\eta_{xx} = \eta_{yy} = -\frac{1}{2}\eta_{zz}$ and $\eta_{\alpha\beta} = 0$ if $\alpha \neq \beta$. The integration is carried out in Appendix B, with the result that

$$\eta_{zz} = \frac{2}{3} - \frac{1}{e_g^2} - \frac{1}{2e_g}\left(1 - \frac{1}{e_g^2}\right)\ln\frac{(1+e_g)}{(1-e_g)} . \qquad (1.19)$$

Furthermore, it can be shown that if U is a general ellipsoid, $\eta_{ii} = -\frac{1}{3} + \frac{N_i}{4\pi}$ where N_i is the demagnetizing factor of the ellipsoid.

1.4 The Dielectric Tensor and the Local Field

The local electric field F_α, experienced by a molecule in the fluid, is given by

$$F_\alpha = E_\alpha + F_{0\alpha} + F_{1\alpha} = E_\alpha + 4\pi L_{\alpha\beta} P_\beta \tag{1.20}$$

where E_α is the applied field, $F_{0\alpha} = \frac{4\pi P_\alpha}{3}$ is the Lorentz cavity field, and $L_{\alpha\beta}$ is the Lorentz-factor tensor introduced by Dunmur (7). Substitution of Eq. (1.13) into Eq. (1.20) yields

$$L_{\alpha\beta} = \frac{1}{3}\delta_{\alpha\beta} + \eta_{\alpha\beta} \ . \tag{1.21}$$

The dielectric permittivity tensor $\varepsilon_{\alpha\beta}$ is obtained from Eq. (1.4) by recalling that $D_\alpha = E_\alpha + 4\pi P_\alpha$; then

$$\varepsilon_{\alpha\beta} E_\beta = E_\alpha + 4\pi P_\alpha \ . \tag{1.22}$$

The expression for the local electric field F_α in terms of the dielectric permittivity is obtained by substituting Eqs. (1.21) and (1.22) into Eq. (1.20); then

$$F_\alpha = \left(\frac{1}{3}(\varepsilon_{\alpha\beta} + 2\delta_{\alpha\beta}) + \eta_{\alpha\gamma}(\varepsilon_{\gamma\beta} - \delta_{\gamma\beta}) \right) E_\beta \ . \tag{1.23}$$

If the assumption is made that the polarization P_α is related to the local field F_α by

$$P_\alpha = \rho \alpha_{\alpha\beta} F_\beta \tag{1.24}$$

where $\alpha_{\alpha\beta}$ is the effective molecular polarizability, substitution of Eqs. (1.20) and (1.24) into Eq. (1.22) yields the anisotropic Clausius-Mossotti equation

$$\varepsilon_{\alpha\beta} - \delta_{\alpha\beta} = 4\pi\rho((\varepsilon_{\alpha\delta} - \delta_{\alpha\delta})L_{\delta\gamma} + \delta_{\alpha\gamma})\alpha_{\gamma\beta} \tag{1.25}$$

or, as expressed in terms of the anisotropy tensor $\eta_{\alpha\beta}$,

$$(\varepsilon_{\alpha\beta} - \delta_{\alpha\beta})(\delta_{\beta\gamma} - 4\pi\rho\eta_{\beta\delta}\alpha_{\delta\gamma}) = \frac{4\pi\rho}{3}(\varepsilon_{\alpha\beta} + 2\delta_{\alpha\beta})\alpha_{\beta\gamma} \ . \tag{1.26}$$

If the permittivity tensor $\varepsilon_{\alpha\beta}$ and the local field anisotropy tensor $\eta_{\alpha\beta}$ are both diagonal, Eq. (1.26) becomes

$$\frac{(\varepsilon_{ii} - 1)}{(\varepsilon_{ii} + 2)}(1 - 4\pi\rho\eta_{ii}\alpha_{ii}) = \frac{4\pi\rho\alpha_{ii}}{3} \ , \tag{1.27}$$

and the local field is given by

$$F_i = \left[\frac{1}{3}(\varepsilon_{ii} + 2) + \eta_{ii}(\varepsilon_{ii} - 1)\right]E_i \tag{1.28}$$

These results have been published in our recent paper (24). If the assumptions made in deriving these relations are valid at optical frequencies, then for a uniaxial fluid, Eq. (1.27) becomes

$$\frac{(n_\ell^2-1)}{(n_\ell^2+2)}\,(1-4\pi\rho\eta_\ell\alpha_\ell) = \frac{4\pi}{3}\rho\alpha_\ell \tag{1.29}$$

since $n_\ell = \sqrt{\varepsilon_\ell}$ where $\ell = \parallel$ or $\perp$. Since $\eta_{\alpha\beta}$ is traceless, $\eta_\parallel = -2\eta_\perp$ and it follows from Eq. (1.29) that

$$\frac{2(n_\perp^2+2)}{(n_\perp^2-1)} + \frac{(n_\parallel^2+2)}{(n_\parallel^2-1)} = \frac{3}{4\pi\rho}\left[\frac{1}{\alpha_\parallel} + \frac{2}{\alpha_\perp}\right] \tag{1.30}$$

All refractive index measurements will be interpreted on the basis of Eq. (1.29); in the case of isotropic fluids, $e_g = 0$, $\eta_{\alpha\beta} = 0$ and Eq. (1.29) reduces to the well known Lorentz-Lorenz relation. In general, however, the refractive indices of a fluid depend on the effective molecular polarizability α_ℓ, the pair-correlation determined anisotropy tensor η_ℓ and the number density ρ. Whereas an exact determination is difficult, an approximate determination of the temperature dependence of these quantities is possible from simple statistical mechanical models.

CHAPTER 2

NEMATIC LIQUID CRYSTALS

2.1 Molecular Order in Liquid Crystals

In crystalline solids, long-range order exists in the three positional degrees of freedom of the constituent molecules. If the molecules are anisotropic, long-range orientational order can also exist. Loss of order in one or more degrees of freedom constitutes a change of phase, and in an isotropic liquid no long-range order remains. The term "mesophase" is applied to the intermediate phases that occur between the phase that has long-range order in the largest number of degrees of freedom and the unordered phase, the isotropic liquid.

Two broad categories of mesophases exist. "Plastic crystals" are characterised by loss of orientational order, while positional order of the crystal lattice is maintained. Commonly occuring examples are solid hydrogen, ammonium halides, and the ferroelectrics barium titanate and rochelle salts. In the strongly ordered phase, the molecules in the crystal lattice have a well-defined orientation, whereas in the less ordered "plastic crystal" mesophase, they commute between several equivalent orientations. In "liquid crystals" the converse is true, orientational order is maintained while positional order is diminished. It follows from the definitions that the constituent molecules of these mesophases must be anisotropic, since one cannot speak of orientation of spherically symmetric molecules, and symmetry

prevents the loss of positional order in fewer than three dimensions. In fact, plastic crystal molecules are nearly spherical in shape, whereas liquid crystal molecules are strongly elongated.

There exists usually a parameter such that a mesophase exists for some range of its values; the end-points of the range corresponding to transitions to more or less ordered phases. If this parameter is temperature, the material is thermotropic, if it is composition (i.e. concentration in a solvent), it is lyotropic. Three categories of liquid crystals are distinguished. In canonic liquid crystals, long range positional order is lost in one dimension, in smectics in two dimensions, and in cholesterics in three. Canonics are regularly packed long rod-like molecules, where the centers of molecules are randomly distributed in one dimension (i.e. one dimensional liquids). Smectics form uniformly separated layers of two-dimensional liquids with oriented molecules; while cholesterics form three-dimensional liquids with well-defined (but not necessarily uniform) orientation.

Compounds capable of forming the liquid crystalline phase are made up of long molecules that are fairly rigid along their long axes. These can be small organic molecules, giving rise to thermotropic phases, long helical rods, giving rise to lyotropic phases or associated structures of molecules and ions, which can be thermo- and/or lyotropic. The general pattern of small organic molecules is two nearly coplanar para-substituted aromatic rings rigidly linked by a double or triple bond (A-B) and short, partly flexible chains, R shown in Fig. 2. The composition of central link A-B and the chains R are

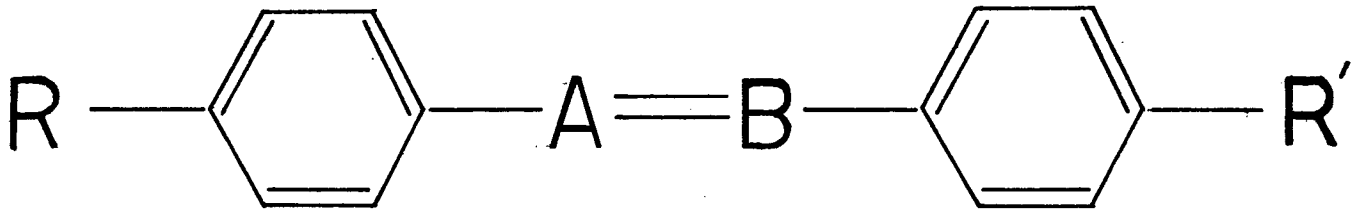

Fig. 2 Structure of common nematogens.

TABLE I. Composition of some common nematic liquid crystals.

	A-B	R	R'	Mol. Wt.
PAA	-N=N- (1, 0)	CH_3-O-	-O-CH_3	258.28
MBBA	-CH=N-	CH_3-O-	-$(CH_2)_3$-CH_3	267.37
EBBA	-CH=N-	C_2H_5O-	-$(CH_2)_3$-CH_3	281.40
BEPC	-O-C- (=O)	CH_3-CH_2-O-	-(CO_3)-$(CH_2)_3$-CH_3	358.39

given in Table I for some common materials. Examples of long helical rods are DNA, tobacco mosaic virus and certain synthetic polypeptides. The typical lengths of these are in the hundreds of angstroms, with widths an order of magnitude smaller. Associated structures consist of long apolar aliphatic chains (10-20 CH_2 groups) having an ionizable polar group at one end, occuring naturally in soaps and phospholipids.

2.2 Types of Liquid Crystalline Order

The different types of liquid crystalline order can best be illustrated graphically. The position and orientation of the molecules is shown by a dash.

In canonics, long rods are hexagonally packed in two dimensions, as shown in Figure 3. The long molecules can be helical rods or groups of associated structures. The probability density of finding a molecule at point (x,y,z) is

$$P(x,y,z) = P(x)\delta(y-dn-\frac{dm}{2}-\alpha)\delta(z-\frac{\sqrt{3}}{2}dm-\beta) ,$$

where δ is the Dirac delta function, d is the repeat distance in the y-direction, m and n are integers and α and β are arbitrary constants. The average value of the orientation of the long axes of the rods is $\bar{\theta} = \frac{\pi}{d}$ and $\bar{\phi} = 0$. Long rods can be made up of associated structures by the following mechanism. The ionic head dissociates in a solvent, making the head hydrophilic and the long tail hydrophobic. End views of the two stable concentration dependent rod-like configurations are shown in Figure 4.

In smectics, long range positional order is retained in one direction, giving rise to a layered liquid structure. In addition, the long axes of the molecules have the same average orientation. The variations smectic A and smectic C are shown in Figure 5. The probability density of finding a molecule at point (x,y,z) is $P(x,y,z) = P(x,y)\delta(z-md-\alpha)$. The average orientation is $\bar{\theta} = \theta_0$ and $\hat{n}$ is a unit

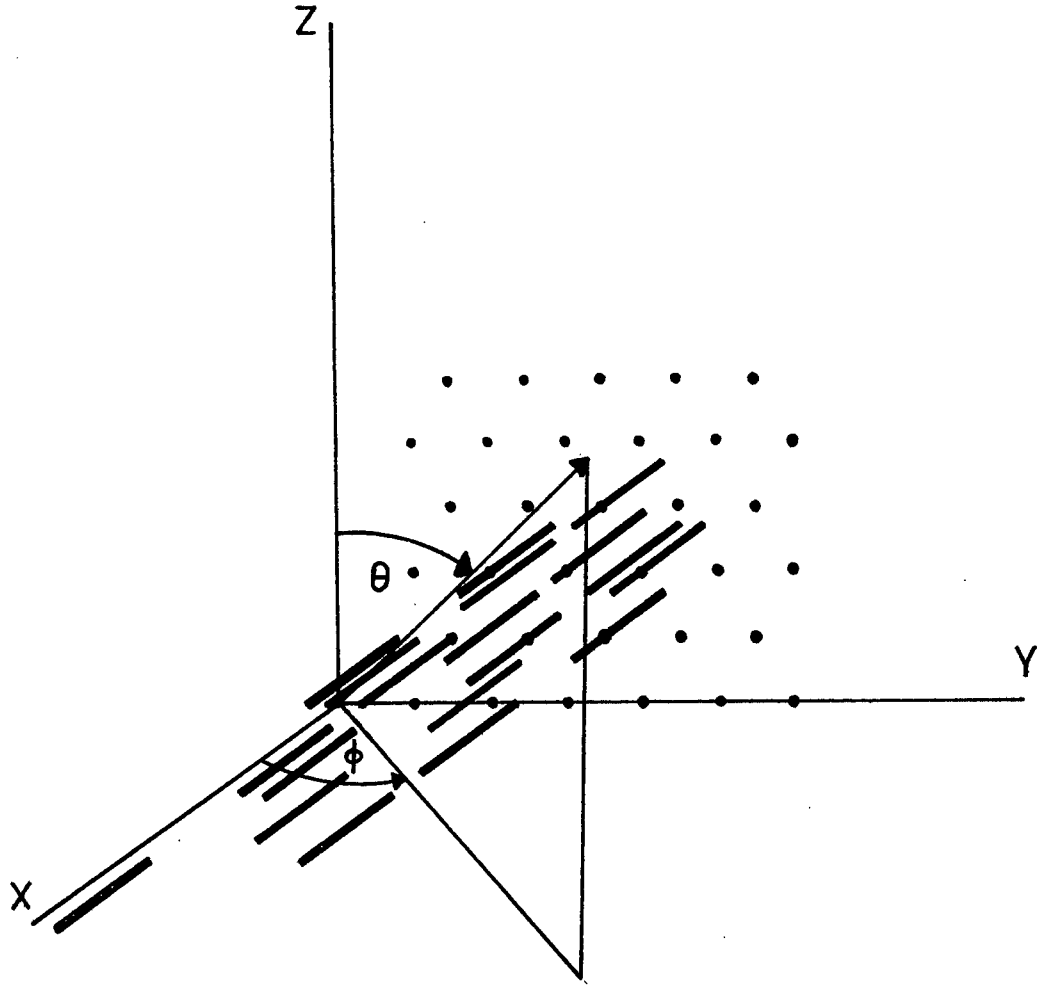

Fig. 3 Canonic order.

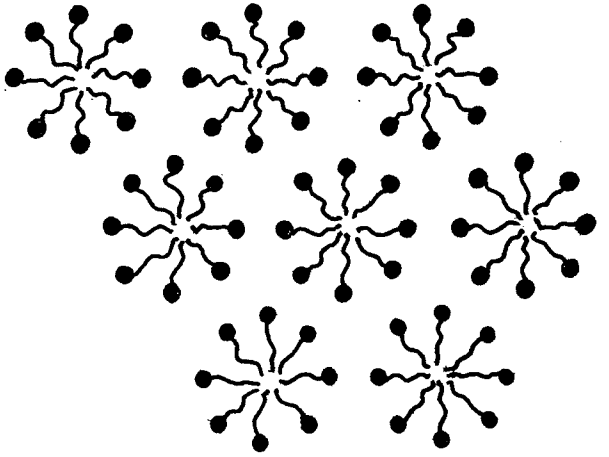

a) Excess solvent .

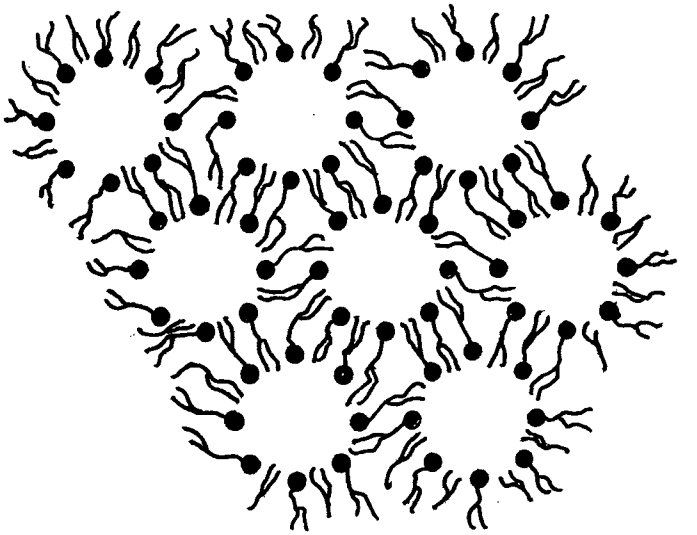

b) Excess solute .

Fig. 4 Hexagonal rod systems .

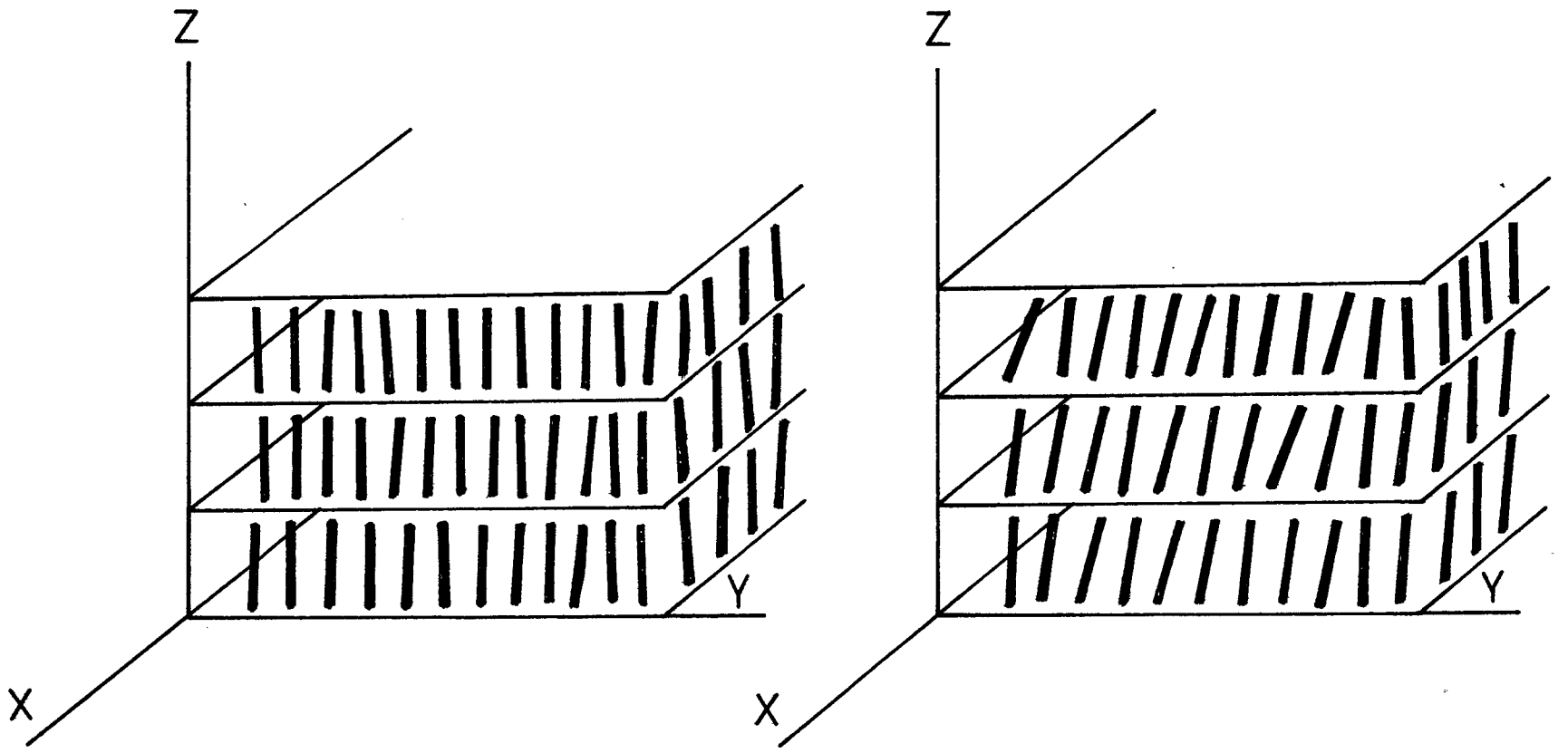

a) Smectic A.

b) Smectic C.

Fig. 5 Arrangement of molecules in smetics.

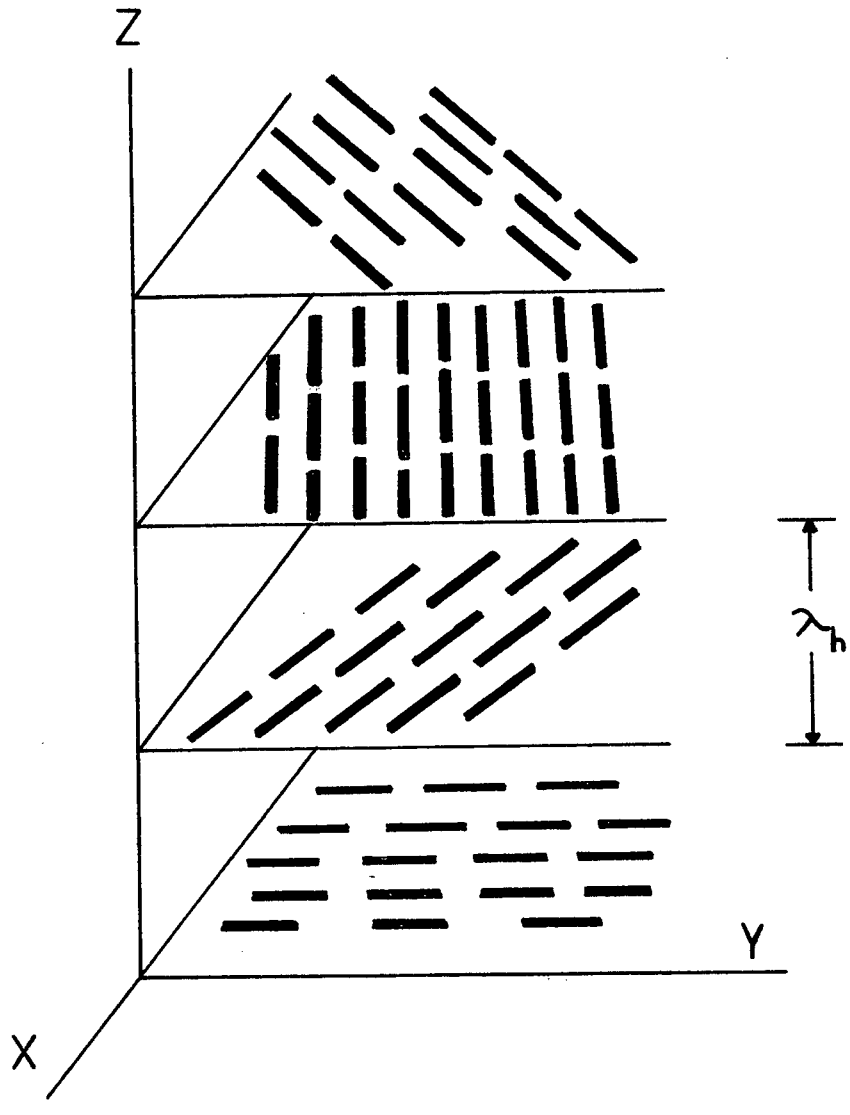

Fig. 6 The cholesteric configuration.

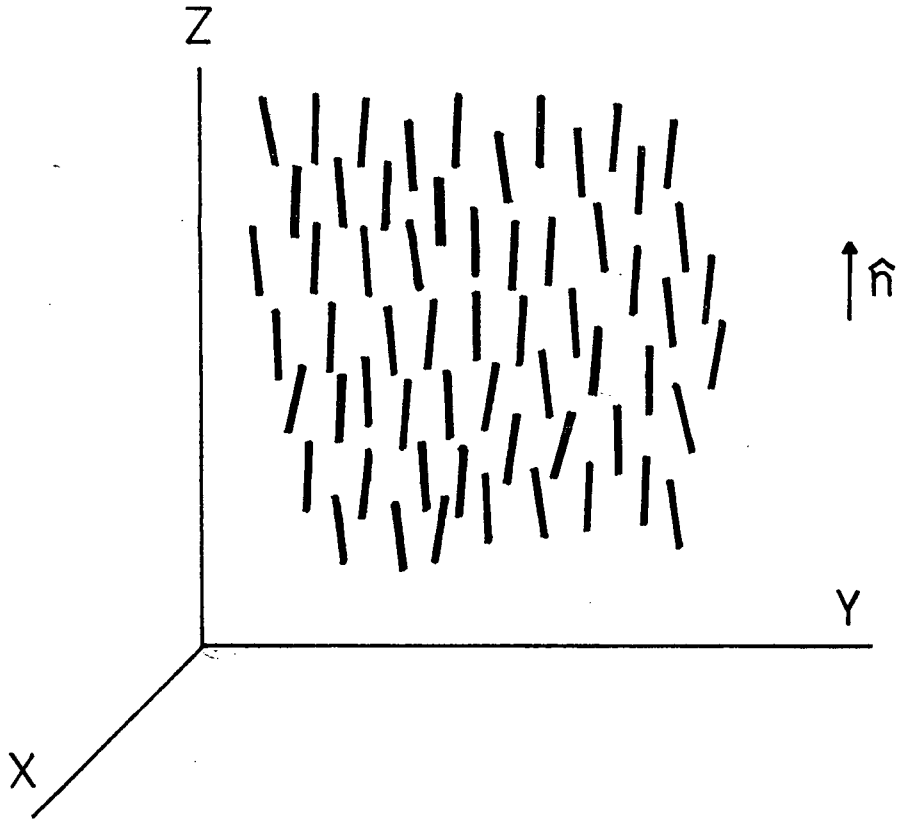

Fig. 7 Arrangement of molecules in the nematic mesophase.

vector pointing in the direction of average orientation. Smectic A is a special case of smectic C, where $\bar{\theta} = 0$.

The arrangement of molecules in the cholesteric phase is shown in Figure 6. In moving through the liquid in the z-direction, $\hat{n}$ (averaged in the x-y plane) is periodic in a distance λ_h. Here $n_x = \cos\left(\frac{2\pi}{\lambda_h}z+\alpha\right)$, $n_y = \sin\left(\frac{2\pi}{\lambda_h}z+\alpha\right)$ and $n_z = 0$. Note that there is no long-range positional order, and that $\hat{n}$ and $-\hat{n}$ are equivalent if the molecules are simple rods.

Arrangement of molecules in the nematic phase is shown in Figure 7. This is a special case of the cholesteric phase, obtained when $\lambda_h \to \infty$. The unit vector $\hat{n}$ pointing in the direction of average orientation is called the nematic director.

In the cholesteric phase, the helical deformation is caused by chiral (left- or right-handed) molecules. The nematic phase is a special case of the cholesteric where the constituents are either achiral or racemic. Because of their relative simplicity, nematics were chosen as the subject of this study. All subsequent discussion is therefore restricted to the nematic mesophase.

2.3 The Order Parameter in Nematics

In order to quantitatively characterize order in a liquid crystalline mesophase, it is desirable to have an order parameter whose value reflects the amount of order present. The molecular order manifests itself as the anisotropy of macroscopic properties of the mesophase. Ideally, then, one would like to relate the anisotropy of measurable physical properties to the molecular order through an order parameter.

To gain this end, we calculate the polarization $\bar{P}$ for an array of spheroidal molecules, carrying permanent dipole moments μ_p along their long axes in an electric field $\vec{F}$. Let $\alpha_{m_{\parallel}}$ and $\alpha_{m_{\perp}}$ be the molecular polarizabilities parallel and perpendicular to the long axis respectively, and let $\hat{n}_i$ be a unit vector along the long axis of the i^{th} molecule, shown in Figure 8. The contribution of the i^{th} molecule to the polarization is

$$p_{i_\alpha} = \mu_p n_{i_\alpha} + T^{-1}_{\alpha\beta}\alpha_{m\beta\gamma}T_{\gamma\delta}F_\delta \tag{2.1}$$

where $T_{\alpha\beta}$ transforms F_α into components parallel and perpendicular to the long axis of the molecule. If θ and ϕ are the usual colatitude and longitude,

$$T_{\alpha\beta} = \begin{bmatrix} -\sin\phi_i & -\cos\phi_i & 0 \\ \cos\theta_i\cos\phi_i & -\cos\theta_i\sin\phi_i & -\sin\theta_i \\ \sin\theta_i\cos\phi_i & -\sin\theta_i\sin\phi_i & \cos\theta_i \end{bmatrix} \tag{2.2}$$

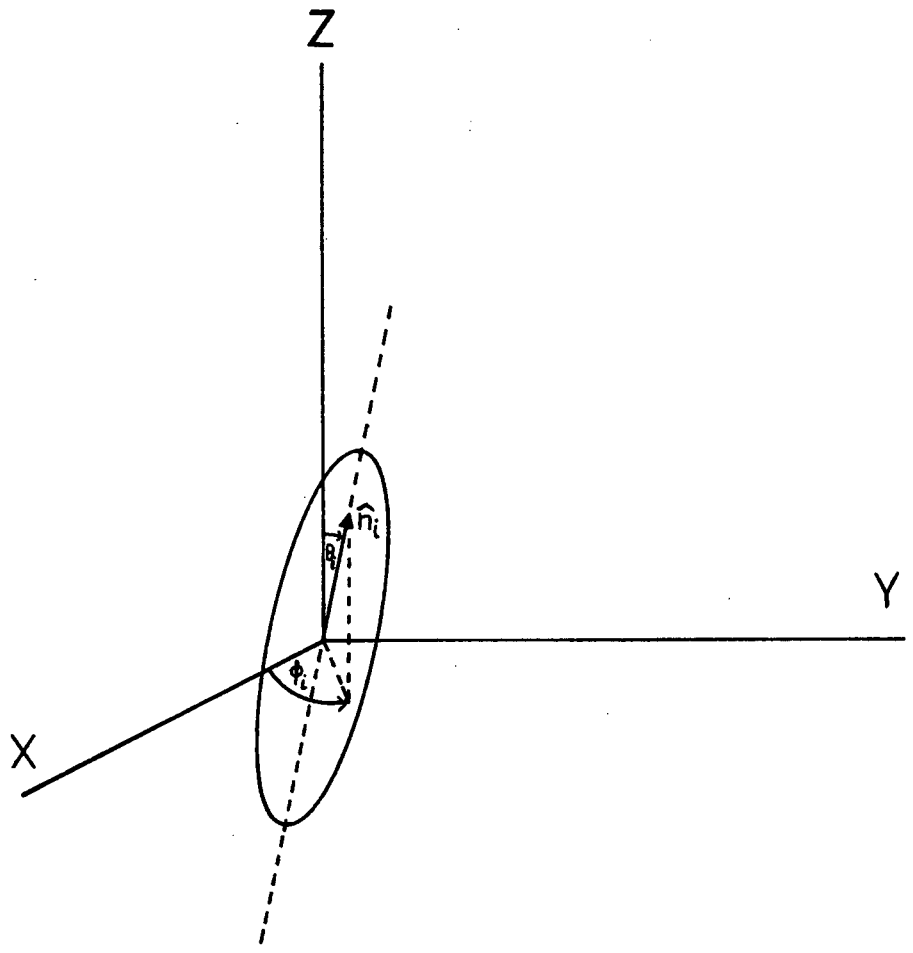

Fig. 8 Co-ordinate system used in the polarization calculation.

$$\alpha_{m_{\alpha\beta}} = \begin{bmatrix} \alpha_{m_\perp} & 0 & 0 \\ 0 & \alpha_{m_\perp} & 0 \\ 0 & 0 & \alpha_{m_\parallel} \end{bmatrix} \tag{2.3}$$

and

$$n_{i_\alpha} = \begin{bmatrix} \sin\theta_i \cos\phi_i \\ \sin\theta_i \sin\phi_i \\ \cos\theta_i \end{bmatrix} . \tag{2.4}$$

$T^{-1}_{\alpha\beta} = T_{\beta\alpha}$ and multiplication yields

$$T^{-1}_{\alpha\beta}\,\alpha_{m\beta\gamma}\,T_{\gamma\delta} = \begin{bmatrix} \alpha_{m_\perp} + 3\Delta\sin^2\theta_i\cos^2\phi_i & -3\Delta\sin^2\theta_i\sin\phi_i\cos\phi_i & 3\Delta\sin\theta_i\cos\theta_i\cos\phi_i \\ -3\Delta\sin^2\theta_i\sin\phi_i\cos\phi_i & \alpha_{m_\perp} + 3\sin^2\theta_i\sin^2\phi_i & -3\sin\theta_i\cos\theta_i\sin\phi_i \\ 3\Delta\sin\theta_i\cos\theta_i\cos\phi_i & -3\Delta\cos\theta_i\sin\theta_i\sin\phi_i & \alpha_{m_\perp} + 3\Delta\cos^2\theta_i \end{bmatrix} \tag{2.5}$$

where $\Delta = (\alpha_{m_\parallel} - \alpha_{m_\perp})/3$. Letting $a = (\alpha_{m_\parallel} + 2\alpha_{m_\perp})/3$, Eq. (2.5) can be re-written as

$$T^{-1}_{\alpha\beta}\alpha_{m_{\beta\gamma}}T_{\gamma\delta} = a\delta_{\alpha\delta} + \Delta\left[3n_{i\alpha}n_{i\delta} - \delta_{\alpha\delta}\right] , \tag{2.6}$$

and

$$p_{i\alpha} = \mu_p n_{i\alpha} + a\delta_{\alpha\beta}F_\beta + \Delta\left[3n_{i\alpha}n_{i\beta} - \delta_{\alpha\beta}\right]F_\beta . \tag{2.7}$$

The polarization $\vec{P}$ is given by

$$P_\alpha = a\rho F_\alpha + \mu_p \rho < n_{i\alpha} > + \Delta\rho F_\beta 2<\tfrac{1}{2}(3n_{i\alpha}n_{i\beta}-\delta_{\alpha\beta})> \tag{2.8}$$

where ρ is the number density, and $< >$ indicates averaging over all molecules. The second and third terms in the r.h.s. of Eq. (2.8) constitute the anisotropic part of $\vec{P}$; they vanish if the material is isotropic and all molecular orientations are equiprobable. We choose, therefore, the vector

$$n_\alpha = <n_{i\alpha}> \tag{2.9}$$

and the symmetric traceless tensor

$$S_{\alpha\beta} = <\tfrac{1}{2}(3n_{i\alpha}n_{i\beta}-\delta_{\alpha\beta})> \tag{2.10}$$

as the dipolar and quadrupolar order-parameters respectively. In a uniaxial material the orientational probability density function does not depend on the angle θ if the symmetry axis of the material coincides with the z-axis. Then, dropping the subscript i,

$$\vec{n} = \begin{bmatrix} 0 \\ 0 \\ R \end{bmatrix} \tag{2.11}$$

where $R = <\cos\theta>$, and

$$S_{\alpha\beta} = \begin{bmatrix} -\frac{1}{2}S & 0 & 0 \\ 0 & -\frac{1}{2}S & 0 \\ 0 & 0 & S \end{bmatrix} \qquad (2.12)$$

where $S = \langle \frac{1}{2}(3\cos^2\theta - 1) \rangle$. If R = 0, the bulk polarizability obtained from Eq. (2.8) is in agreement with published results (21). The two scalars R and S are thus sufficient to describe order in uniaxial materials; they have the value of unity if all the molecules are aligned, and they vanish in the completely disordered isotropic phase. R distinguishes between molecules flipped end for end, whereas S does not. Note that R and S are not independent, the condition $S \geq \frac{1}{2}(3R^2-1)$ must be satisfied, (i.e. $S = 0 \not\rightarrow R = 0$) and that negative and positive values of R describe the same physical configuration, whereas for S they do not. In fact, negative values of S indicate molecules perpendicularly aligned to the symmetry axis, randomly distributed otherwise.

2.4 The Landau Theory

In the thermotropic nematic phase, as the temperature is increased, the angular distribution of the symmetry axes of the molecules becomes more random, until the value of the order parameter(s) drops to zero catastrophically at some temperature T_c. Experimentally, the diminishing order can be seen by measuring the anisotropy of such macroscopic properties as the magnetic susceptibility, the dielectric constant and the refractive index.

If the nature of the intermolecular interaction is known, it is possible in principle to calculate the temperature dependence of the order parameters. In practice, exact solutions for three-dimensional systems have not yet been obtained. A great deal of qualitative information can, however be obtained from the elegant Landau theory of phase-transitions (8). We start with the partition function Q, given by

$$Q = \sum_i e^{-\beta E_i} = \int \Omega(\zeta) e^{-\beta E(\zeta)} d\zeta = \int e^{-\beta(E(\zeta)-kT\ln\Omega(\zeta))} d\zeta \qquad (2.13)$$

where $\beta = \frac{1}{kT}$, ζ is the order parameter, and $\Omega(\zeta)$ is the density of states. The Landau free energy density $F(\zeta,T)$ is defined by

$$F(\zeta,T) = \frac{1}{V}[E(\zeta)-kT\ln\Omega(\zeta)] \qquad (2.14)$$

where V is the volume.

The basic assumption of the Landau theory is that F has a minimum value for some ζ, say ζ_c, and that F may be expanded near ζ_c in a power series in ζ. Then

$$F(\zeta,T) = F(\zeta_c,T) + a_2(\zeta-\zeta_c)^2 + \ldots; \tag{2.15}$$

$a_1 = 0$ since $\left.\frac{\partial F}{\partial \zeta}\right|_{\zeta=\zeta_c} = 0$. Substitution of Eq. (2.15) into Eq. (2.14) and Eq. (2.13) yields

$$Q \cong e^{-\beta V F(\zeta_c,T)} \int e^{-\beta V a_2(\zeta-\zeta_c)^2} d\zeta \, , \tag{2.16}$$

and the average value of ζ is given by

$$\langle\zeta\rangle = \frac{e^{-\beta V F(\zeta_c,T)}}{Q} \int \zeta \, e^{-\beta V a_2(\zeta-\zeta_c)^2} d\zeta \tag{2.17}$$

As $V \to \infty$, clearly $\langle\zeta\rangle \to \zeta_c$, and the Helmholtz free energy density F is given by

$$F = -\frac{kT}{V} \ln Q = F(\zeta_c,T) - \frac{kT}{V} \ln \int e^{-\beta V a_2(\zeta-\zeta_c)^2} d\zeta \to F(\zeta_c,T) \tag{2.18}$$

Eq. (2.15) can therefore be regarded as an expansion of the Helmholtz free energy about its equilibrium value; the expected value of the order parameter is that which minimizes $F(\zeta,T)$. It is convenient to define a quantity $\Delta F = F(\zeta,T)-F(\zeta_c,T)$; since $\zeta_c \leq \zeta \leq 1$, we assume that ΔF can be expanded about $\zeta = 0$. Then

$$\Delta F = a_2\zeta^2 + a_3\zeta^3 + a_4\zeta^4 \tag{2.19}$$

and a stable ordered phase will occur if ΔF is negative and is a minimum. Since for a low temperature ordered phase to exist a_2 must change sign near the transition temperature, it is assumed to have the form $a_2 = q(T-T_0)$, where q and T_0 are positive constants. The other a's are assumed to be constants.

If the interaction is predominantly the permanent dipole-dipole type, that is, the pair interaction potential is not invariant if one molecule is turned end for end, the configurational free energy ΔF can be expanded in terms of R, and is given by

$$\Delta F = a_2 R^2 + a_4 R^4 + a_6 R^6 \tag{2.20}$$

where we have chosen somewhat arbitrarily to retain only the first three terms. There are no odd powers of R, since +R and -R describe physically equivalent orientations. At the phase transition, $\Delta F = 0$, $R = R_c$ and $T = T_c$. There are two solutions which minimize ΔF; if $a_4 > 0$ and $a_6 < 0$, then $R_c = 0$ and

$$R^2 \equiv \left(\frac{q}{2a_4}\right)(T_c - T) \tag{2.21}$$

where $T_c = T_0$. The details of the calculations in this section are given in Appendix C. The free energy ΔF and R are shown in Figure 9. If $a_4 < 0$ and $a_6 > 0$, then $R_c = \sqrt{\frac{-a_4}{2a_6}}$ and

$$R^2 \cong \frac{2}{3} R_c^2 + k_1' \sqrt{T_c^+ - T} \tag{2.22}$$

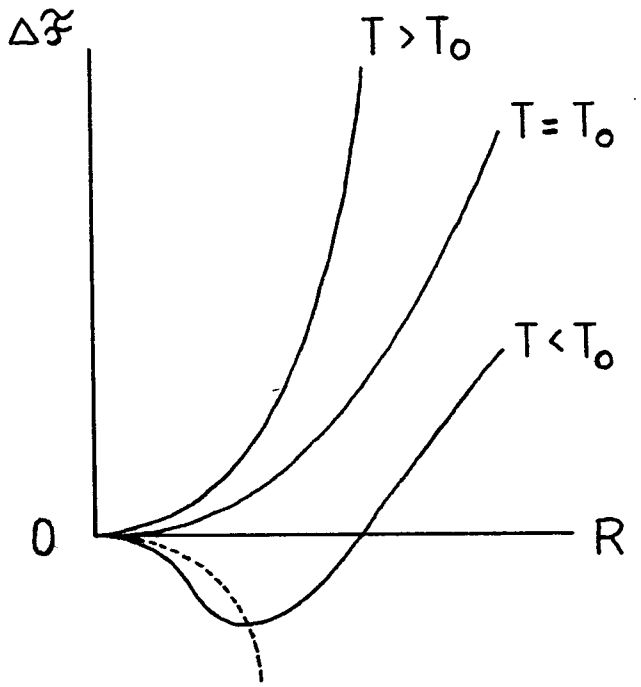

a) the Landau free energy

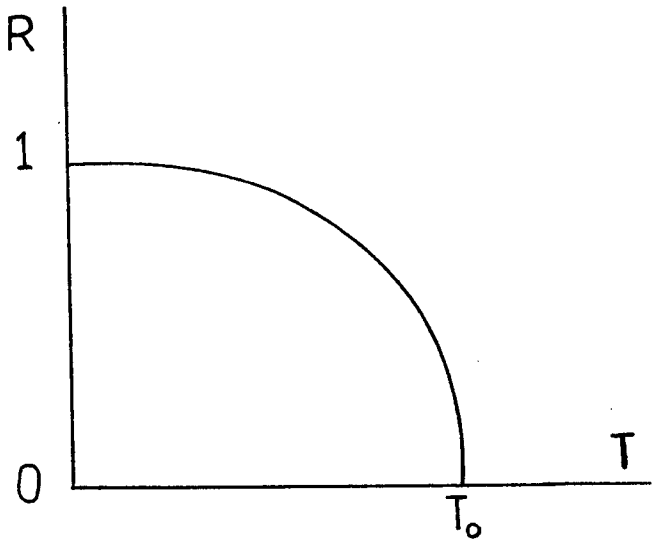

b) the order parameter R as a function of temperature

Fig. 9 Free energy and order parameter R; continuous transition.

where $k_1'^2 = \frac{q}{3a_6}$ and $T_c = T_0 + \frac{a_4^2}{4qa_6}$. Furthermore $\frac{\partial \Delta F}{\partial R} = 0$ for $T \leq T_c^+ = T_0 + \frac{a_4}{3qa_6}$; a metastable ordered phase can therefore persist, on heating, up to a temperature $T = T_c^+$ with $R^2 \Big|_{T_c^+} = \frac{5}{6} R_c^2$. Similarly, since for small R, $\frac{\partial \Delta F}{\partial R} \simeq 2a_2 R$, a metastable unordered (R = 0) phase can exist, on cooling, down to a temperature $T = T_0$ with $R^2 \Big|_{T_0} = \frac{3}{2} R_c^2$. The free energy ΔF and R are shown in Figure 10.

If the interaction is predominantly induced dipole-dipole type, that is, the pair interaction potential is invariant if one molecule is turned end for end, ΔF can be expanded in terms of S and is given by

$$\Delta F = b_2 S^2 + b_3 S^3 + b_4 S^4 \qquad (2.23)$$

where, as before $b_2 = q(T-T_0)$. The salient feature here is the inclusion of odd powers of S in the expansion; b_3 cannot be zero since negative and positive values of S correspond to physically different configurations.

At the transition, $\Delta F = 0$, $S = S_c$ and $T = T_c$. There are two solutions which minimize ΔF; if $b_3 > 0$ and $b_4 < 0$, then $S_c = 0$ and

$$S \simeq \frac{2q}{3b_3} (T_c - T) \qquad (2.24)$$

where $T_c = T_0$. This solution corresponds to a local minimum only, however; energetically an ordered phase with S = -1 will always be favorable. Behaviour of the type given by Eq. (2.24) is therefore not expected to occur. Molecular symmetry thus forces the second solution, where $b_3 < 0$ and $b_4 > 0$, then $S_c = \frac{-b_3}{2b_4}$, $T_c = T_0 + \frac{b_3^2}{4qb_4}$ and

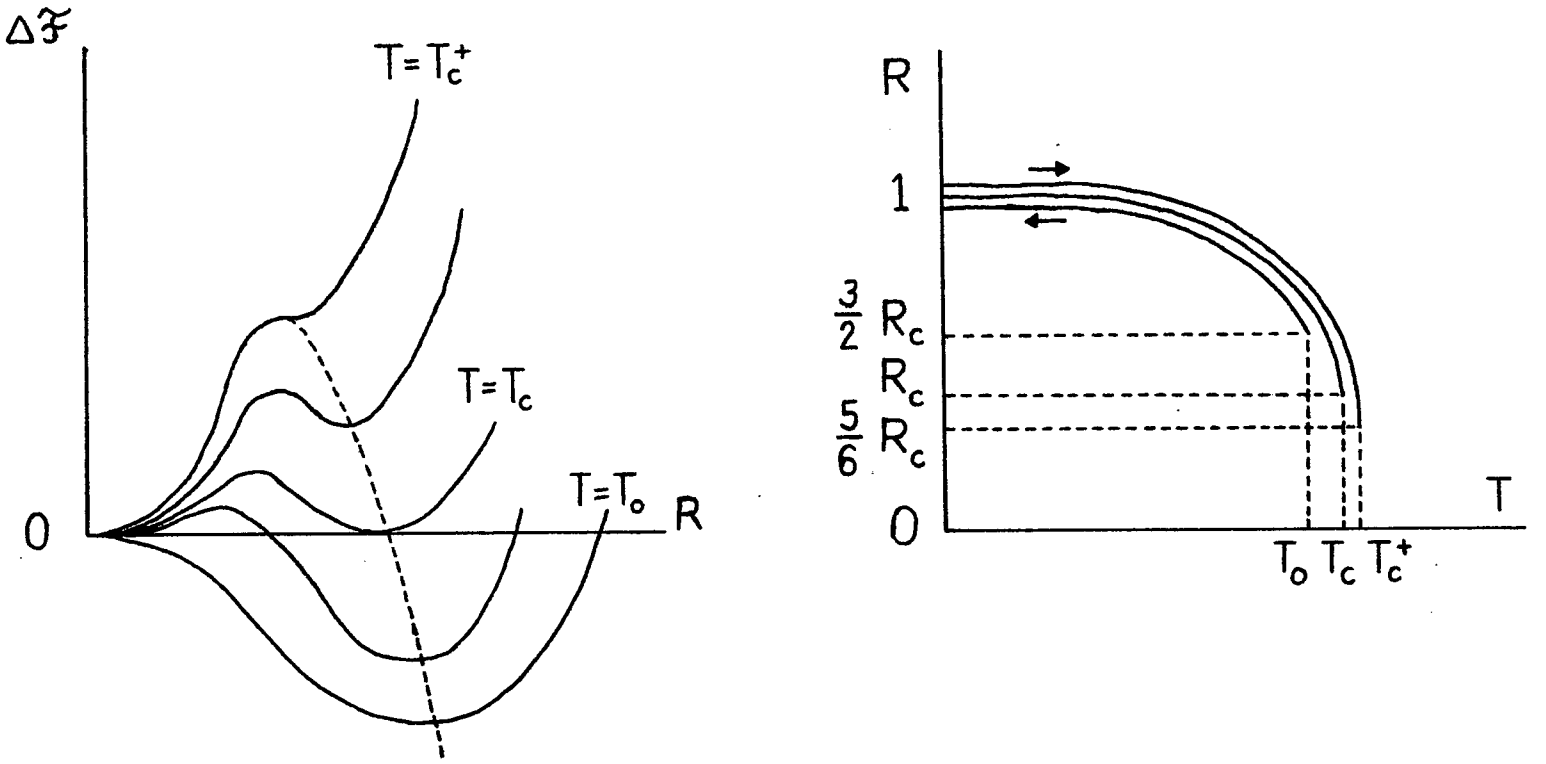

a) the Landau free energy

b) the order parameter R as a function of temperature

Fig. 10 Free energy and order parameter R; discontinuous transition.

$$S \cong \frac{3}{4} S_c + k_2' \sqrt{T_c^+ - T} \tag{2.25}$$

where $T_c^+ = T_0 + \frac{qb_3^2}{32qb_4}$ and $k_2'^2 = \frac{q}{2b_4}$.

As previously, a metastable ordered phase can persist, on heating, up to a temperature T_c^+, with $S\Big|_{T_c^+} = \frac{3}{4} S_c$; and a metastable unordered (S = 0) phase can exist, on cooling, down to a temperature $T = T_0$ with $S\Big|_{T_0} = \frac{3}{2} S_c$. The free energy ΔF and S are shown in Figure 11.

For most nematic liquid crystals, the predominant interaction is assumed to be the anisotropic Van der Waals interaction, and the constant b_3 is known to be negative. Thus, the temperature dependence of the order parameter is expected to be similar to that of Eq. (2.25); in fact, experimental measurements (9) indicate extremely good agreement with Eq. (2.25). The presence of metastable phases near the critical point whose stability is enhanced by sample impurities (10), however, make accurate comparison between theory and experiment difficult.

In addition to the nematic-isotropic transition, it is interesting to consider the liquid-vapor transition in a fluid. Using the so-called lattice gas model, we consider a volume V, divided into 2N identical cells, containing N molecules. If a liquid and a vapor phase coexist in V, then we denote the number of occupied and unoccupied cells in the liquid by N_1 and N_2 respectively; we assume that each cell can either be empty, or contain only one molecule. If the law of rectilinear diameters holds, i.e. $N_1+N_2 = N$, then the number of occupied and unoccupied cells in the vapor phase is given N_2 and N_1 respectively. The probability of a cell being occupied in the liquid or a cell being

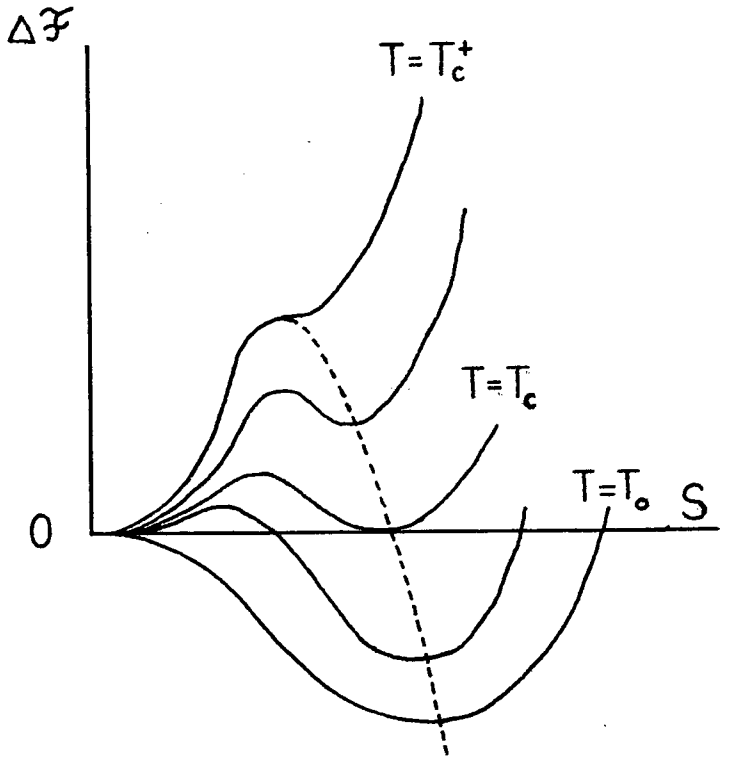

a) the Landau free energy.

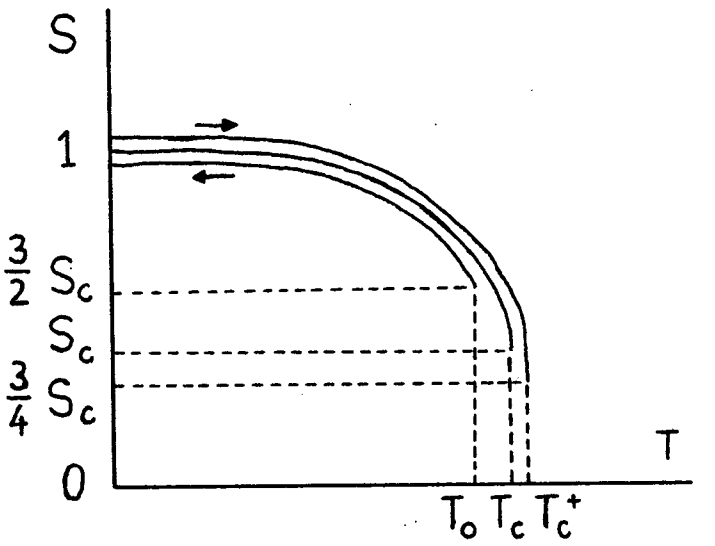

b) the order parameter S as a function of temperature.

Fig. 11 Free energy and order parameter S; discontinuous transition.

empty in the vapor is $\frac{N_1}{N_1+N_2}$; whereas the probability of a cell, anywhere in V, being either empty or full is $\frac{1}{2}$. The deviation of the probability in either phase from its average value of $\frac{1}{2}$ is $\gamma = \frac{N_1}{N_1+N_2} - \frac{1}{2} = \frac{N_1-N_2}{2N}$. If there is only a single homogeneous phase existing, then $\gamma = 0$; thus γ may be regarded as the order parameter. In terms of densities, $\gamma = \frac{\rho_L-\rho_V}{\rho_c}$, where $\rho_L = \frac{2N_1}{V}$, $\rho_V = \frac{2N_2}{V}$ and $\rho_c = \frac{N}{V}$. Since $+\gamma$ and $-\gamma$ describe the same physical configuration, the expansion of the Landau free energy in even powers of γ is appropriate. If the coefficient of the second term in the expression is positive, then Eq. (2.21) yields immediately

$$\rho_2-\rho_V = c_1(T_c-T)^{\beta} \tag{2.26}$$

where $\beta = \frac{1}{2}$ and $c_1 = \rho_c \left(\frac{q}{2a_4}\right)^{1/2}$. In view of the simplicity of the model, Eq. (2.26) gives a remarkably accurate description of the liquid-vapor transition.

CHAPTER 3

MEAN FIELD THEORY

3.1 One-body Pseudopotential in the Mean Field Approximation

For a classical fluid of N identical molecules contained in a volume V, the configurational partition function Q_N, n-particle distribution function $P^{(n)}$ and n-particle correlation function $g^{(N)}$ can be written

$$Q_N = \frac{\int\cdots\int \exp(-\beta U_N)\, d\vec{\gamma}_1 \ldots d\vec{\gamma}_N}{N!(4\pi)^N} = \frac{Z_N}{N!(4\pi)^N} \tag{3.1}$$

$$P^{(n)}(\vec{\gamma}_1 \ldots \vec{\gamma}_n) = \frac{N!\int\cdots\int \exp(-\beta U_N)\, d\vec{\gamma}_{n+1} \ldots d\vec{\gamma}_N}{(N-n)!\, Z_N} \tag{3.2}$$

$$g^{(n)}(\vec{\gamma}_1 \ldots \vec{\gamma}_n) = P^{(n)}(\vec{\gamma}_1 \ldots \vec{\gamma}_n) \Bigg/ \left[\prod_{i=1}^{n} P^{(1)}(\vec{\gamma}_i)\right] \tag{3.3}$$

where U_N is the N-particle configurational potential energy, $\vec{r}_i$ and Ω_i denote, respectively, the position and orientation of molecule i, $\beta = 1/kT$ and $d\vec{\gamma}_i = d\vec{r}_i d\Omega_i = d\vec{r}_i \sin\theta_i d\theta_i d\phi_i$.

If the molecules are interacting pair-wise, then

$$U_N = \frac{1}{2} \sum_{i=1}^{N} \sum_{\substack{j=1 \\ j\neq 1}}^{N} W_{i,j}(\vec{\gamma}_i, \vec{\gamma}_j) \tag{3.4}$$

where $W_{i,j}(\vec{r}_i,\vec{r}_j)$ is the interaction energy of the pair i,j, and the potential energy of say, molecule 1, ε_1 is given by

$$\varepsilon_1(\vec{r}_1\ldots\vec{r}_N) = \frac{1}{2}\sum_{j=2}^{N} W_{i,j}(\vec{r}_1,\vec{r}_j) \tag{3.5}$$

The mean-field approximation consists of replacing the sum in Eq.(3.5) by its average value; all thermodynamic properties of the system can then be obtained from the resulting one-body pseudopotential $\bar{\varepsilon}_1(\vec{r}_1)$.

Since the system is a fluid, $\bar{\varepsilon}_1(\vec{r}_1) = \bar{\varepsilon}_1(\Omega_1)$ and

$$U_N = \sum_{i=1}^{N} \bar{\varepsilon}_i(\Omega_i) \tag{3.6}$$

From Eq. (3.2),

$$P^{(1)}(\vec{r}_1) = \rho f(\Omega_1) \tag{3.7}$$

where $\rho = N/V$,

$$f(\Omega_1) = \frac{\exp(-\beta\bar{\varepsilon}_1(\Omega))}{\int \exp(-\beta\bar{\varepsilon}_1(\Omega_1))d\Omega_1} \tag{3.8}$$

and self-consistency requires that the average value of U_N

$$\bar{U}_N = N\int \bar{\varepsilon}(\Omega)f(\Omega)d\Omega \ . \tag{3.9}$$

In most mean-field theories of the nematic state, molecular interactions consist explicitly only of anisotropic long-range attractive forces (13),(15),(25). Repulsive interactions are taken into account implicitly through assumptions made about the positional distribution of particles in the calculation of the one-body pseudopotential $\bar{\varepsilon}(\Omega)$. These assumptions, (the most frequent one being that of spherical symmetry), are usually not well justified. It is possible, however, to obtain an exact expression for $\bar{\varepsilon}(\Omega)$ in the mean-field approximation, since the molecular distribution is consistently determined by the form of the interaction potential $W_{1,2}$.

The average value of $\bar{\varepsilon}(\Omega)$ is given by

$$\bar{\varepsilon}_1(\vec{\gamma}_1) = \frac{1}{2}\int W_{i,j} \frac{P^{(2)}(\vec{\gamma}_1,\vec{\gamma}_j)}{P^{(1)}(\vec{\gamma}_1)} d\vec{\gamma}_j \quad . \tag{3.10}$$

Substitution from Eqs. (3.3) and (3.7) yields

$$\bar{\varepsilon}_1(\Omega_1) = \frac{1}{2}\rho\int W_{i,j}\, g^{(2)}(\vec{\gamma}_1,\vec{\gamma}_j) f(\Omega_j) d\vec{\gamma}_i \quad . \tag{3.11}$$

The pair-correlation function can be evaluated by considering pairs of particles; the potential energy of the pair of molecules, say 1 and 2 is given by

$$\varepsilon_{1,2}(\vec{\gamma}_1 \ldots \vec{\gamma}_N) = W_{1,2} + \frac{1}{2}\sum_{j=3}^{N} W_{i,j} + \frac{1}{2}\sum_{j=3}^{N} W_{2,j} \quad . \tag{3.12}$$

As before, the mean field approximation consists of replacing the sums in (3.12) by their average value; then, as $N \to \infty$,

$$\bar{\varepsilon}_{1,2}(\vec{\gamma}_1,\vec{\gamma}_2) = W_{1,2} + \bar{\varepsilon}_1(\Omega_1) + \bar{\varepsilon}_2(\Omega_2) \tag{3.13}$$

$g^{(2)}(\vec{\gamma}_1,\vec{\gamma}_2)$ can now be evaluated, since $U_N = \bar{\varepsilon}_{1,2} + \bar{\varepsilon}_{3,4} + \ldots \bar{\varepsilon}_{N-1,N}$

$$g^{(2)}(\vec{\gamma}_1,\vec{\gamma}_2) = \frac{N!\,\exp(-\beta\bar{\varepsilon}_{1,2})\left[\int \exp(-\beta\bar{\varepsilon}_{i,j})d\vec{\gamma}_i,d\vec{\gamma}_j\right]^{\frac{N}{2}-1}}{(N-2)!\left[\int\exp(-\beta\bar{\varepsilon}_{i,j})d\vec{\gamma}_i,d\vec{\gamma}_j\right]^{\frac{N}{2}}\rho f(\Omega_1)\rho f(\Omega_2)}$$

$$= \frac{N(N-1)\exp(-\beta\bar{\varepsilon}_{1,2})}{\hat{\rho}^2 f(\Omega_1)f(\Omega_2)\int\exp(-\beta\bar{\varepsilon}_{1,2})d\vec{\gamma}_1,d\vec{\gamma}_2} \tag{3.14}$$

In principle, for a given interaction potential $W_{1,2}$, the one-body pseudopotential $\bar{\varepsilon}_1(\Omega_1)$ can be obtained from Eqs. (11) and (14). As the resulting integral equation appears intractable, the assumption is made that $g^{(2)}(\vec{\gamma}_1,\vec{\gamma}_2)$ may be approximated in Eq. (11) by its average value $\bar{g}^{(2)}(\vec{r}_1,\vec{r}_2)$ where $\bar{}$ denotes averaging over molecular orientations. Letting $\vec{r} = \vec{r}_1 - \vec{r}_2$,

$$\bar{g}^{(2)}(\vec{r}) = \int g^{(2)}(\vec{\gamma}_1,\vec{\gamma}_2)f(\Omega_1)f(\Omega_2)d\Omega_1 d\Omega_2$$

$$= K\int\exp(-\beta\bar{\varepsilon}_{1,2})d\Omega_1 d\Omega_2 \tag{3.15}$$

where K is the normalization factor such that as $r \to \infty$, $\bar{g}^{(2)} \to 1$ given by

$$K^{-1} = \frac{\rho^2 \int \exp(-\beta \bar{\varepsilon}_{1,2}) d\vec{\gamma}_1, d\vec{\gamma}_2}{N(N-1)} = \int \exp(-\beta \bar{\varepsilon}_1) d\Omega_1 \int \exp(-\beta \bar{\varepsilon}_1) d\Omega_2 \tag{3.16}$$

as $N \to \infty$.

3.2 Pair-Correlation in a Hard Spheroid Model

In order to take steric repulsion of the molecules into consideration explicitly, the interaction potential $W_{1,2}$ is assumed to consist of a short-range repulsive part $U(\vec{r}_1,\vec{r}_2)$ and a long range attractive part $V(\vec{r}_1,\vec{r}_2)$. Then

$$\varepsilon_1(\Omega_1) = \frac{1}{2}\sum_{j=1}^{N}\left[U_{1,j}(\vec{r}_1,\vec{r}_j) + V_{1,j}(\vec{r}_1,\vec{r}_j)\right] \tag{3.17}$$

and

$$\bar{\varepsilon}_{1,2}(\vec{r}_1,\vec{r}_2) = U_{1,2}(\vec{r}_1,\vec{r}_2) + \bar{\varepsilon}_1(\Omega_1) + \bar{\varepsilon}_2(\Omega_2) \tag{3.18}$$

where $V_{1,2}(\vec{r}_1,\vec{r}_2)$ is assumed to be contained in $\bar{\varepsilon}_1$ and $\bar{\varepsilon}_2$. If the molecules are represented by cylindrically symmetric "hard" surfaces, whose orientation is given by Ω, a convenient form for $U_{1,2}$ is

$$U_{1,2}(\bar{r},\Omega_1,\Omega_2) = \lim_{\sigma\to\infty} -\ln\left(\frac{1}{2} + \frac{1}{\pi}\tan^{-1}\sigma[r-d_{1,2}(\Omega_1,\Omega_3,\hat{r})]\right) \tag{3.19}$$

where $\vec{r} = r\hat{r}$ is the intermolecular vector and $d_{1,2}$ is the distance between molecular centers when the surfaces are in point contact externally.

The anisotropy of the pair-correlation function $g^{(2)}(r\hat{r})$ may be obtained from $D(\hat{r})$, defined to be the effective hard core diameter given by

$$D(\hat{r}) = \int_0^{\infty}(1-\bar{g}^{(2)}(r\hat{r}))dr; \tag{3.20}$$

in order to simplify the notation, henceforth we shall write $\bar{g}^{(2)}(r\hat{r})$ as $g(r\hat{r})$.

We assume that there exists a radial scaling transformation $r = r'f(\hat{r})$ which renders $g(r\hat{r})$ isotropic; then, as in Section 1.3, $g(r\hat{r}) = g(r'f(\hat{r})\hat{r}) = g_0(r')$. From Eq. (3.20), it follows that

$$D(\hat{r}) = \int_0^\infty (1-g(r\hat{r}))dr = f(\hat{r})\int_0^\infty (1-g_0(r'))dr' \tag{3.21}$$

and $f(\hat{r}) = (2R_0)^{-1}D(\hat{r})$ where R_0, the effective hard-sphere radius, is assumed constant. Thus, if $D(\hat{r})$ is known, the average values of expressions involving two-particle interactions can be evaluated by simple scaling.

Substitution of Eqs. (3.15), (3.18) and (3.19) into Eq. (3.20) yields

$$D(\hat{r}) = \lim_{\sigma\to\infty} K\int\int_0^\infty \left(\frac{1}{2} - \frac{1}{\pi}\tan^{-1}_{\sigma}[r-d(\Omega_1,\Omega_2,\hat{r})]\right)dr \times \tag{3.22}$$

$$\exp(-\beta[\bar{\varepsilon}_1(\Omega_1)+\bar{\varepsilon}_2(\Omega_2))d\Omega_1 d\Omega_2$$

and integration over r yields

$$D(\hat{r}) = K\int d_{1,2}(\Omega_1,\Omega_2,\hat{r})\exp(-\beta[\bar{\varepsilon}_1(\Omega_1)+\bar{\varepsilon}_2(\Omega_2))d\Omega,d\Omega_2 = \bar{d}(\hat{r}) \tag{3.23}$$

In this model, the molecules are represented by hard spheroids, whose equation is

$$r_m^2(1-e^2(\hat{r}_m\cdot\hat{n}_m)^2) = R_0^2 \tag{3.24}$$

where $\vec{r}_m = r_m\hat{r}_m$ is a position vector originating at the center of the m^{th} molecule, $\hat{n}_m$ is a unit vector along its symmetry axis and e is the eccentricity. Unfortunately, it has not been possible to obtain a closed-form expression for the distance of closest approach $d_{1,2}$ in spite of considerable effort; consequently bounds on it must be considered.

If $d_{1+}(\hat{r},\Omega_1)$ is the length of the normal projection of surface 1 onto a line through its center in the direction $\hat{r}$, and $d_{1-}(\hat{r},\Omega_1)$ is the length of the intercepted segment of the same line, as shown in Figure 12, then clearly

$$\frac{1}{2}d_{1-}(\hat{r},\Omega_1) + \frac{1}{2}d_{2-}(\hat{r},\Omega_2) \leq d_{1,2} \leq \frac{1}{2}\, d_{1+}(\hat{r},\Omega_1) + \frac{1}{2}\, d_{2+}(\hat{r},\Omega_2) \tag{3.25}$$

Letting $\bar{d}_{\pm}(\hat{r}) = \int d_{\pm}(\hat{r},\Omega)f(\Omega)d\Omega$,

$$\bar{d}_-(\hat{r}) \leq D(\hat{r}) \leq \bar{d}_+(\hat{r}) \tag{3.26}$$

from elementary geometry, as shown in Appendix D,

$$d_-(\hat{r},\Omega) = \frac{2R_0}{(1-e^2(\hat{r}\cdot\hat{n})^2)^{1/2}} \quad \text{and} \quad d_+(\hat{r},\Omega) = 2R_0(1 + \frac{e^2}{1-e^2}\,(\hat{r}\cdot\hat{n})^2)^{1/2}. \tag{3.27}$$

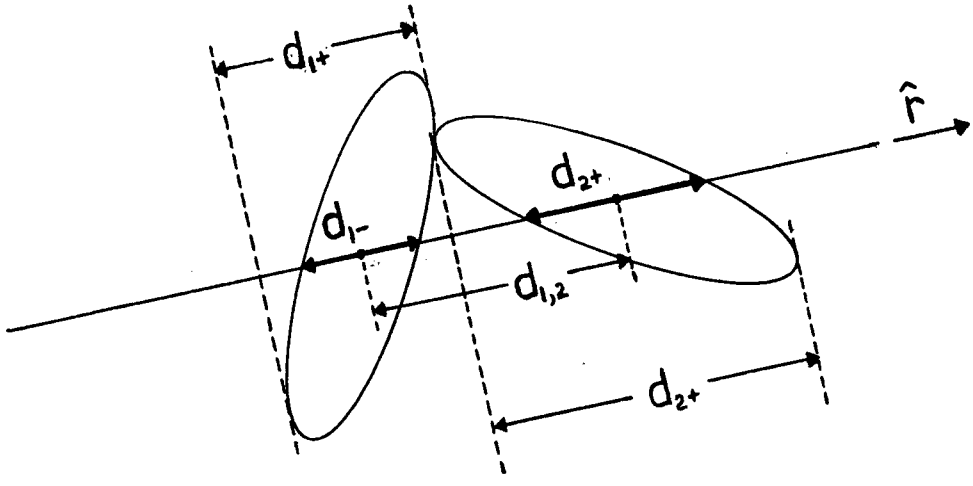

Fig. 12 The geometry of closest approach.

Since $\bar{d}_-(\hat{r}) \geq d_-(\overline{(\hat{r}\cdot\hat{n})^2})$ and $\bar{d}_+(\hat{r}) \leq d_+(\overline{(\hat{r}\cdot\hat{n})^2})$,

$$d_-(\overline{(\hat{r}\cdot\hat{n})^2}) \leq D(\hat{r}) \leq d_+(\overline{(\hat{r}\cdot\hat{n})^2}) \quad . \tag{3.28}$$

Eq. (3.28) can be expressed interms of the order parameter $S_{\alpha\beta}$ as follows:

$$(\hat{r}\cdot\hat{n})^2 = r_\alpha(n_\alpha n_\beta)r_\beta = \frac{2}{2}\, r_\alpha\left[\frac{1}{2}\,(3n_\alpha n_\beta - \delta_{\alpha\beta})\right]r_\beta + \frac{1}{3} \tag{3.29}$$

and

$$\overline{(\hat{r}\cdot\hat{n})^2} = \frac{2}{3}\, r_\alpha S_{\alpha\beta} r_\beta + \frac{1}{3} \tag{3.30}$$

Substitution of Eq. (3.30) into Eq. (3.27) finally yields

$$R_0\left(1 - \frac{e^2}{3}(1+2r_\alpha S_{\alpha\beta} r_\beta)\right)^{-1/2} \leq D(\hat{r}) \leq 2R_0\left(1 + \frac{e^2}{3(1-e^2)}(1+2r_\alpha S_{\alpha\beta} r_\beta)\right)^{1/2}$$

(3.31)

It is worth noting that there have been no specific assumptions made regarding the attractive part of the pair-interaction potential in obtaining Eq. (3.31), and that in a condensed phase, $D(\hat{r})$ may be thought of as the average repeat distance of molecules in the direction $\hat{r}$.

The bounds $d_{\pm}(r_\alpha S_{\alpha\beta} r_\beta)$ on $D(\hat{r})$, given in Eq. (3.31) are shown in Figure13 for $\hat{r}$ in the z and x (or y) directions as a function of the order parameter $S = S_z$, for the case when the length to width ratio of the hard core is 2:1, (i.e. $e^2 = \frac{3}{4}$), and the symmetry axis of the material is in the z-direction. As can be seen from Fig. 13, for this model of hard spheroids, an essential feature of the ordered phase is the anisotropy of the molecular distribution. In order to avoid the necessity of performing two sets of calculations, one for each bound, we assume

$$D(\hat{r}) = \frac{1}{2}(d_-(r_\alpha S_{\alpha\beta} r_\beta) + d_+(r_\alpha S_{\alpha\beta} r_\beta)). \tag{3.32}$$

This choice of $D(\hat{r})$ preserves the essential features of the molecular distribution; in fact, it is plausible that it is the exact effective hard core diameter for some elongated hard core potential. To simplify the notation somewhat, in analogy with tetragonal crystals we shall denote $D(\hat{r})$ by "c" if $\hat{r}$ is in the z-direction, and by "a" if $\hat{r}$ is in the x or y directions for the case when the symmetry axis of the material is in the z-direction. Eq. (3.31) suggests that a more general treatment might be to expand $D(\hat{r})$ in a power series in $r_\alpha S_{\alpha\beta} r_\beta$; in order to avoid introducing additional parameters, however, we continue with the spheroidal model.

The local field anisotropy tensor $\eta_{\alpha\beta}$ can now be evaluated; the eccentricity of $D(\hat{r})$ and hence of $f_s(\hat{r})$ is

$$e_g^2 = 1 - \frac{a^2}{c^2} \tag{3.33}$$

Fig. 13 Bounds on the effective hard-core diameter $\hat{D}(r)$.

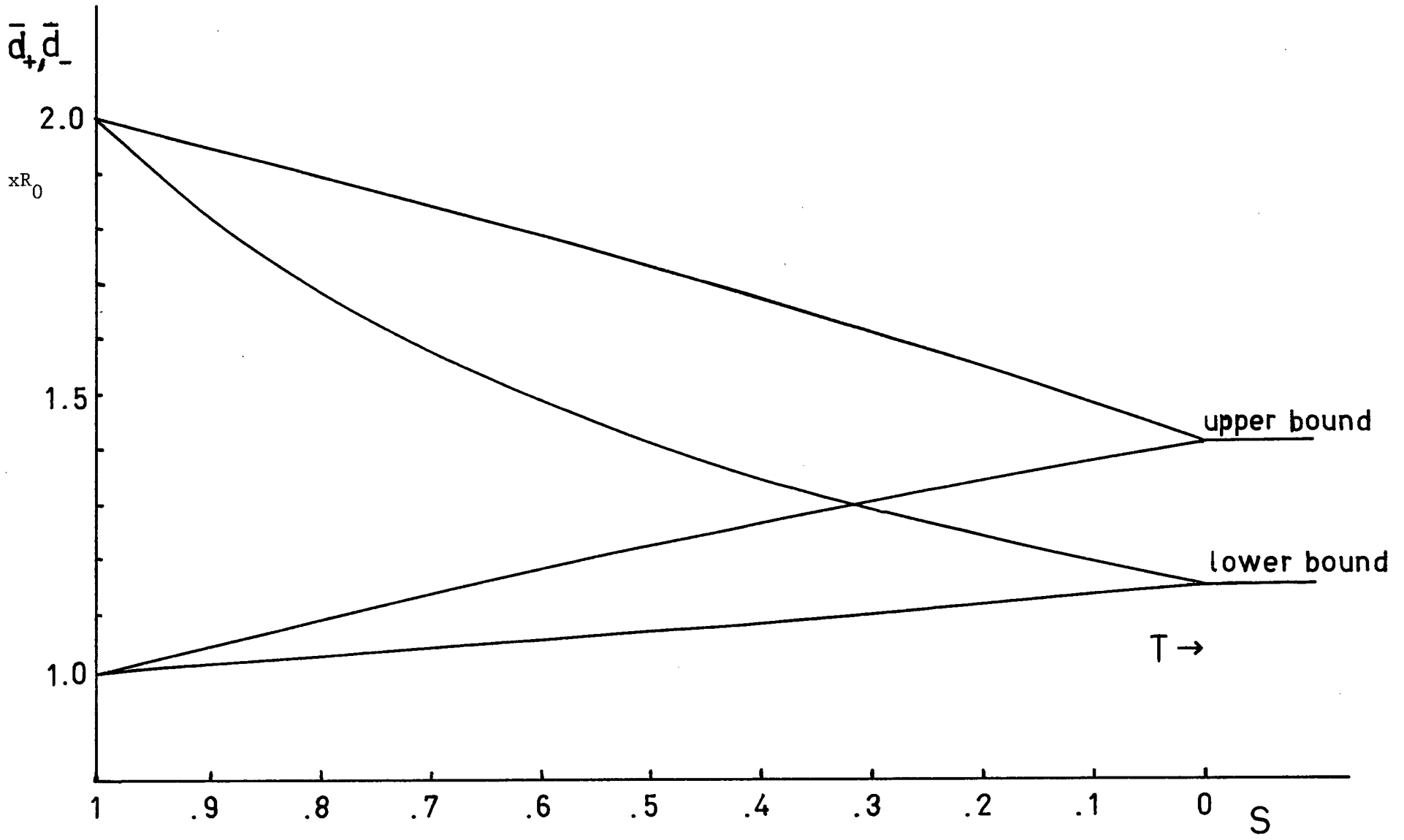
$\bar{d}_+, \bar{d}_-$
2.0
xR_0
1.5
1.0
upper bound
lower bound
T →
1
.9
.8
.7
.6
.5
.4
.3
.2
.1
0
S

where, from Eqs. (3.32) and (3.31)

$$c = R_0 \left[\left(1 - \frac{e^2}{3}(1+2S)\right)^{1/2} + \left(1 + \frac{e^2}{3(1-e^2)}(1+2S)\right)^{-1/2} \right] \qquad (3.34)$$

and

$$a = R_0 \left[\left(1 - \frac{e^2}{3}(1-S)\right)^{1/2} + \left(1 + \frac{e^2}{3(1-e^2)}(1-S)\right)^{-1/2} \right] \qquad (3.35)$$

The value of η_{zz} is shown in Figure 14 as a function of S for several values of the molecular eccentricity e. Values of η_{zz} obtained from refractive index measurements of PAA(26) are also shown; giving reasonable agreement with theory. The small deviation of the experimental values from the linear S-dependence predicted by the theory may in part be caused by a decrease in the molecular eccentricity e as a function of temperature due to molecular vibrations.

Once $f_s(\hat{r}) = (2R_0)^{-1} D(\hat{r})$ is known, the one particle pseudopotential $\bar{\varepsilon}_1(\Omega_1)$ can be evaluated from Eq. (3.11) as follows. By noting that, for a general hard-core repulsive potential U,

$$\int U(\vec{\gamma}_1, \vec{\gamma}_2) g^{(2)}(\vec{\gamma}_1, \vec{\gamma}_2) d\vec{\gamma}_2 = 0 \qquad (3.36)$$

where $g^{(2)}$ is given by Eq. (3.14), Eq. (3.11) yields

$$\bar{\varepsilon}_1(\Omega_1) = \frac{1}{2} \rho \int V_{1,j}(\vec{\gamma}_1, \vec{\gamma}_j) g^{(2)}(\vec{\gamma}_1, \vec{\gamma}_j) f(\Omega_j) d\vec{\gamma}_j . \qquad (3.37)$$

Fig. 14 The local field anisotropy tensor as a function of the order parameter.

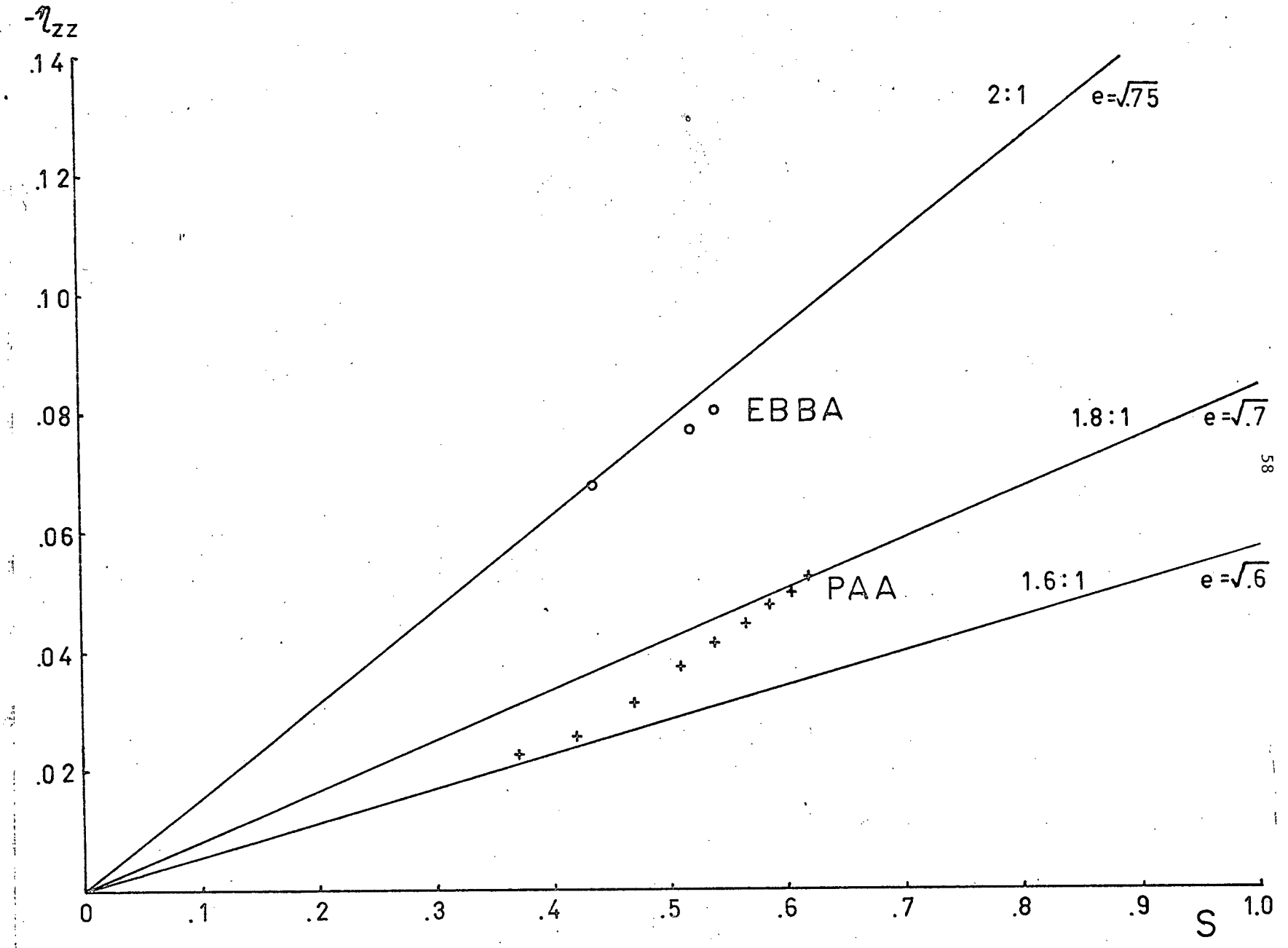
$-\eta_{zz}$
.14
.12
.10
.08
.06
.04
.02
0
.1
.2
.3
.4
.5
.6
.7
.8
.9
1.0
S
2:1
e=√.75
EBBA
1.8:1
e=√.7
PAA
1.6:1
e=√.6

Replacing $g^{(2)}(\vec{r}_1,\vec{r}_j)$ by $g(\vec{r})$, where $\vec{r} = \vec{r}_j - \vec{r}_1$

$$\bar{\varepsilon}_1(\Omega_1) = \frac{1}{2}\rho\int V_{1,j}(\Omega_1,\Omega_j,\vec{r})g(\vec{r})f(\Omega_j)d\Omega_j d\vec{r} \ . \tag{3.38}$$

Letting $d\vec{r} = r^2 dr d\Omega_r$ and $r = r' f_s(\hat{r})$,

$$\bar{\varepsilon}_1(\Omega) = \frac{1}{2}\rho\int V_{1,j}(\Omega_1,\Omega_j,r' f_s(\hat{r})\hat{r})g_0(r')f(\Omega_j)f_s^3(r)r'^2 dr' d\Omega_r d\Omega_j \ . \tag{3.39}$$

3.3 Dependence of Density on the Order Parameter

The equation of state can be obtained from the partition function, which, in the mean field approximation is given by

$$Q = \frac{\left[\int \exp(-\beta\bar{\varepsilon}(\Omega))\,d\vec{\gamma}\right]^N}{N!\,(4\pi)^N} \tag{3.39}$$

The free volume seen by one particle is $V_f = \int d\vec{r} = V - NV_m$, where V_m, the volume effectively occupied by one molecule is

$$V_m = \frac{1}{2^3 h}\int (1-g(\vec{r}))r^2 dr d\Omega. \tag{3.40}$$

where h is the packing fraction. Since, from Eq. (3.11) $\bar{\varepsilon}(\Omega)$ is proportional to the number density, we may write $\bar{\varepsilon}(\Omega) = -\rho z(\Omega)$. The pressure P is given by $P = -\left(\frac{\partial F}{\partial V}\right)_T$ and the free energy F is given by $F = -\frac{1}{\beta}\ln Q$. Then

$$P = \frac{1}{\beta}\left[\frac{\partial}{\partial V}\ln Q\right]_T = \frac{1}{\beta}\left[\frac{N}{V-NV_m} - \frac{N^2}{V^2}\beta\,\frac{\int z(\Omega)\exp(\beta\,\frac{N}{V}\,z(\Omega))\,d\Omega}{\int \exp(\beta\,\frac{N}{V}\,z(\Omega))\,d\Omega}\right] \tag{3.41}$$

and

$$\left(\frac{P}{\rho^2\bar{z}} + 1\right)(1 - \rho V_m) = \frac{kT}{\rho\bar{z}} \quad . \tag{3.42}$$

Far below the liquid-vapor transition ($kT << \rho\bar{z}$) in the condensed phase at low pressure ($P << \rho^2\bar{z}$) Eq. (3.42) yields

$$\rho = \frac{1}{V_m} - \frac{kT}{\bar{z}} + \ldots\ldots \tag{3.43}$$

We suppose most of the volume dependence at $T \approx T_c$ to reside in V_m; although it is clear from Eq. (3.41) that $\bar{z}$ may change considerably across the transition. As a first order approximation we let $\rho^{-1} = V_m$, then making the transformation $r = r'f(\hat{r})$, Eq. (3.40) yields

$$\rho^{-1} = \frac{1}{2^3 h}\int_0^\infty (1-g_0(r'))r'^2 dr' \int f^3(\hat{r})d\Omega_r \tag{3.44}$$

Since $f_s(\hat{r}) = D(\hat{r})/2R_0$

$$\rho^{-1} = \frac{1}{24h}\int D^3(\hat{r})d\Omega_r \quad . \tag{3.45}$$

If $D(\hat{r})$ is a spheroid with eccentricity $e_g^2 = 1 - \frac{a^2}{c^2}$, then $D(\hat{r}) = a(1-e_g^2\cos^2\theta_r)^{-\frac{1}{2}}$ and

$$\rho^{-1} = \frac{\pi a^3}{12h}\int \frac{\sin\theta_r d\theta_r}{(1-e_g^2\cos^2\theta_r)^{3/2}} = \frac{\pi a^2 c}{6h} \tag{3.46}$$

where a and c are given by Eqs. (3.34) and (3.35). In order to further simplify calculations, we replace a and c in Eq. (3.46) by a linear approximation,

$$a \cong A - \delta S \tag{3.47}$$

and

$$c \cong A + 2\delta S \tag{3.48}$$

where $A = \frac{2R_0}{3}(\kappa+2)$ and $\delta = \frac{2R_0}{3}(\kappa-1)$ and κ is the molecular length to width ratio $\kappa = \frac{1}{\sqrt{1-e^2}}$. This is equivalent to letting

$$D(\hat{r}) = 2R_0\left[1 + \frac{(\kappa-1)}{3}(1 + 2r_\alpha S_{\alpha\beta} r_\beta)\right]. \tag{3.49}$$

The exact values of a and c and the linear approximations are shown in Figure 15. The volume V(S) is given by

$$V(S) = \frac{4\pi R_0^3}{81h} N \left[(\kappa+2) - (\kappa-1)S\right]^2 \left[(\kappa+2) + 2(\kappa-1)S\right] \tag{3.50}$$

or

$$\frac{V(S)}{V(0)} = 1 - 3\left(\frac{\kappa-1}{\kappa+2}\right)^2 S^2 + 2\left(\frac{\kappa-1}{\kappa+2}\right)^3 S^3 \tag{3.51}$$

The thermal expansivity is obtained from Eq. (3.51), and

$$\frac{1}{V}\frac{\partial V}{\partial T} \cong -6\left(\frac{\kappa-1}{\kappa+2}\right)^2 S \frac{dS}{dT} \quad . \tag{3.52}$$

Fig. 15 Approximations to the effective hard-core diameter.

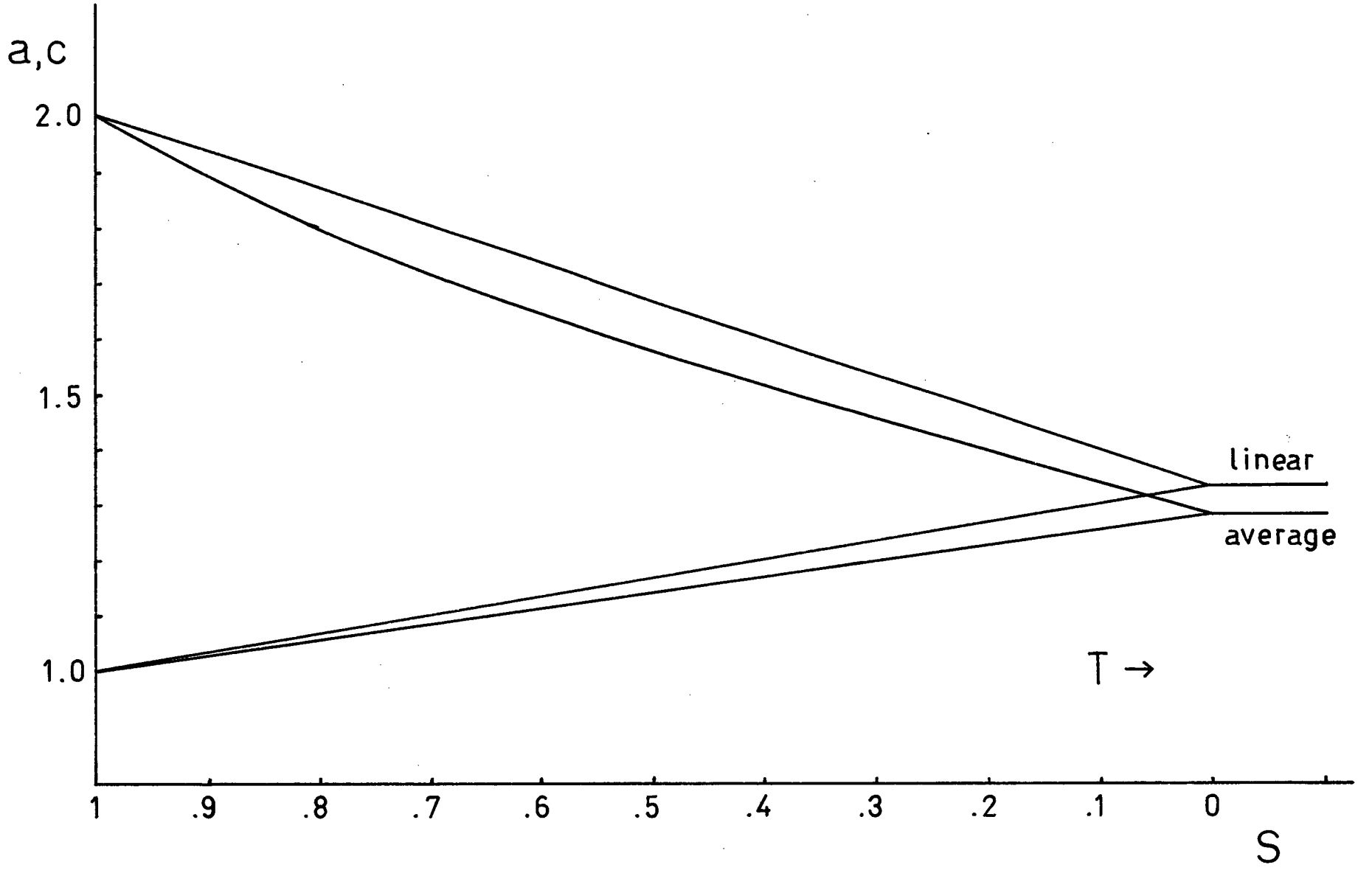
a,c
2.0
1.5
1.0
linear
average
T →
1
.9
.8
.7
.6
.5
.4
.3
.2
.1
0
S

From Eq. (2.25), near the transition $S = \frac{3}{4} S_c + k_2' \sqrt{T_c^+ - T}$, and

$$\frac{1}{V}\frac{\partial V}{\partial T} = 3\left(\frac{\kappa-1}{\kappa+2}\right)^2 k_2'^2 \left[1 + \frac{3S_c}{4k_2'} (T_c^+ - T)^{-\frac{1}{2}}\right]. \tag{3.53}$$

Arrott and Press (10) have shown that experimentally obtained values of the expansion coefficients of MBBA obey such a relation. Their experimental values were fitted to

$$\frac{1}{V}\frac{\partial V}{\partial T} = \beta_0 + Z(T_c^+ - T)^{-G} \tag{3.54}$$

with the result that $G = 0.56 \pm .1$ and $Z = 0.435 \times 10^{-3}/°C^{1/2}$. We can estimate Z from Eq. (3.42) where we take $\kappa = 1.6$ as suggested by local field results, and $\kappa_2' = 0.08$, then

$$Z \cong \frac{9}{h}\left(\frac{\kappa-1}{\kappa+2}\right)^2 k_2' S_c = 1.512 \times 10^{-3}/°C^{1/2} .$$

The value of k_2' was obtained from published values of Landau expansion coefficients for MBBA (11). In view of the approximations made in obtaining Eq. (3.53), the agreement is considered satisfactory.

The discontinuous volume change across the nematic-isotopic transition is given approximately by

$$\frac{V(0)-V(S_c)}{V(0)} \cong 3\left(\frac{\kappa-1}{\kappa+2}\right)^2 S_c^2 \tag{3.55}$$

For $\kappa = 1.6$ and $S_c \cong 0.3$, Eq. (3.55) yields a volume change of 0.75%. If a and c given by Eqs. (3.34) and (3.35) are used instead of the linear approximation, then the volume change is further reduced to 0.25%. Experimental results (10) for MBBA suggest 0.13% as a minimum estimate, the existence of a two-phase region in the neighborhood of the transition makes accurate determination of the discontinuous volume change difficult.

3.4 Dipole-Dipole Interaction

The interaction energy between two point dipoles $\mu\hat{n}_i$ and $\mu\hat{n}_j$ separated by $\bar{r} = r\hat{r}$ is

$$V_{ij} = -\frac{\mu^2}{r^3}\left[3(\hat{n}_i\cdot\hat{r})(\hat{n}_j\cdot\hat{r}) - \hat{n}_i\cdot\hat{n}_j\right] , \tag{3.56}$$

substitution into Eq. (3.38) yields, for a spherical sample of radius R

$$\bar{\varepsilon}_1(\Omega_1) = -\frac{1}{2}\rho\mu^2 n_{1\alpha}\int \frac{(3r_\alpha r_\beta - \delta_{\alpha\beta})n_{j\beta}}{r^3}\, g(\bar{r})f(\Omega_j)d\Omega_j d\bar{r} . \tag{3.57}$$

Performing the transformation $r = r'f_s(\hat{r})$ yields

$$\bar{\varepsilon}_1(\Omega_1) = -2\pi\rho\mu^2 n_{1\alpha}\int n_{j\beta}f(\Omega_j)d\Omega_j \cdot \frac{1}{4\pi}\iint_0^{R/f_s(\hat{r})} \frac{g_0(r')dr'}{r'} \times$$

$$\times \ (3r_\alpha r_\beta - \delta_{\alpha\beta})d\Omega_r \tag{3.58}$$

where the first integral is just the dipolar (vector) order parameter n_α of Eq. (2.9), and the second integral is the local field anisotropy tensor $\eta_{\alpha\beta}$ of Eqs. (1.14) and (1.16). Then

$$\bar{\varepsilon}_1(\Omega_1) = -2\pi\rho\mu^2 n_{1\alpha}n_\beta\eta_{\alpha\beta} . \tag{3.59}$$

If the symmetry axis of the fluid is in the z-direction, then Eq. (3.59) becomes, on dropping the subscript 1,

$$\bar{\varepsilon}(\Omega) = -2\pi\rho\mu^2\cos\theta R\eta_{zz} \tag{3.60}$$

and the quantity $2\pi\rho\mu R\eta_{zz} = H_E$ may be thought of as the effective molecular field. The orientational probability density function $f(\Omega)$ is obtained by substituting Eq. (3.60) into Eq. (3.8), and from Eq. (3.9), the self-consistent equation for R is

$$R = \frac{\int_0^{\pi} \cos\theta \exp(\beta\mu H_E \cos\theta)\sin\theta d\theta}{\int_0^{\pi} \exp(\beta\mu H_E \cos\theta)\sin\theta d\theta} \tag{3.61}$$

The quadrupolar order parameter S is similarly given by

$$S = \frac{\int_0^{\pi} \frac{1}{2}(3\cos^2\theta - 1)\exp(\beta\mu H_E \cos\theta)\sin\theta d\theta}{\int_0^{\pi} \exp(\beta\mu H_E \cos\theta)\sin\theta d\theta} \tag{3.62}$$

The integrals are evaluated in Appendix E with the results that

$$R = L(\beta\mu H_E) \tag{3.63}$$

and

$$S = 1 - \frac{3}{\beta\mu H_E} L(\beta\mu H_E) \tag{3.64}$$

where L is Langevin's function, $L(x) = \coth(x) - \frac{1}{x}$. The sensitivity of the solution to the anisotropy of the molecular distribution is apparent. If, as is frequently assumed, the distribution is isotropic, then $\eta_{zz} = H_E = 0$, and $R = S = 0$. If, as assumed by Born (12) and later by Chandrasekhar (13) the distribution is anisotropic but independent of the temperature, then $H_E = \mu c_1 R$ where c_1 is a constant and the solution for R is identical to the magnetization in the Weiss theory of ferromagnetism. $L(x)$ may be expanded about $x = 0$, and letting

$$T_c = \frac{\mu^2 c_1}{3k}$$

$$R = \frac{T_c}{T} R - \frac{3}{5}\left(\frac{T_c}{T}\right)^3 R^3 + \ldots \tag{3.65}$$

and, for small R,

$$R = \left(\frac{T}{T_c}\right)\left[\frac{5}{3}\left(1 - \frac{T}{T_c}\right)\right]^{1/2} \tag{3.66}$$

while

$$S = 1 - \frac{3RkT}{\mu^2 c_1 R} = 1 - \frac{T}{T_c} \quad . \tag{3.67}$$

We have shown, however, that the anisotropy of the distribution is temperature dependent; as can be seen from Figure 14, $\eta_{zz} \cong c_2 S$ where c_2 is a constant if changes in the density are neglected. Since, for prolate molecules $c_2 \leq 0$, $R = S = 0$; from Eq. (3.41) it is clear that

for a given R antiparallel alignment is energetically favorable. Oblate molecules may be considered by replacing the hard-core (prolate) eccentricity $+e^2$ by $\frac{-e_0^2}{1-e_0^2}$ where e_0^2 is the eccentricity of an oblate spheroid. Then $\eta_{zz} \geq 0$ hence $c_2 \geq 0$, and letting $H_E = \mu_2 c_2 RS$ and $T_c = \frac{\mu^2 c_2}{12k}$ yields, from Eq. (3.64)

$$S = \frac{1}{2} \pm \frac{1}{2} \sqrt{1 - \frac{T}{T_c}} \tag{3.68}$$

where only + gives a physically meaningful solution, and

$$R = L\left[12\frac{T_c}{T} RS\right] \cong S^{1/2} \tag{3.69}$$

where the result $R^2 \cong S$ has been obtained by numerical means.

3.5 London-van der Waals Interaction

If molecule i has a dipole moment $\mu_s \hat{n}_i$ caused by a spontaneous charge fluctuation, the resulting electric field of a point $\vec{r} = r\hat{r}$ is given by

$$\vec{E} = \frac{\mu_3}{r^3}\left[3(\hat{n}_i\cdot\hat{r})\hat{r}-\hat{n}_i\right]. \tag{3.70}$$

If molecule j at $\bar{r}$ has a polarizability $\alpha_{\parallel}$ along its symmetry axis and $\alpha_{\perp}$ perpendicular to it, and if $\alpha_{\parallel} >> \alpha_{\perp}$, then the induced dipole is $(\vec{E}\cdot\hat{n}_j)\alpha_{\parallel}\hat{n}_j$. The interaction energy of the two dipoles is

$$V_{i,j} = -\alpha_{\parallel}(\vec{E}\cdot\hat{n}_j)^2 = -\frac{\alpha_{\parallel}\mu_s^2}{r^6}\,(3(\hat{n}_i\cdot\hat{r})(\hat{n}_j\cdot\hat{r}) - \hat{n}_i\cdot\hat{n}_j)^2 \ . \tag{3.71}$$

The same form of $V_{i.j}$ is obtained from quantum mechanical calculation of the dipole-dipole contribution to the dispersion energy (14). Substitution into Eq. (3.38) yields for the one-body pseudopotential

$$\bar{\varepsilon}_1(\Omega) = -\frac{1}{2}\,\rho\mu_s^2\alpha_{\parallel}n_{1\alpha}n_{1\gamma}\int n_{j\beta}n_{j\delta}\,\frac{(3r_\alpha r_\beta-\delta_{\alpha\beta})(3r_\gamma r_\delta-\delta_{\gamma\delta})}{r^6} \tag{3.72}$$

$$\cdot\, g(\vec{r})f(\Omega_j)d\Omega_j d\bar{r}$$

Performing the transformation $r = r'f_s(\hat{r})$ yields

$$\bar{\varepsilon}_1(\Omega) = -\frac{1}{2}\rho\mu_3^2\alpha_{\shortparallel}n_{1\alpha}n_{1\gamma}\int n_{j\beta}n_{j\delta}f(\Omega_j)d\Omega_j$$

$$\cdot\int\int_0^{R/f_s(\hat{r})}\frac{g_0(r')dr'}{r'^4}\;\frac{(3r_\alpha r_\beta-\delta_{\alpha\beta})(3r_\gamma r_\delta-\delta_{\gamma\delta})}{f_s^3(\hat{r})}\,d\Omega_r \qquad (3.73)$$

The first integral can be expressed in terms of $S_{\alpha\beta}$, and integration over r' yields, for large R,

$$\bar{\varepsilon}_1(\Omega) = -\frac{\rho\mu_s^2\alpha_{\shortparallel}n_{1\alpha}n_{1\gamma}}{48R_0^3}\left[\frac{1}{3}(2S_{\beta\delta}+\delta_{\beta\delta})\right]$$

$$\cdot\int\frac{(9r_\alpha r_\beta r_\gamma r_\delta-3r_\alpha r_\beta\delta_{\gamma\delta}-3r_\gamma r_\delta\delta_{\alpha\beta}+\delta_{\alpha\beta}\delta_{\gamma\delta})d\Omega r}{f_s^3(\hat{r})} \qquad (3.74)$$

If there exists rotational symmetry about the z-axis, then, as shown in Appendix F, Eq. (3.58) becomes

$$\bar{\varepsilon}_1(\Omega_1) = -\frac{\pi\rho\mu_{\shortparallel}^2}{24R_0^3}\int\left[\frac{2}{3}+\frac{2}{3}\left(\frac{3\cos^2\theta_r-1}{2}\right)\left(S+\frac{(3\cos^2\theta_1-1)}{2}\right)\right. \qquad (3.75)$$

$$\left.+\,S\,\frac{(3\cos^2\theta_1-1)}{2}\,(9\cos^4\theta_r-8\cos^2\theta_r+1)\right]\frac{\sin\theta_r d\theta_r}{f_s^3(\hat{r})}\,.$$

If a spherically symmetric molecular distribution is supposed, then $f_S(\hat{r}) = 1$ and the usual Maier-Saupe pseudopotential is obtained; dropping the subscript 1,

$$\bar{\varepsilon}(\Omega) = S(3\cos^2\theta-1) \text{ x constant} . \tag{3.76}$$

If the molecular distribution is anisotropic, then, as before

$$f(\hat{r}) = \frac{D(\hat{r})}{2R_0} = \frac{a}{2R_0}(1-e_g^2\cos^2\theta_r)^{-1/2} \quad \text{when} \quad e_g^2 = 1 - \frac{a^2}{c^2} .$$

Furthermore, the density ρ is given by $\rho = \frac{6h}{\pi a^2 c}$, and Eq. (3.75) becomes, on omitting the terms not containing θ_1 from the integrand

$$\bar{\varepsilon}(\Omega) = -\frac{2\mu_S^2\alpha_u h}{a^5 c}\frac{(3\cos^2\theta-1)}{2}\int_0^{\pi}(1-e_g^2\cos^2\theta_r)^{3/2}\left[\frac{2}{3}\frac{(3\cos^2\theta_r-1)}{2}\right.$$

$$\left. + S(9\cos^4\theta_r-8\cos^2\theta_r+1)\right]\sin\theta d\theta . \tag{3.77}$$

The dependence of $\bar{\varepsilon}(\Omega)$ on S may be condensed into a function $\phi(S)$, then

$$\bar{\varepsilon}(\Omega) = -\frac{1}{2}(3\cos^2\theta-1)\phi(S) \tag{3.78}$$

and S is obtained self-consistently from Eq. (3.9)

$$S = \frac{\int_0^{\pi}\frac{1}{2}(3\cos^2\theta-1)\exp\left[\frac{\beta}{2}\phi(S)(3\cos^2\theta-1)\right]\sin\theta d\theta}{\int_0^{\pi}\exp\left[\frac{\beta}{2}\phi(S)(3\cos^2\theta-1)\right]\sin\theta d\theta} . \tag{3.79}$$

Eq.(3.79) cannot be solved analytically; the temperature dependence of S has been obtained using numerical methods. The method is described in Appendix G, and the results are shown in Figure 16. The effect of the elongated hard core is to make the transition more abrupt; the behavior of the system varies continuously from the Maier-Saupe solution (15) to Onsager's result for hard rods (23) as the length to width ratio of the repulsive potential is increased. Since this behavior is not in agreement with experimental results, a more realistic interaction potential should be considered; a model in which the molecular polarizability perpendicular to the symmetry axis is not neglected may predict more physical behavior.

Fig. 16 The effect of the anisotropic hard-core on the order parameter in the mean field approximation.

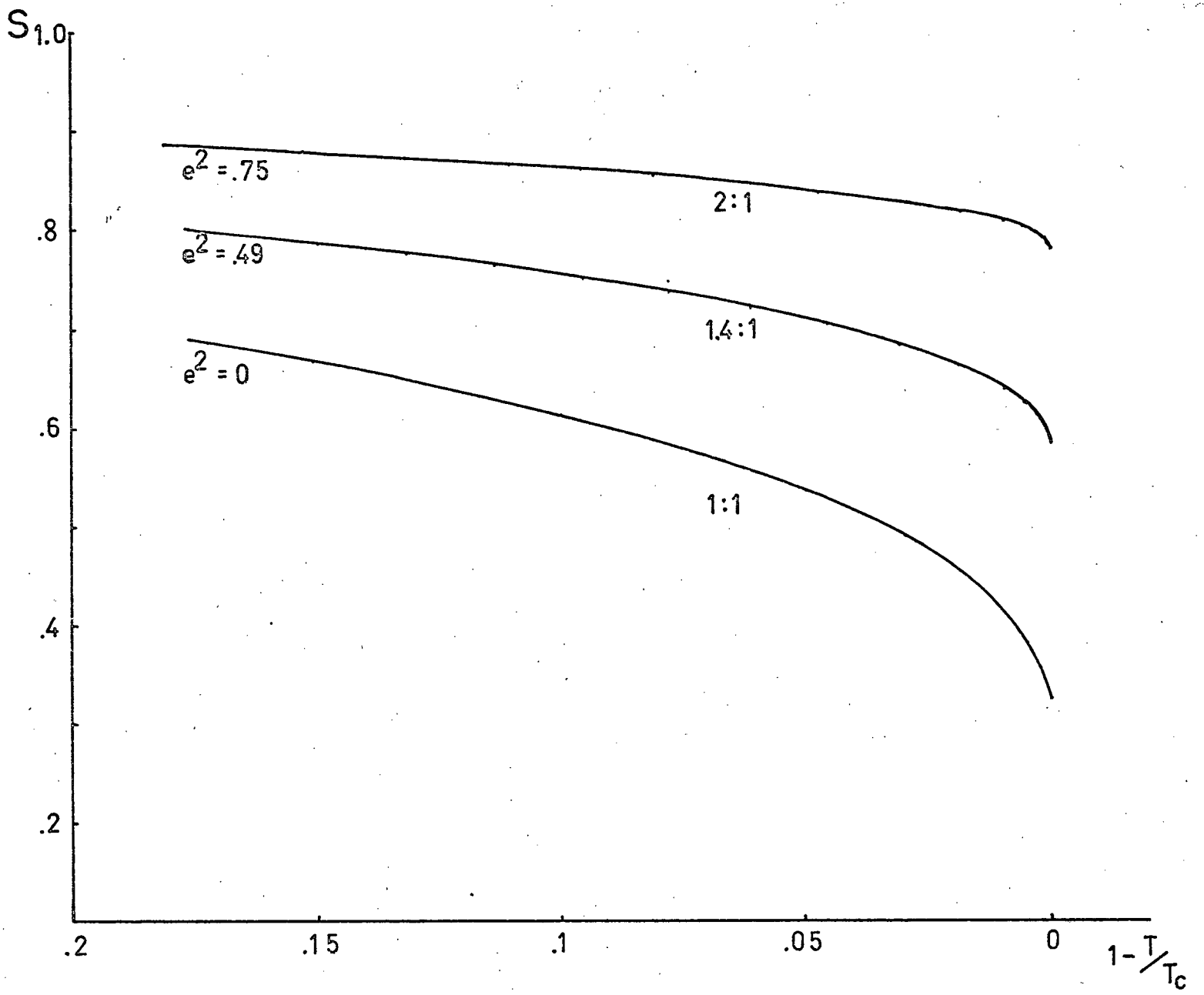
S 1.0
.8
.6
.4
.2
e^2 = .75
2:1
e^2 = .49
1.4:1
e^2 = 0
1:1
.2
.15
.1
.05
0
1 - T/Tc

CHAPTER 4

PURE FLUIDS - EXPERIMENTAL

4.1 The Lorentz-Lorenz Relation

In an isotropic fluid, the pair-correlation function $g(\vec{r})$ is spherically symmetric; the local field anisotropy tensor $\eta_{\alpha\beta}$ therefore vanishes and Eq. (1.29) reduces to the well-known Lorentz-Lorenz relation

$$\frac{n^2-1}{n^2+2} = L\rho_M \, . \tag{4.1}$$

The Lorentz-Lorenz coefficient L is given by

$$L = \frac{4\pi_\alpha M}{3Av} \tag{4.2}$$

where α is the effective molecular polarizability, M is the gram molecular weight and Av is Avogadro's number and ρ_M is the mass density. It is of interest to investigate the validity of Eq. (4.1) across the liquid-vapor transition, since optical techniques are commonly used (16,17) to measure the order parameter $\frac{\rho_c-\rho_v}{\rho_c}$ near the critical point. The Lorentz-Lorenz coefficients for sulfur hexafluoride and germane have been measured together with their critical constants. Refractive indices and density are both measured in the same experiment, yielding values of L accurate to 0.05 per cent for densities near critical. The method utilizes a prism-

shaped high-pressure cell which can be removed from a temperature controlled holder and weighed on a precision balance. The cell is equipped with a needle valve which allows the high pressure gas to be bled out in steps, refractive indices are thus measured as a function of weight and hence density.

4.2 Details of the Experiment

Optical equipment used in this experiment is schematically illustrated in Figure (17). A laser beam, rendered uniphase and collimated by a beam expanding telescope and pinhole filter, traverses a prism-shaped sample vessel and is reflected by a mirror into a telescope. The prism is oriented with its axis vertical; the beam is refracted horizontally through an angle which depends on the index of refraction of the fluid in the prism-vessel. The beam is reflected into an autocollimating telescope (Davison model D275) by a differential-micrometer driven mirror (Lansing Research Corp. Model 10.253).

The high pressure sample vessel is shown in Figure 18. The body is made of aluminum with a brass needle valve at one end. Two sapphire windows, clamped in place by flanges, form a prism-shaped region at the end of the vessel. The space between the windows is kept to a minimum in order to keep the light path length small. The long cylindrical portion of the vessel provides a reasonably large volume of fluid. Experimental error decreases with increasing volume of the vessel, but the precision balance available for this experiment had a limit of 200 gm. Therefore, the sample vessel was designed to obtain a large volume of fluid but under the restriction that the mass of the vessel and contents not exceed the limit of the balance. The prism angle between the sapphire windows was measured to be 20.088°.

The relationship between the refractive index, n, of the fluid and the angle of deviation, θ, through the prism vessel for a ray incident normally to the front face of the prism is derived in Appendix H and is

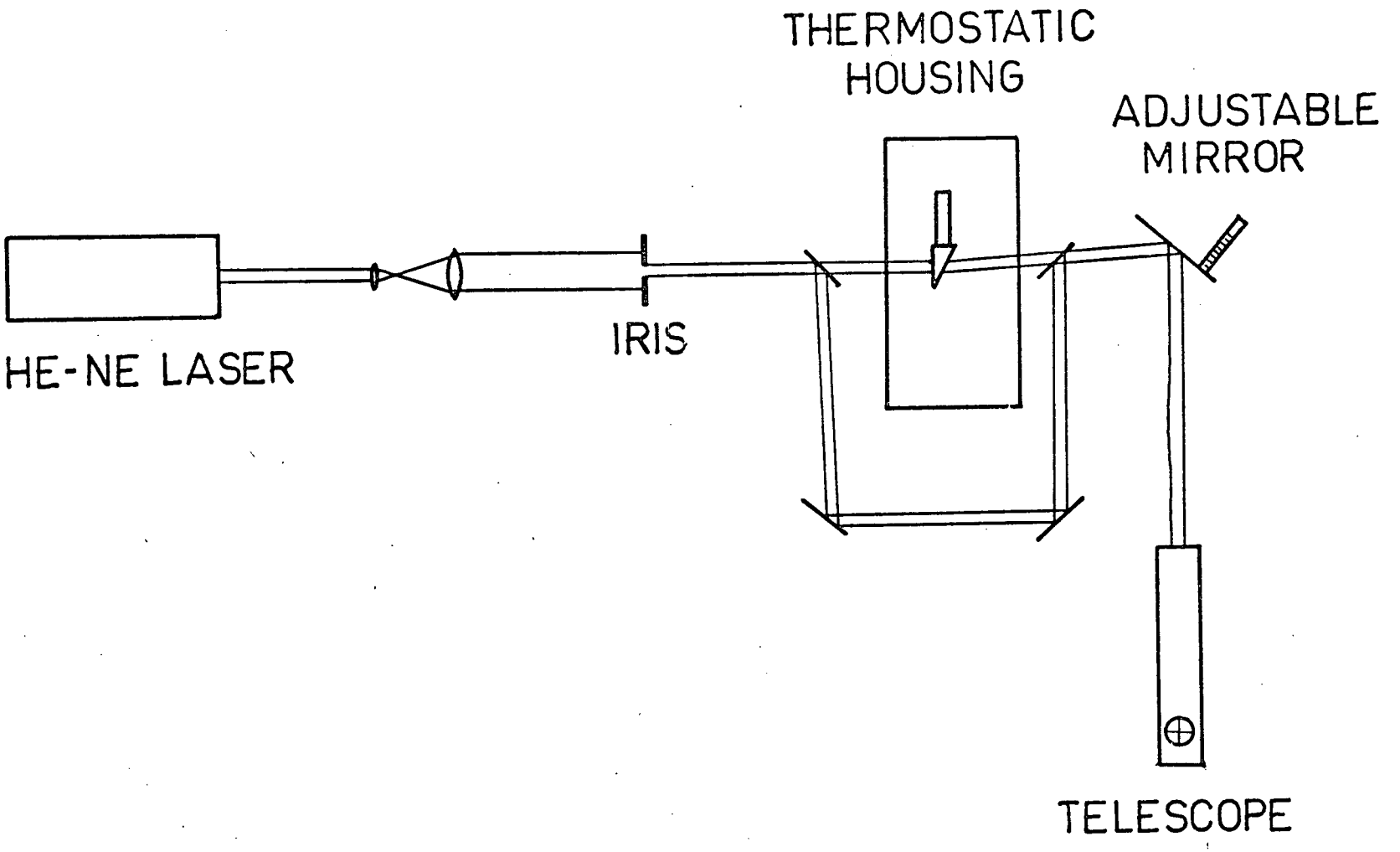

Fig. 17 Schematic illustration of optical equipment.

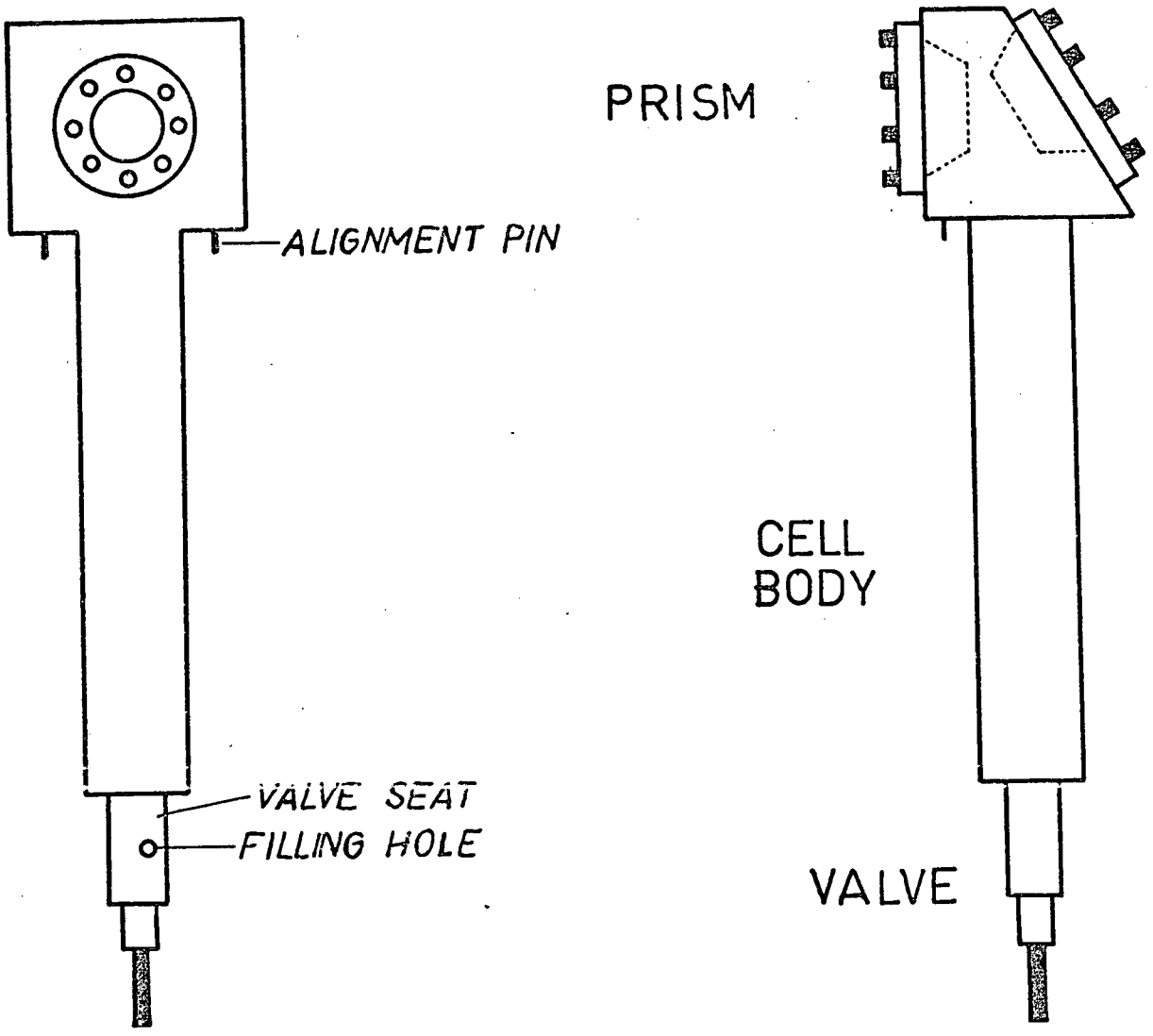

Fig. 18 Drawing of sample cell.

$$n = n_a + (\sin\theta - \sin\theta_a)[B + C(\sin\theta + \sin\theta_a)]$$

where n_a is the refractive index of air, θ_a is the angle of deviation for air in the sample cell, and B and C depend on the cell geometry.

The angle of deviation through the prism is measured by adjustment of the micrometer screw on the mirror mount. The mirror is adjusted until the beam is centered on the cross hairs of the autocollimator, the reading of the micrometer is then recorded. The procedure is repeated ten times and the readings are averaged. Five readings are taken with the micrometer screw turned clockwise and five C.C.W. This is done in order to eliminate backlash in the screw and in order to eliminate the effect that would occur if the amount of backlash were not a constant amount, but depended on the particular orientation of the screw. A reference angle is obtained when the cell is removed for weighing. This reference angle is measured on the micrometer screw each time the cell is removed in order to avoid any problems due to alterations in the alignment of the optical system during the course of the experiment. The zero angle used for calculation of the deviation angle is obtained with the cell containing air at N.T.P.

The relationship between the angle of deviation and the readings of the micrometer screw is established by calibrating using a 50 line per inch Ronchi ruling in place of the sample vessel. The micrometer readings for sixty-five orders were measured, and a relationship between $\sin\theta$ and micrometer screw reading was established. The relationship is linear except for a small correction which is nearly

negligible except for larger angles. (It should be noted that the maximum angle of deviation encountered in the experiment is only 3 degrees.)

The measurement of the refractive index described above yields two values, n_l and n_v, when both liquid and vapour are present in the cell. The density and temperature of interest is in the single phase region at the coexistence curve boundary. The sample vessel was initially filled to an average density ρ' such that it was nearly all liquid at room temperature with only a small amount of vapour present. The sample vessel was then placed in the thermostatic housing at temperature T_1. If T_1 is below T'_1 both liquid and vapour are present, and $n_l(T_1)$ and $n_v(T_1)$ can both be measured (see Fig. 19). The temperature was then increased to T_2 resulting in an increase in the fraction of liquid present. The values of $n_l(T_2)$ and $n_v(T_2)$ were then measured. The temperature was then increased to T_3 and measurements of n repeated. As the temperature approaches T', the meniscus rises in the vessel and it becomes impossible to measure n_v. For temperatures above T', measurements of n result in obtaining $n(\rho',T)$. $n(\rho',T)$ is almost independent of T for $T > T'$ and it is easy to extrapolate to obtain $n(\rho',T')$ which is the value sought in this work. Following the carrying out of the above procedure for obtaining $n(\rho',T')$ the sample vessel was removed from the thermostatic housing and weighed. The density was obtained using the known volume and the mass of the vessel when evacuated.

Fig. 19 Coexistence curve on a temperature-density plot illustrating procedure for obtaining data.

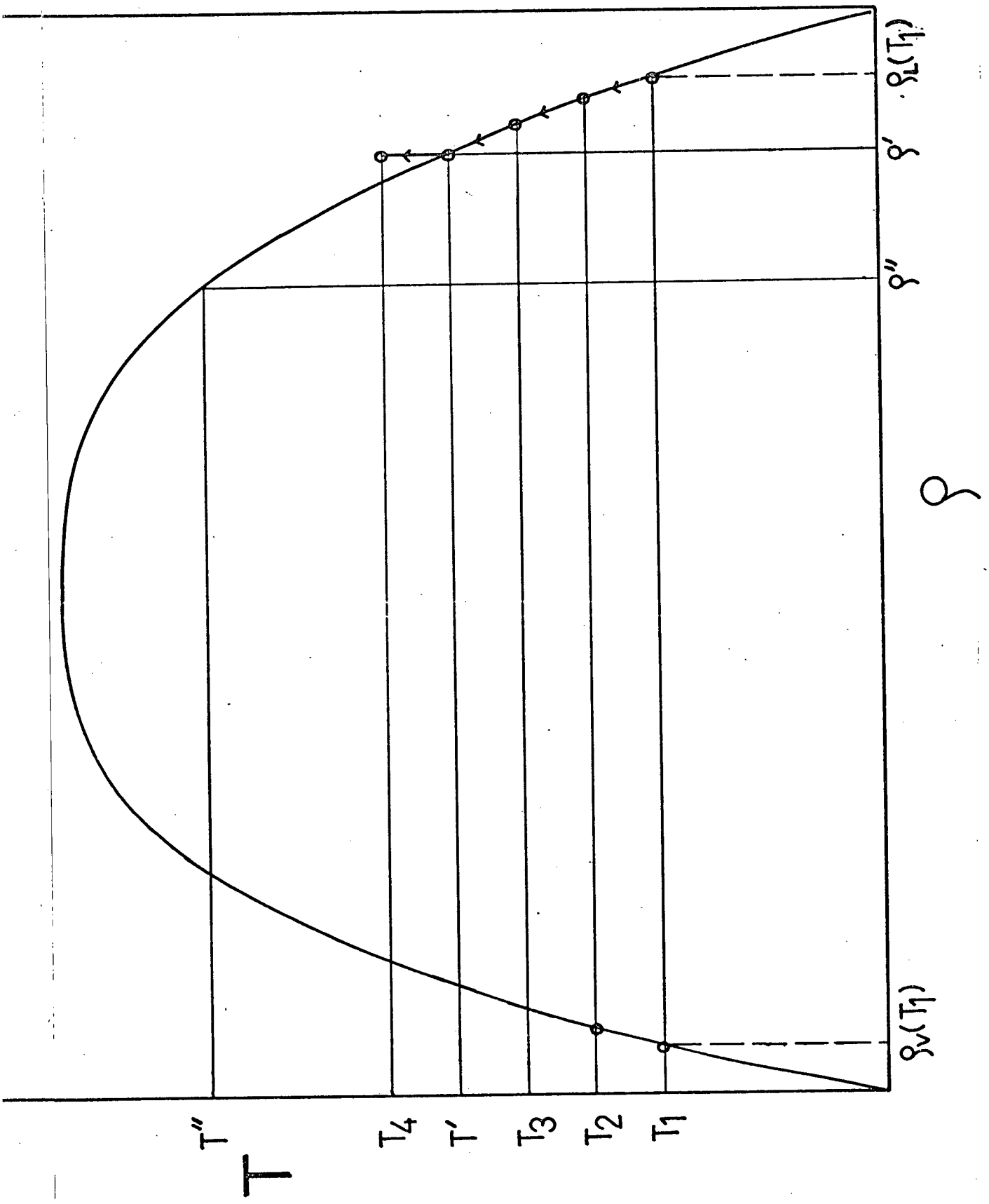
T
T''
T4
T'
T3
T2
T1
ρv(T1)
ρ''
ρ'
ρL(T1)
ρ

The density was then decreased by bleeding out a small amount of fluid with the needle valve. The procedure was then repeated to obtain a value corresponding to $n(\rho'',T'')$, etc.

As the critical point is approached at the top of the coexistence curve, the large compressibility of the fluid results in large density gradients. Therefore, it is difficult to obtain n at the coexistence curve boundary near the critical point. The values used for calculating the Lorentz-Lorenz coefficient, L, are those obtained at temperatures shown in the shaded area in Figure 20.

The measurements on the vapour side of the coexistence curve are made in a similar way except the meniscus level decreases with increasing temperature and only vapour is present for temperatures above the coexistence curve. The values used in obtaining L are obtained in the shaded region. The measurements were continued for densities for which the coexistence curve is well below room temperature and L for these points correspond to $n(\rho,T_{room})$.

The mass of the evacuated vessel was obtained by weighing it after evacuating it. The volume of the vessel was obtained by filling it with distilled water and weighing it. Small corrections were made for the change in volume of the cell with temperature. Small corrections were also made for the change in volume of the cell with pressure although the accuracy of this correction is less reliable because of the difficulty of estimating the change in volume with pressure for the oddly shaped vessel.

Fig. 20 Temperature and density region of which data points are obtained. The existence of large density gradients creates difficulties in obtaining data at the coexistence curve near the critical point.

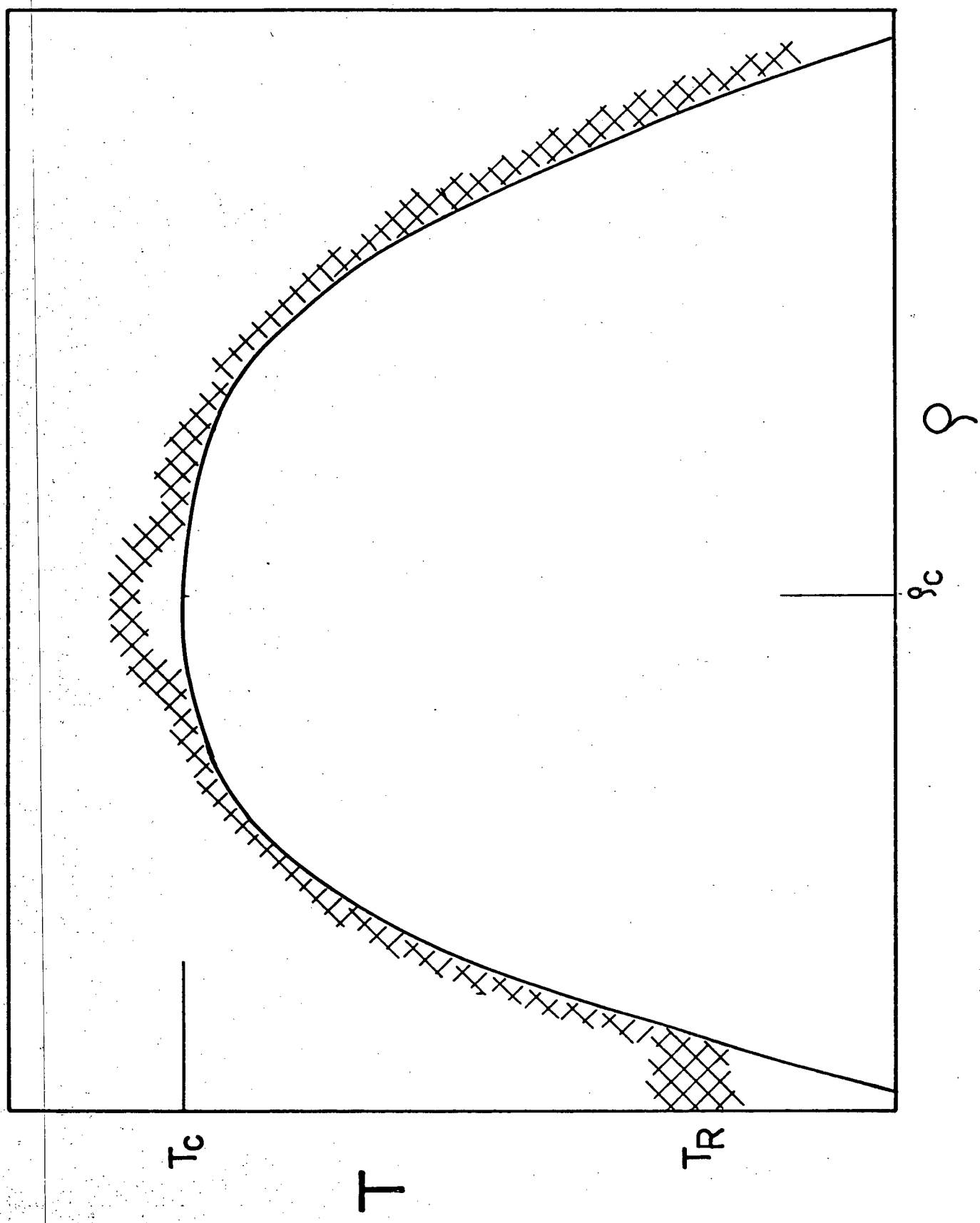
ρ
ρc
T
Tc
TR

4.3 Temperature Control

The temperature control systems used both in the pure fluid and the nematic liquid crystal experiments consist of two basic parts; an outer housing, whose temperature is controlled by a fluid circulating through it, and an inner cell-holder, carrying heating coils, embedded in a thermally insulating foam. The circulating fluid in this experiment was water pumped by a Forma Scientific Model 2095 whose temperature was constant to within ±0.05°C. In some of the liquid crystal experiments at higher temperatures, a Haake Model E12 circulator of similar thermostatic accuracy was used with Shell Vitrea Oil 21. Temperature sensing was done with high-resistance Fenwal thermistors, whose resistance was greater than 2000 Ω near the operating temperature. The thermistors were epoxied into 1/4" copper bolts, which in turn were screwed into tapped holes in the cell-holder. Thermistor resistance was measured by means of specially constructed Wheatstone bridges utilizing matched resistors and individually calibrated to each thermistor. The output of each Wheatstone bridge was measured by a Hewlett-Packard Model 419A DC null voltmeter. Temperature control was effected by feeding the proportional output of the d.c. null meter into a low output impedance operational amplifier, Kepco Operational Power Supply 7-2B, whose gain was adjustable. The operational amplifier then supplied current to the non-inductive windings on the cell holder. The Wheatstone bridges used in temperature control had, in addition to the usual balancing decade box, a 25-turn motor-driven heli-pot, which could be used to sweep temperature continuously. The circuit diagram for the

temperature control system is shown in Figure (21). The thermistors, their associated bridges and decade boxes, were calibrated using a Hewlett-Packard Model DY-2801A quartz thermometer. Deviations from the theoretically predicted resistance $R = R_0 e^{\beta/T}$ where R_0 and β are characteristic constants of each thermistor were fitted by polynomials in T, thus reducing the uncertainty in the measured temperature to ±0.0001°C. The decade boxes used in temperature monitoring were General Radio Type 1433, with a specified temperature coefficient of resistance less than ±20 ppm/°C; in addition, every attempt was made to regulate room temperature during the course of the experiment. The temperature control was accurate to ±0.0005°C over an eight hour period. In some of the liquid crystal experiments, the quartz thermometer was used in addition to thermistor resistance measurements; the thermistor characteristics appeared to remain constant over the course of the experiments. The cell containers showing the location of the heating coil and thermistors is shown in Figure (22).

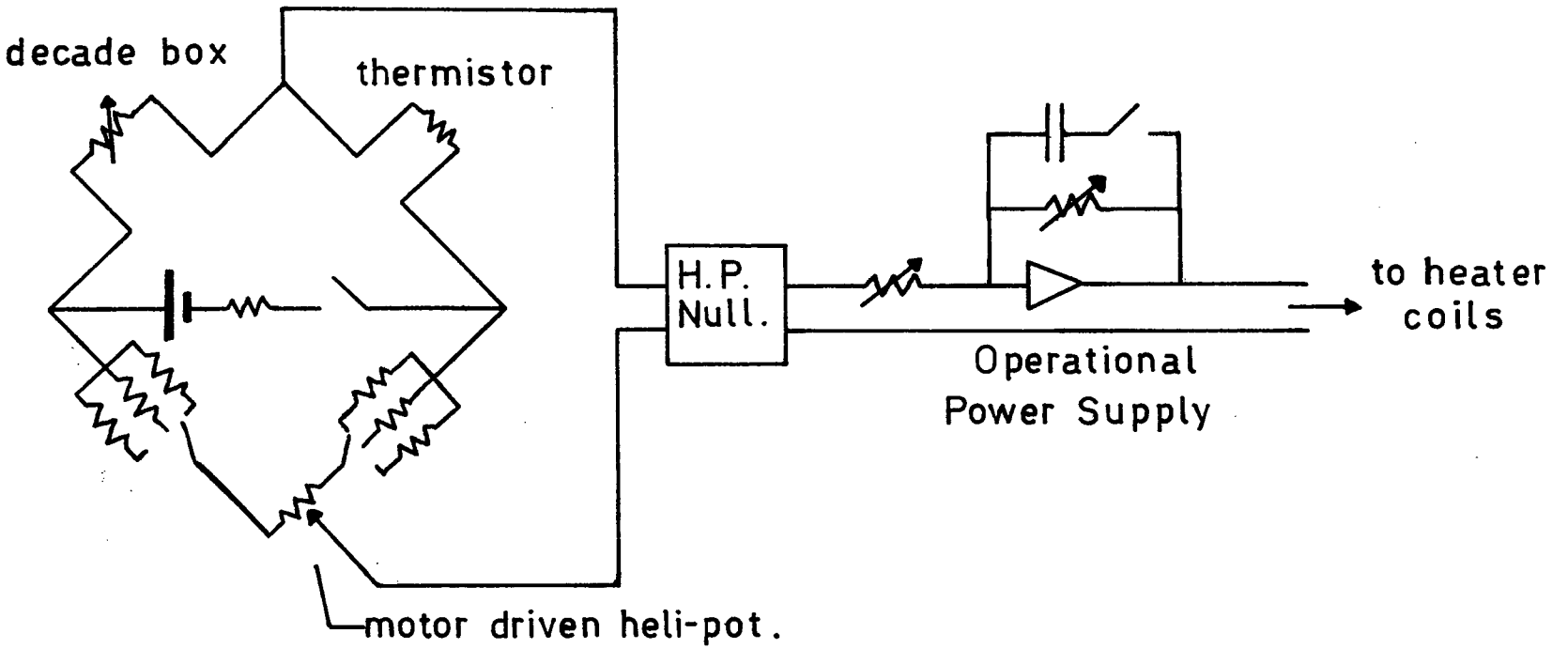

Fig. 21 Circuit diagram of the temperature control system.

Fig. 22 The cell containers.

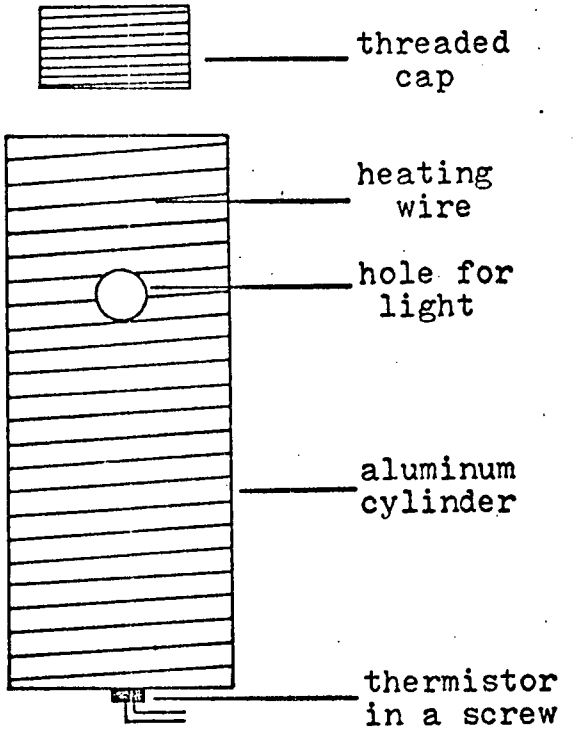
threaded cap
heating wire
hole for light
aluminum cylinder
thermistor in a screw
Side View

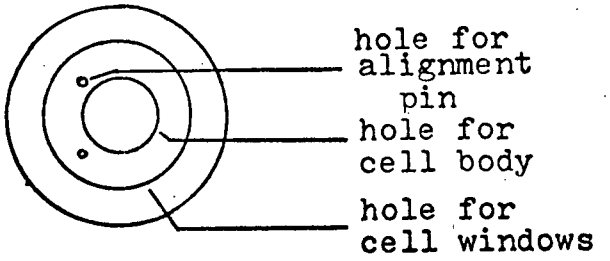
hole for alignment pin
hole for cell body
hole for cell windows
End View

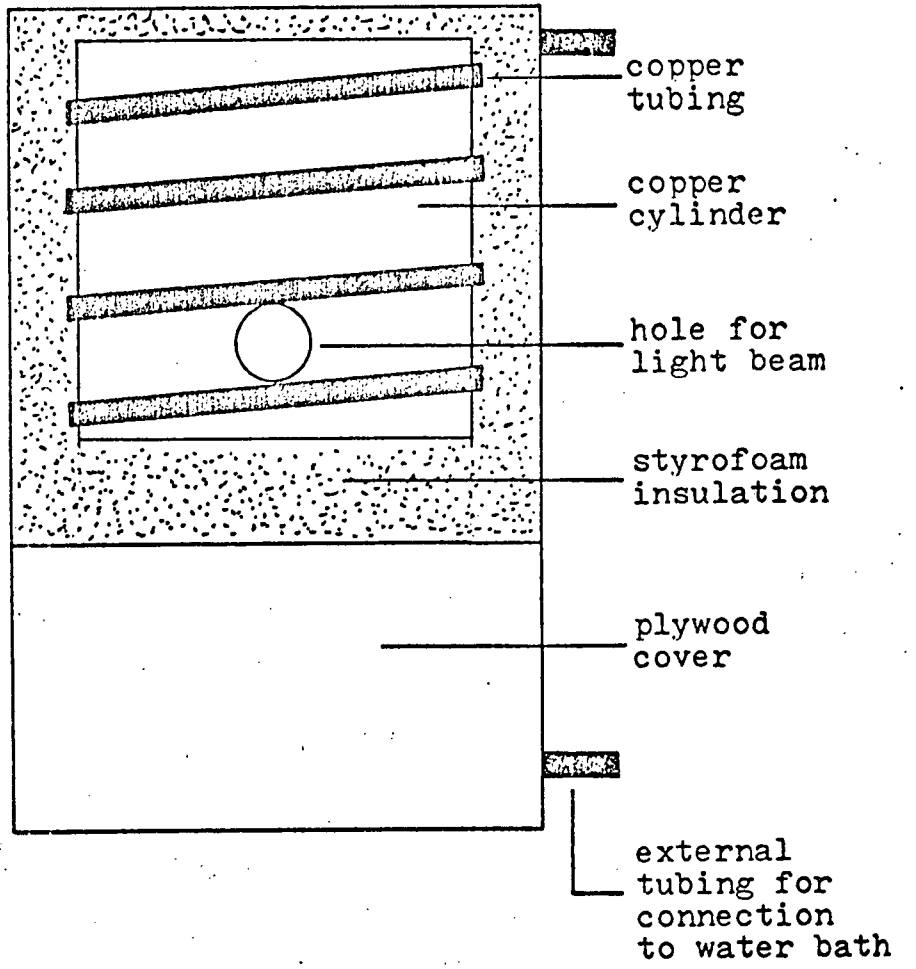
copper tubing
copper cylinder
hole for light beam
styrofoam insulation
plywood cover
external tubing for connection to water bath

4.4 Results

The experimental procedure described above was carried out for SF_6 and GH_4. Figures (23) and (24) show the results for the Lorentz-Lorenz coefficient for λ = 6328 Å as a function of density, the results for SF_6 have appeared in the literature (27). The coefficient is essentially constant within $\pm$0.5% over the range covered, although a small decrease is observed with increasing density.

The decrease in L with increasing density is opposite to the prediction of Yaris and Kurtman (18) who predicted an increase with density. The decrease with density agrees with the conclusions of Chapman, Finnimore, and Smith (22) for xenon. The precision of the measurements presented in Figures (23) and(24) is almost an order of magnitude better than Smith's xenon data because density and refractive index are both measured in this experiment whereas analysis of the xenon refractive index data required use of published PVT data for interpretation.

The critical density and temperature for GeH_4 were measured for the first time in this experiment; the obtained values are ρ_c = 0.5029 gm/cm^3 and T_c = 38.925°C.

Fig. 23 The Lorentz-Lorenz coefficient for SF_6 as a function of density.

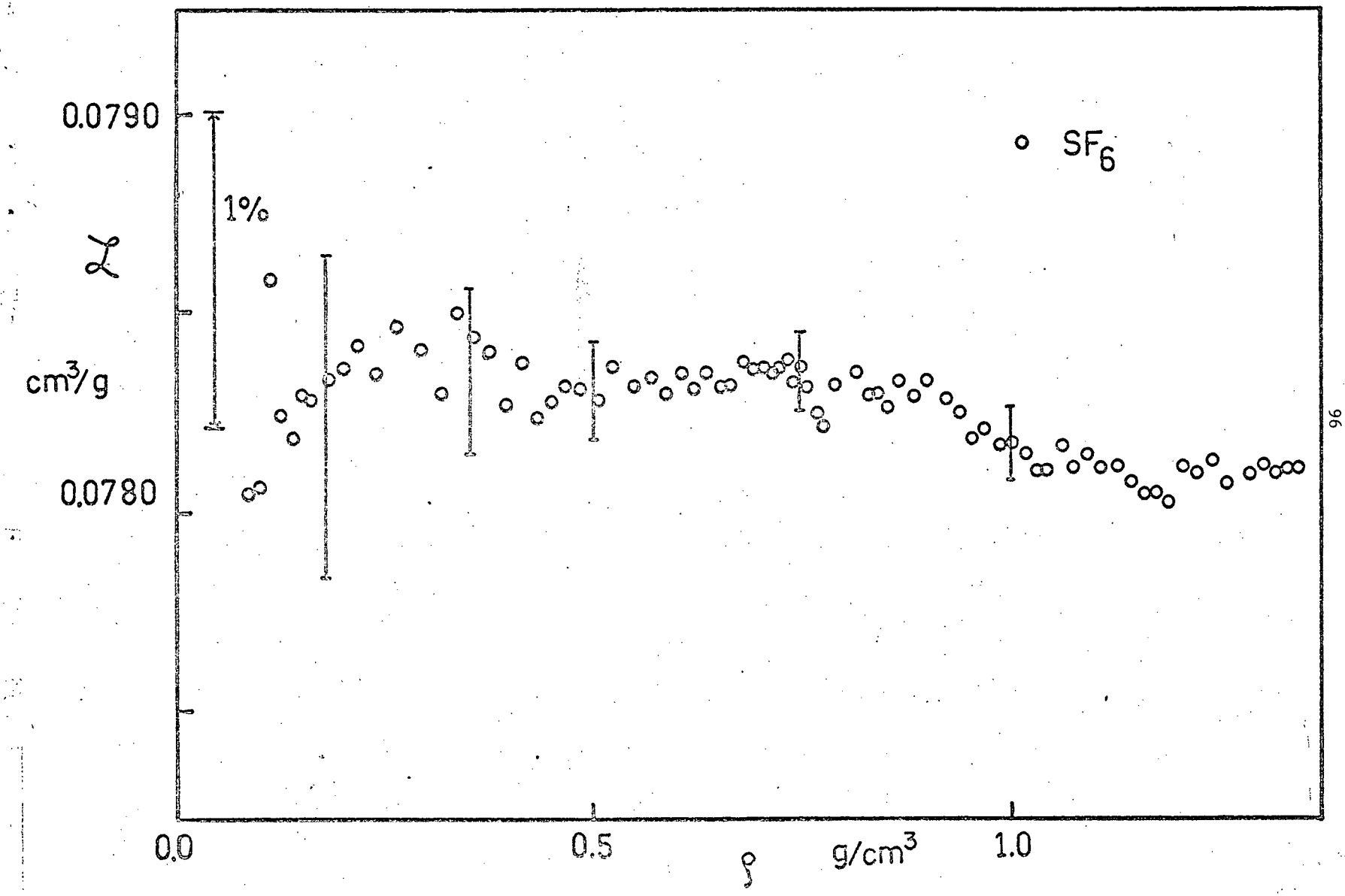
0.0790
0.0780
1%
$\mathcal{L}$
cm³/g
SF6
0.0
0.5
1.0
ρ
g/cm³

Fig. 24 The Lorentz-Lorenz coefficient for GeH_4 as a function of density.

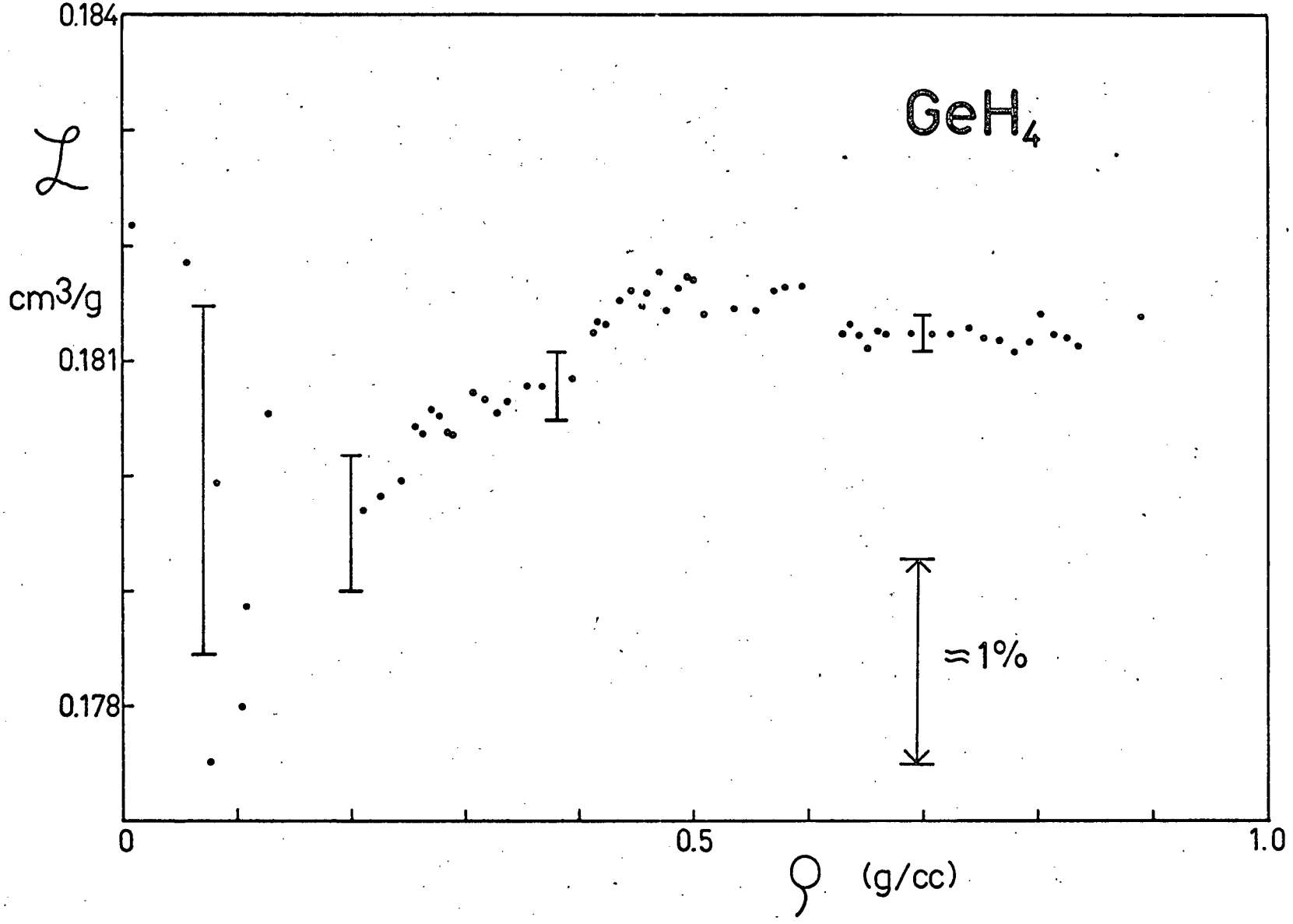
0.184
$\mathcal{L}$
cm3/g
0.181
0.178
GeH_4
≈1%
0
0.5
1.0
ϱ (g/cc)

Fig. 25 Coexistence curve of GeH_4.

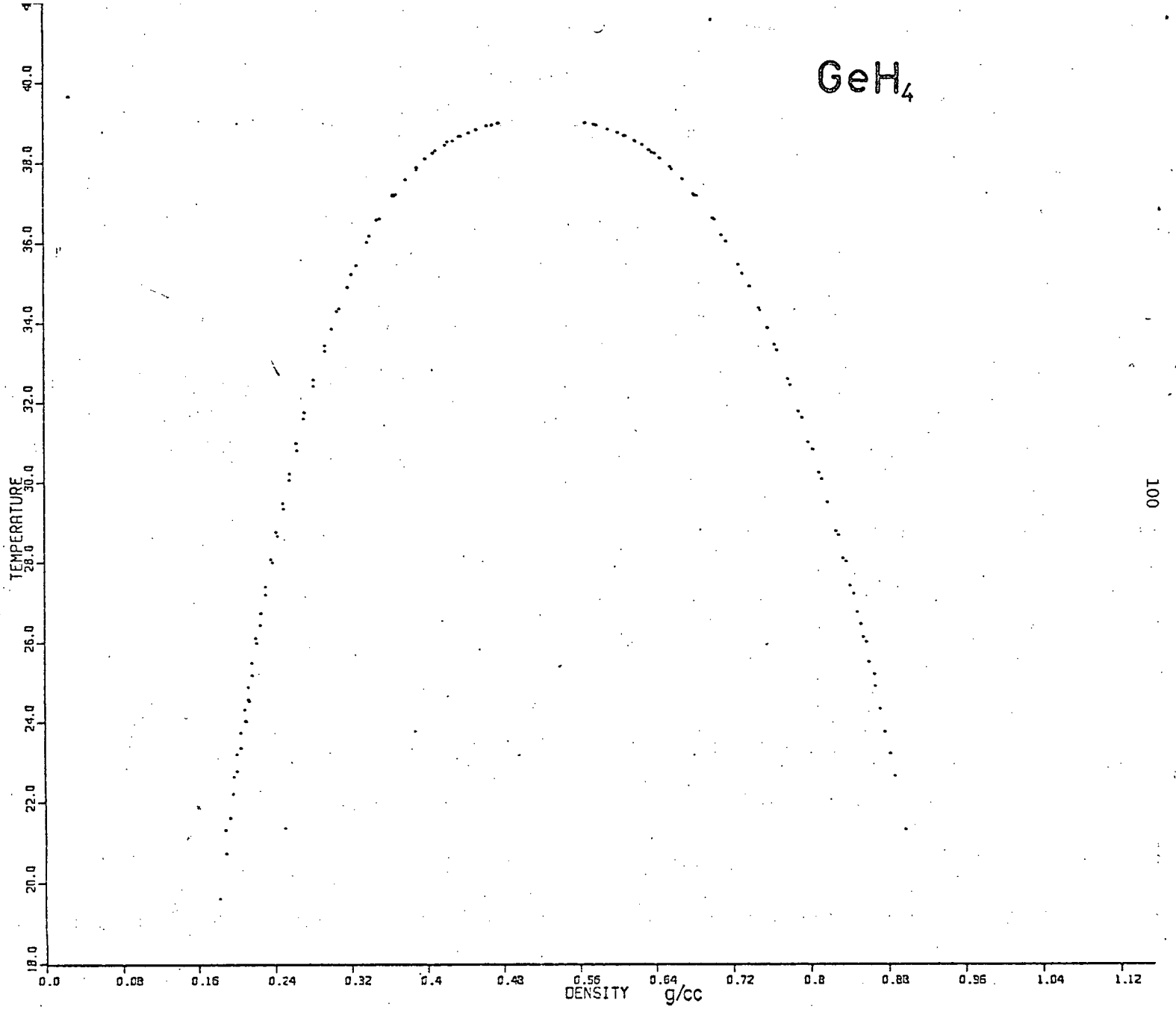
GeH4
TEMPERATURE
40.0
38.0
36.0
34.0
32.0
30.0
28.0
26.0
24.0
22.0
20.0
18.0
0.0
0.08
0.16
0.24
0.32
0.4
0.48
0.56
0.64
0.72
0.8
0.88
0.96
1.04
1.12
DENSITY g/cc

CHAPTER 5

NEMATIC LIQUID CRYSTALS - EXPERIMENTAL

5.1 The Anisotropic Lorentz-Lorenz Relation

For nematic liquid crystals, the relation between refractive indices, number density, polarizability and local field anisotropy is given by Eq. (1.29). In a principal axis system, for a uniaxial material, Eq. (1.29) yields

$$\frac{(n_{\parallel}^2-1)}{(n_{\parallel}^2+2)}(1-4\pi\rho\eta_{\parallel}\alpha_{\parallel}) = \frac{4\pi}{3}\rho\alpha_{\parallel} \tag{5.1}$$

and

$$\frac{(n_{\perp}^2-1)}{(n_{\perp}^2+2)}(1-4\pi\rho\eta_{\perp}\alpha_{\perp}) = \frac{4\pi}{3}\rho\alpha_{\perp} \; . \tag{5.2}$$

The polarizabilities α for the medium are given by Eq. (2.8); since for a system of prolate molecules $R = \langle\cos\theta\rangle = 0$,

$$\alpha_{\parallel} = \frac{1}{3}(\alpha_{m_{\parallel}}+2\alpha_{m_{\perp}}) + \frac{2S}{3}(\alpha_{m_{\parallel}}-\alpha_{m_{\perp}}) \tag{5.3}$$

and

$$\alpha_{\perp} = \frac{1}{3}(\alpha_{m_{\parallel}} + 2\alpha_{m_{\perp}}) - \frac{S}{2}(\alpha_{m_{\parallel}} - \alpha_{m_{\perp}}) \tag{5.4}$$

where the α_m denote molecular polarizability. The order parameter S may be eliminated from Eqs. (5.3) and (5.4) to yield

$$\alpha_{\parallel} + 2\alpha_{\perp} = \alpha_{m_{\parallel}} + 2\alpha_{m_{\perp}} \quad . \tag{5.5}$$

Since the anisotropy tensor $\eta_{\alpha\beta}$ is traceless and the material is uniaxial

$$\eta_{\parallel} + 2\eta_{\perp} = 0. \tag{5.6}$$

If the refractive indices and the number density are known, then the four equations Eq. (5.1), (5.2), (5.5) and (5.6) may be solved for the four unknowns $\alpha_{\parallel}$, $\alpha_{\perp}$, $\eta_{\parallel}$, $\eta_{\perp}$ at a given temperature. The order parameter S can then be obtained from

$$S = \frac{\alpha_{\parallel} - \alpha_{\perp}}{\alpha_{m_{\parallel}} - \alpha_{m_{\perp}}} \quad . \tag{5.7}$$

In this experiment, the refractive indices $\eta_{\parallel}$ and $\eta_{\perp}$ are measured as a function of temperature using a modified Rayleigh interferometer. The difference between the refractive indices is separately measured by use of a previously reported (20) conoscopic techniques. Thermal expansivity measurements were obtained by filling conventional mercury and alcohol thermometers with liquid crystal samples and measuring the height of the meniscus in the capillary as a function of temperature. The nematic

liquid crystals used in the measurements reported here were EBBA (p-Ethoxy Benzylidene-p-n-Butylaniline) and BEPC (Butyl p-(p-Ethoxy-phenoxycarbonyl) phenyl Carbonate) obtained from Eastman Kodak Co.

5.2 The Modified Rayleigh Interferometer

The liquid crystal samples were contained in rectangular fused quartz cells manufactured by Hellma Ltd. The inside dimensions of the cells are 1 cm x 5 cm x 0.2 cm; with a window thickness of 0.12 cm. The cells were connected to a vacuum system and pumped on for a period of 24 hours prior to filling. They were then approximately one-half filled with the liquid crystal sample in the isotropic phase, and were then immediately reconnected to the vacuum system and were pumped on again in order to remove air dissolved in the sample and from the rest of the cell. The cells were then vacuum sealed, and kept at a sufficiently high temperature to prevent sample recrystallization. The cell containing the sample to be measured was then placed inside the temperature controlled cell holder. Sample alignment was effected by placing the cell holder between the poles of a conventional electromagnet. The pole-piece separation was 8", providing a B-field of 1.8 kG at a 5 A supply current with 99.8% homogeneity over the volume occupied by the cell.

The light source used was a Hughes Model 3178H 0.5 mW He-Ne laser. The beam was collimated and rendered uniphase by a beam expanding telescope and a 10μ pinhole filter, it was then passed through a 1 cm diameter iris and a Spindler-Hoyer polarizer. The beam was normally incident on the cell in such a way that approximately one half of the beam passed through the liquid crystal sample in the lower portion of the cell, while the rest of the beam traversed the upper portion of the cell containing only vapor from the sample. The two beams were mixed using a 1.5 cm x 1.5 cm x 1.5 cm beam cube and the

resulting interference pattern was enlarged using a simple f/2.8 f = 4.5 cm lens. Due to imperfections in the alignment of the two halves of the beam cube, the interference pattern consisted of approximately 15 vertical fringes, spaced a distance λ_f apart. Using a 0.5 mm slit, a 2.5 cm x 0.5 mm horizontal portion was continuously recorded on film. The optical system and the interference pattern is shown in Figures 26 and 27. As the temperature of the sample was varied, the optical path length difference of the beam through the liquid and of the beam through the vapor varied, resulting in horizontal movement of the fringes. A displacement of the fringes through a distance λ_f corresponds to a change in the phase difference of the two beams of 2π radians. Since the vapor pressure of the samples is much less than one atmosphere, changes in the optical path length due to vapor density variations are neglected. For light polarized parallel or perpendicular to the optic axis, the change in the corresponding refractive index Δn_α is thus

$$\Delta n_\alpha = \frac{\Delta N \lambda}{\ell} \tag{5.8}$$

where ℓ = 2 mm is the sample thickness, λ = 6328 Å is the free-space wavelength of the laser and ΔN is the number of fringes that move past any given point within the interference pattern.

In addition to photographing the interference pattern, the movement of fringes was monitored by a silicon photocell, whose amplified output was recorded on a strip-chart recorder. Sample temperature was

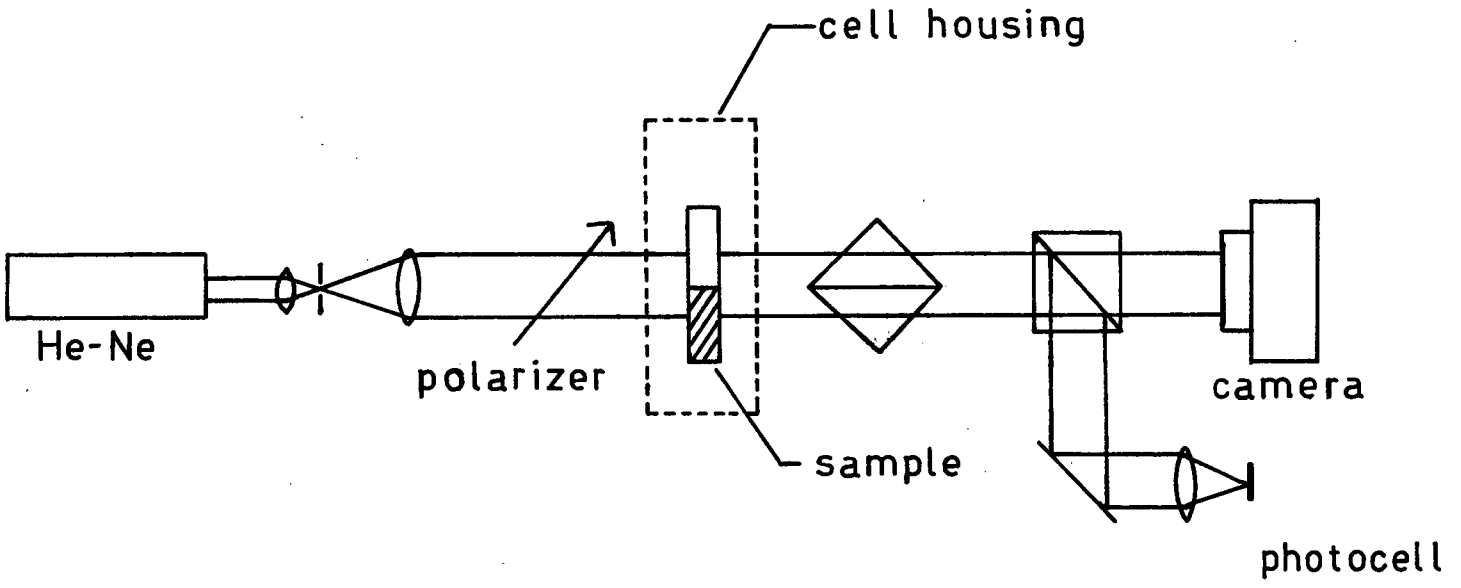

Fig. 26 The modified Rayleigh interferometer.

Fig. 27 Interference pattern obtained from the modified Rayleigh interferometer.

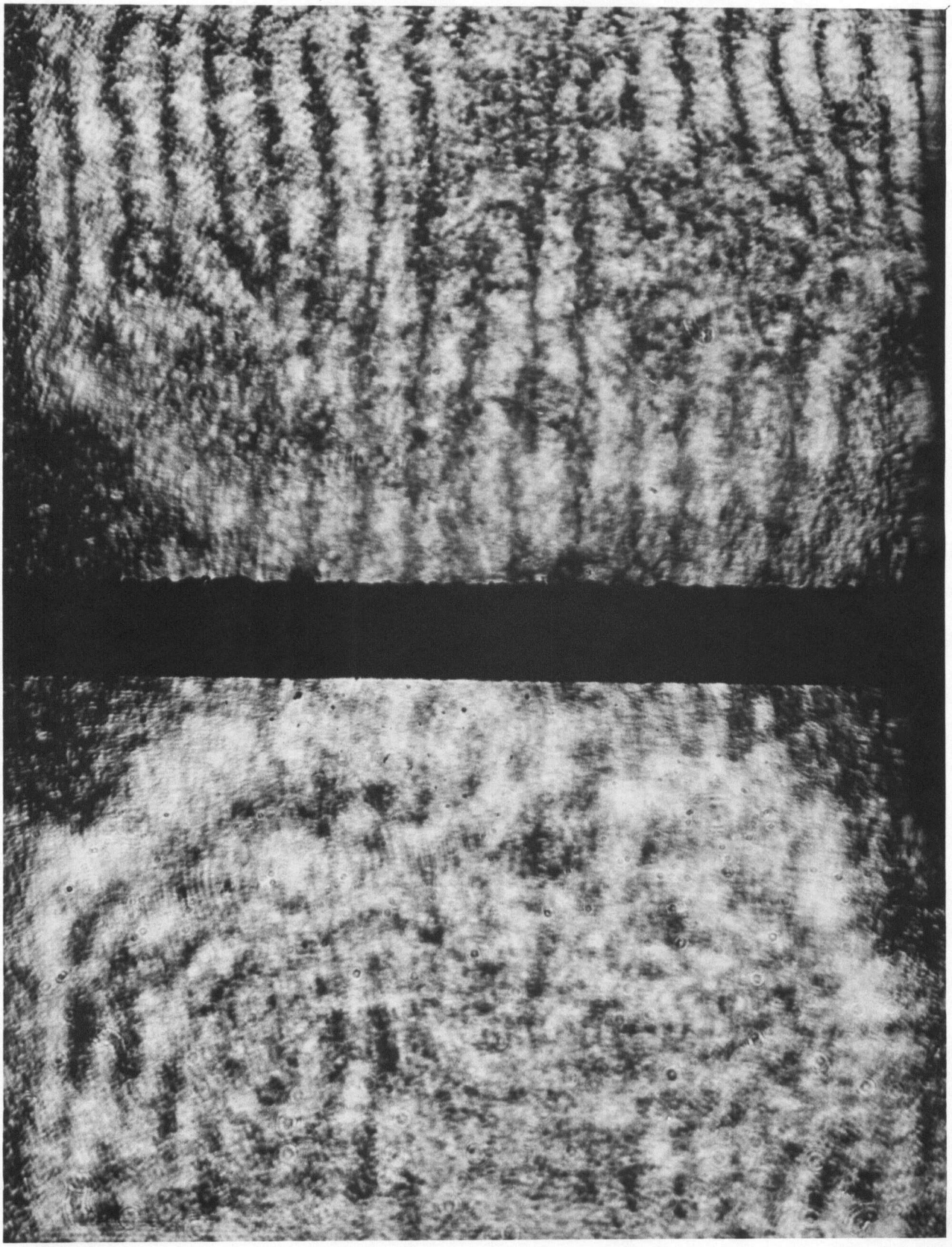

recorded by photographing the display of the quartz thermometer every 5 minutes, and in addition, by manually balancing the monitor thermistor bridge and recording the thermistor resistance. Temperature was continuously increased from approximately 20°C below the transition temperature to 10°C above it; with sweep rates of .5°C/hr far from the transition, and .002°C/hr near it. Two separate runs were made for each sample; one with light polarized along the optic axis, and one with light polarized perpendicular to it. The direction of motion of the fringes was opposite in the two cases. The refractive index in the isotropic phase is known to decrease with increasing temperature due to decreasing density. Since the direction of fringe movement when the polarization was along the optic axis and the sample was in the nematic phase was in the same direction as that in the isotropic phase, it was concluded that the extraordinary refractive index decreases with increasing temperature, while the ordinary index increases. The number of fringes moving past the center of the interference pattern corresponding to changes in the refractive indices is shown in Figures (28) and (29). Since fringe displacements of $\lambda_f/2$ corresponding to $\Delta N = \frac{1}{2}$ are easily detected, the accuracy in measuring the change in the refractive indices is better than one part in three thousand; an order of magnitude better than previously reported (21) refractive index measurements.

The absolute value of the ordinary index at a given temperature was obtained by slowly rotating the cell about its vertical axis, and counting the fringes as they moved past a given point near the center of the pattern. The cell rotation was accomplished by using a 1/240 r.p.m.

Fig. 28 Results of fringe number measurements corresponding to changes in the refractive indices of EBBA.

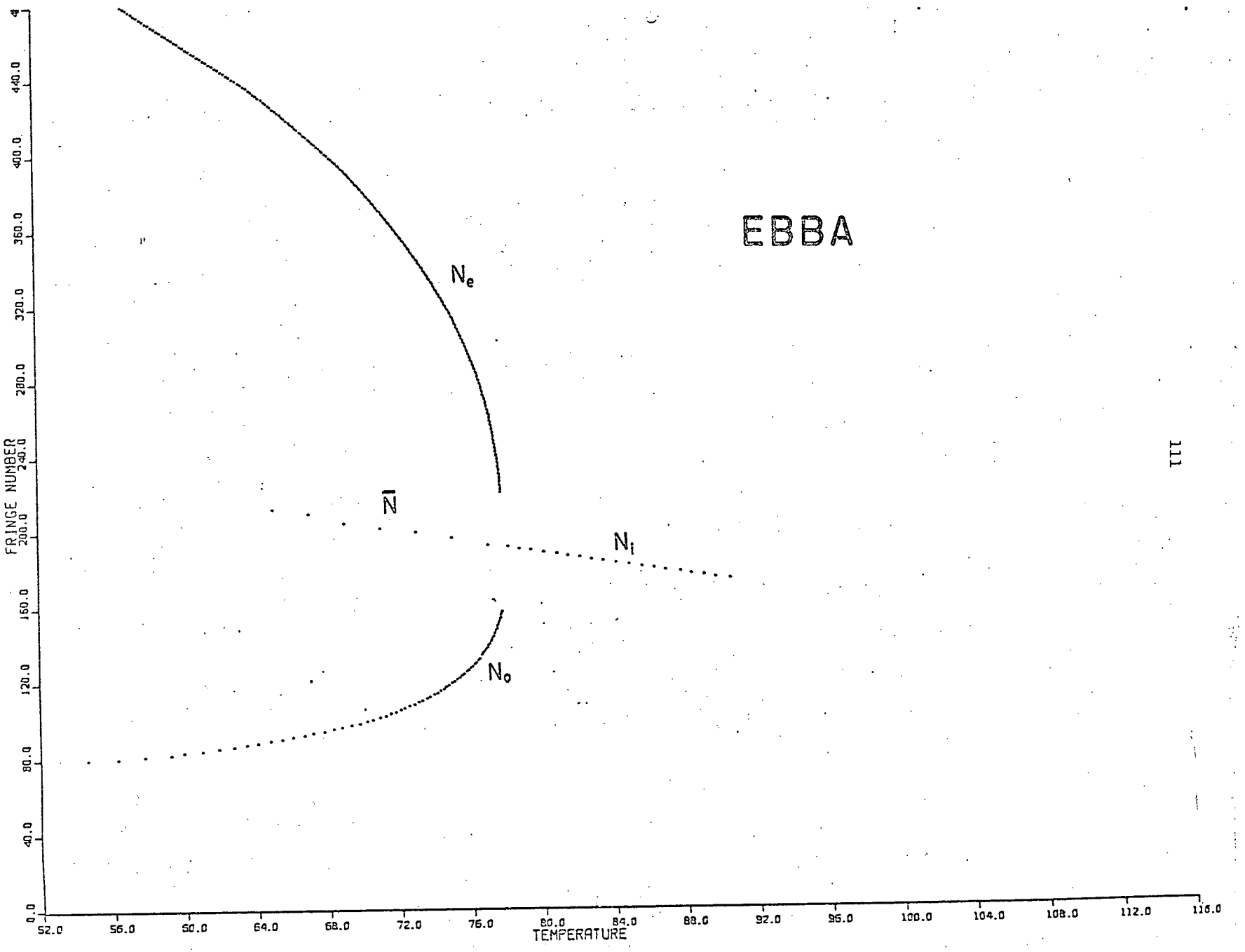
EBBA
N_e
$\bar{N}$
N_l
N_o
FRINGE NUMBER
TEMPERATURE
0.0
40.0
80.0
120.0
160.0
200.0
240.0
280.0
320.0
360.0
400.0
440.0
52.0
56.0
60.0
64.0
68.0
72.0
76.0
80.0
84.0
88.0
92.0
96.0
100.0
104.0
108.0
112.0
116.0

Fig. 29 Results of fringe number measurements corresponding to changes in the refractive indices of BEPC.

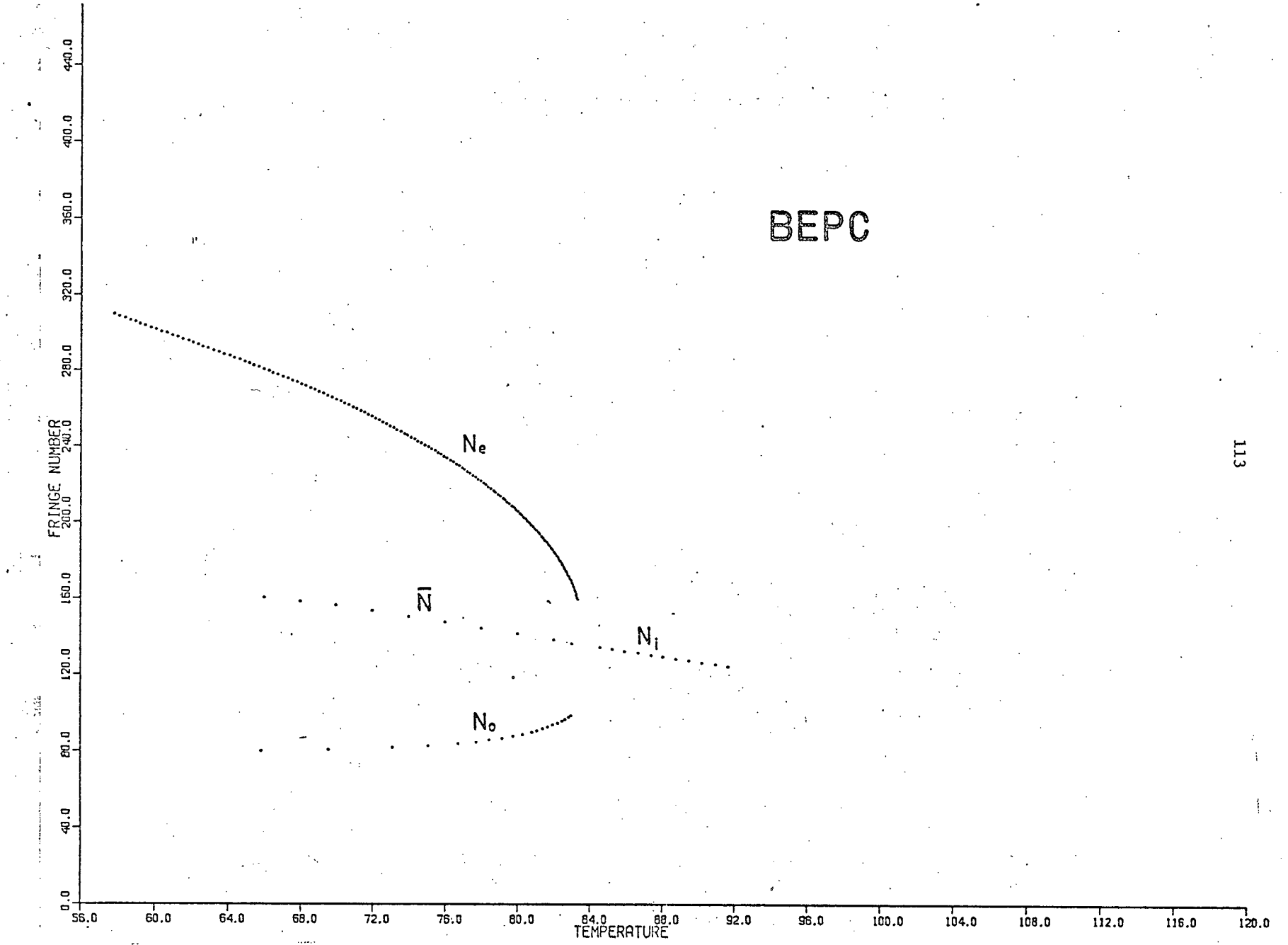
BEPC
FRINGE NUMBER
0.0
40.0
80.0
120.0
160.0
200.0
240.0
280.0
320.0
360.0
400.0
440.0
N_e
$\bar{N}$
N_i
N_o
56.0
60.0
64.0
68.0
72.0
76.0
80.0
84.0
88.0
92.0
96.0
100.0
104.0
108.0
112.0
116.0
120.0
TEMPERATURE

A.C. motor manufactured by Graham Canada Ltd., Model 267777. Care was taken to mount the motor in such a way as to minimize vibration of the sample. A 10-tooth spur gear on the motor output shaft was used to drive a 96-tooth spur gear mounted on the vertical axis of the cylindrical cell holder; the angular velocity of cell rotation was 9.375°/hr. Cell rotation was initiated with the cell positioned at +30° from its normal position perpendicular to the beam, and was rotated through 0° to a final orientation of -30°. In order to correct for errors due to the gear being slightly off axis, the cell was rotated 180° and the above procedure was repeated. As shown in Appendix I, the relation between $n_\perp$ and ΔN is given by

$$x^2 + \sin^2\theta = ax + b \tag{5.9}$$

where

$$x = \frac{\Delta M\lambda}{d} + \cos\theta - 1$$

$$a = -2\left(\frac{\varepsilon\lambda}{d} + n_\perp\right)$$

$$b = n_\perp^2 - \left(\frac{a}{2}\right)^2$$

and ε is a constant between zero and unity.

The fringes plotted on the chart paper were symmetric about $\theta = 0$; the angle corresponding to each intensity maximum was calculated from the known rotation rate. The quantity x was evaluated for each

Fig. 30 Analysis of cell rotation data; x vs. $x^2 + \cos^2\theta$ for EBBA.

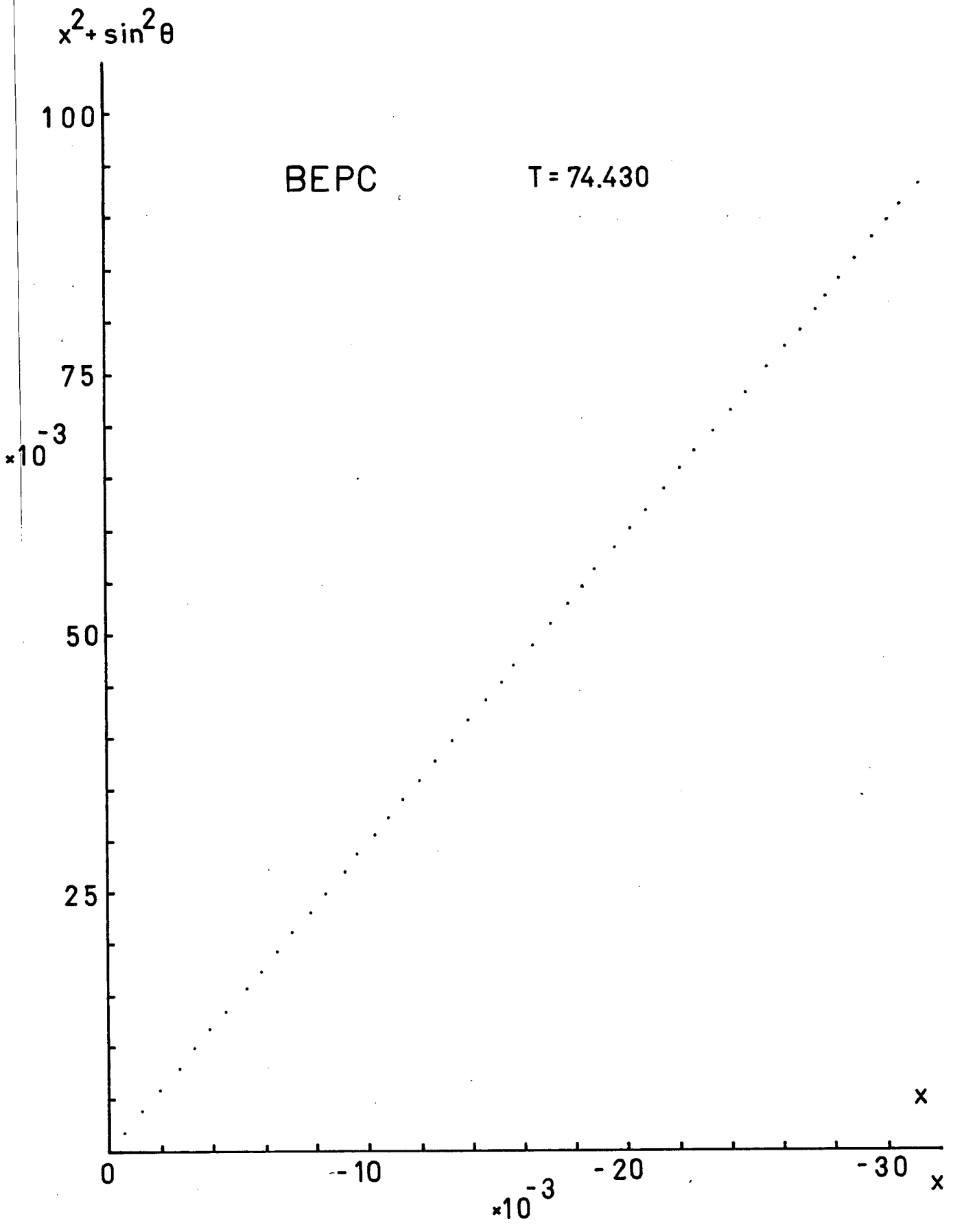
$x^2 + \sin^2\theta$
100
75
$\times 10^{-3}$
50
25
BEPC
T = 74.430
x
0
-10
-20
-30
$\times 10^{-3}$
x

fringe (ΔM = integer) and $x^2 + \sin^2\theta$ was then plotted vs. x. The refractive index $n_\perp$ was calculated from the slope and intercept of the resulting straight line, since

$$n_\perp = \sqrt{(\frac{a}{2})^2+b} \quad . \tag{5.10}$$

A typical graph is shown in Figure 30; the error in $n_\perp$ is estimated to be ± 0.005.

In principle, a similar procedure could have been used to determine the absolute value of $n_\parallel$. Rotation of the cell, however, necessitates the continuous re-alignment of the nematic director along the applied $\bar{B}$-field. Although the observed time constant for this relaxation process was less than one second, it was felt that more reliable results could be obtained by using the conoscopic method described in the next section.

The advantages of the modified Rayleigh interferometer described in this section that merit mention are its simplicity, its relative ease of alignment, its inherent insensitivity to the optical path length of the sample container (i.e. cell windows) and its insensitivity to building vibrations. Although the steel frame table supporting the optical bench and magnet was floated on 14 automobile tire innertubes, an identical experiment using a Mach-Zender interferometer could not be made to yield reliable results due to building vibrations. No such problems were encountered during the course of this experiment.

5.3 Conoscopic Measurements

The difference between the principal refractive indices of the liquid crystal samples were measured using a conoscopic technique. A converging beam focussed approximately 0.5 cm below the meniscus of the sample was obtained by placing compound f/1.8 f = 85 mm lenses directly in front of and behind the sample. The beam cube of Figure 24 was replaced by an analyzer. The polarizer and analyzer were crossed in such a way that the polarization of the incident light was at an angle of 45° to the optic axis. The resulting interference pattern is shown in Figure 31. As the difference between the refractive indices decreased due to increasing temperature, fringes were observed to move towards the center of the pattern in the horizontal direction and away from the center in the vertical direction.

A silicon photocell was used to monitor the intensity variations due to fringes sweeping through the center of the pattern. The number of fringes ΔN that move past the center as the difference between the refractive indices changes is given by

$$\Delta N = \frac{\ell}{\lambda} (n_{\parallel} - n_{\perp}) - N_0 \tag{5.11}$$

Where N_0 is a constant. Changes in the refractive index difference can therefore be measured with an accuracy greater than one part in six thousand; ΔN is shown in Figures 32 and 33 as a function of temperature. These results may be compared with changes in the refractive index difference calculated from the modified Rayleigh interferometer results of the previous section; the two sets of results agree to within ± 1 fringe.

Fig. 31 Conoscopic diffraction pattern.

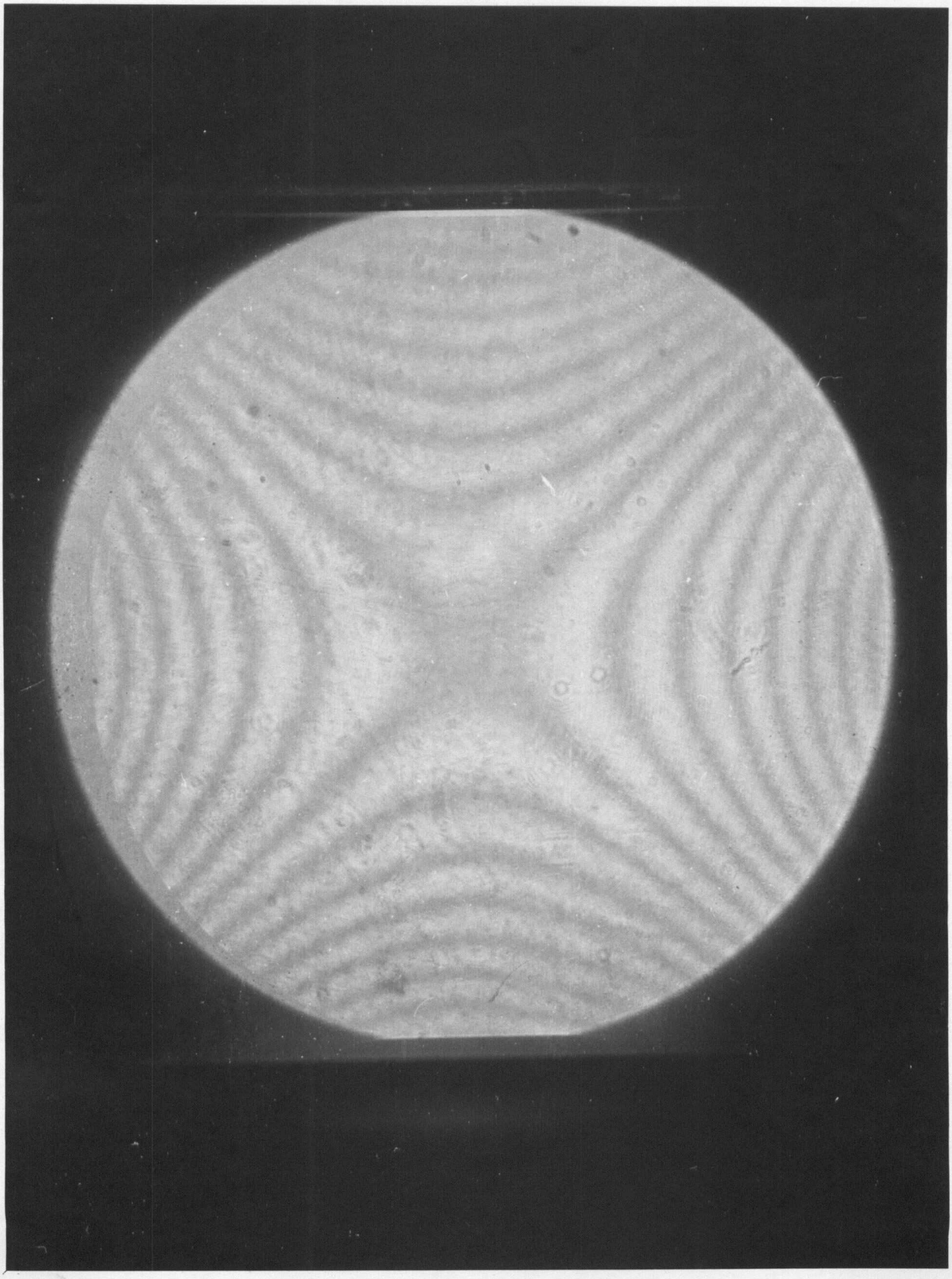

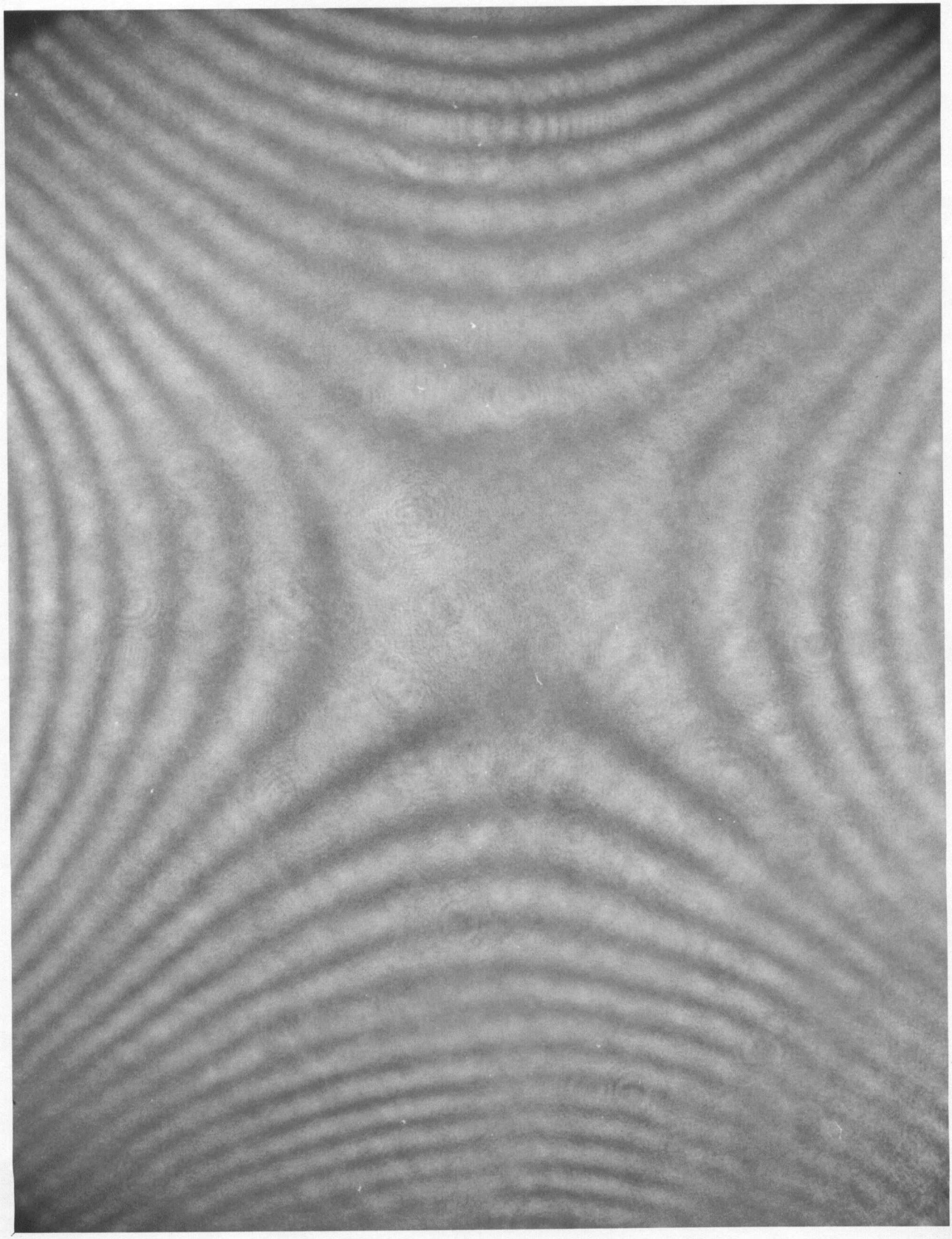

Fig. 32 Conoscopic fringe number measurements for EBBA.

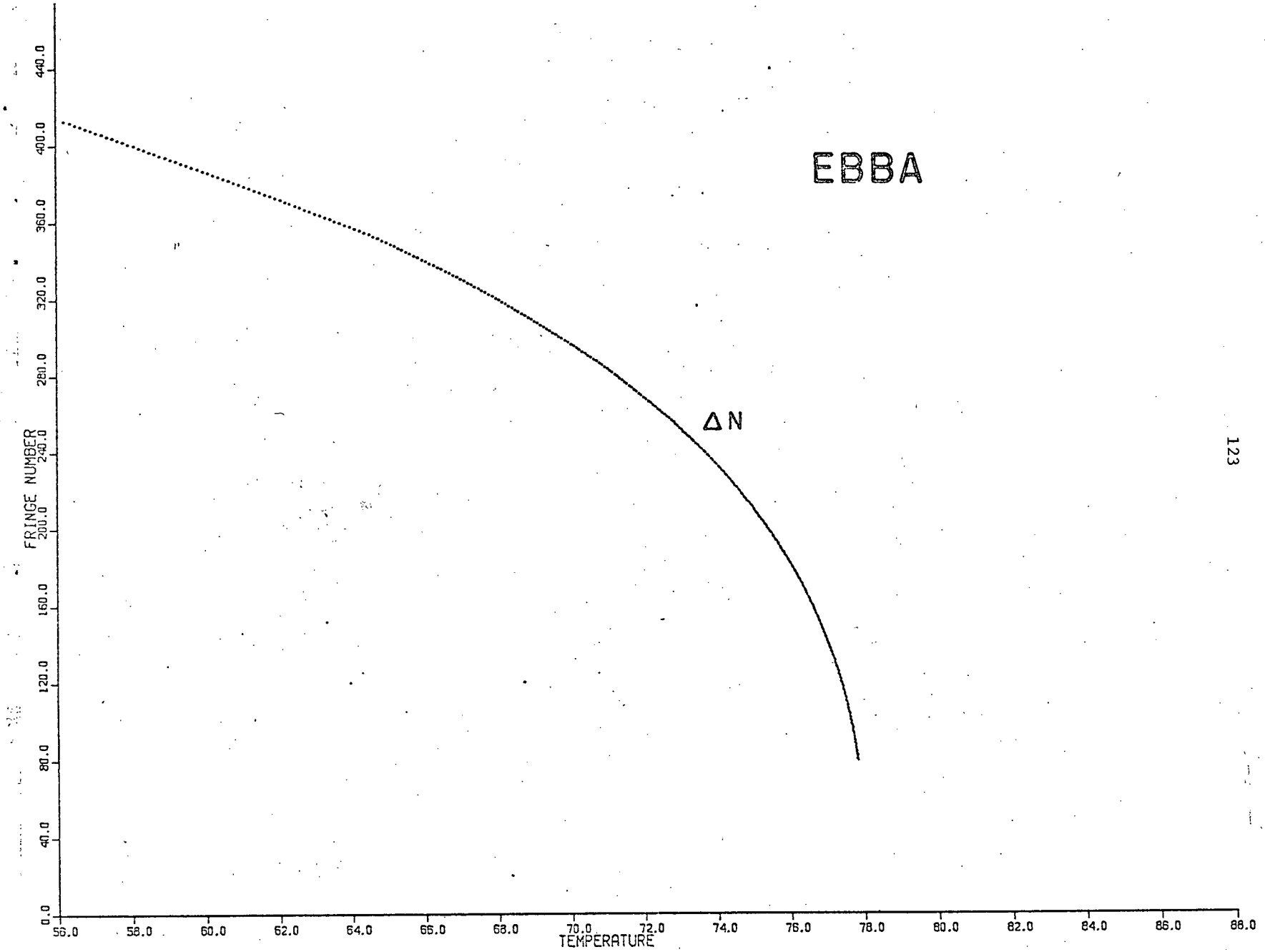
EBBA
ΔN
FRINGE NUMBER
0.0
40.0
80.0
120.0
160.0
200.0
240.0
280.0
320.0
360.0
400.0
440.0
56.0
58.0
60.0
62.0
64.0
66.0
68.0
70.0
72.0
74.0
76.0
78.0
80.0
82.0
84.0
86.0
88.0
TEMPERATURE

Fig. 33 Conoscopic fringe number measurements for BEPC.

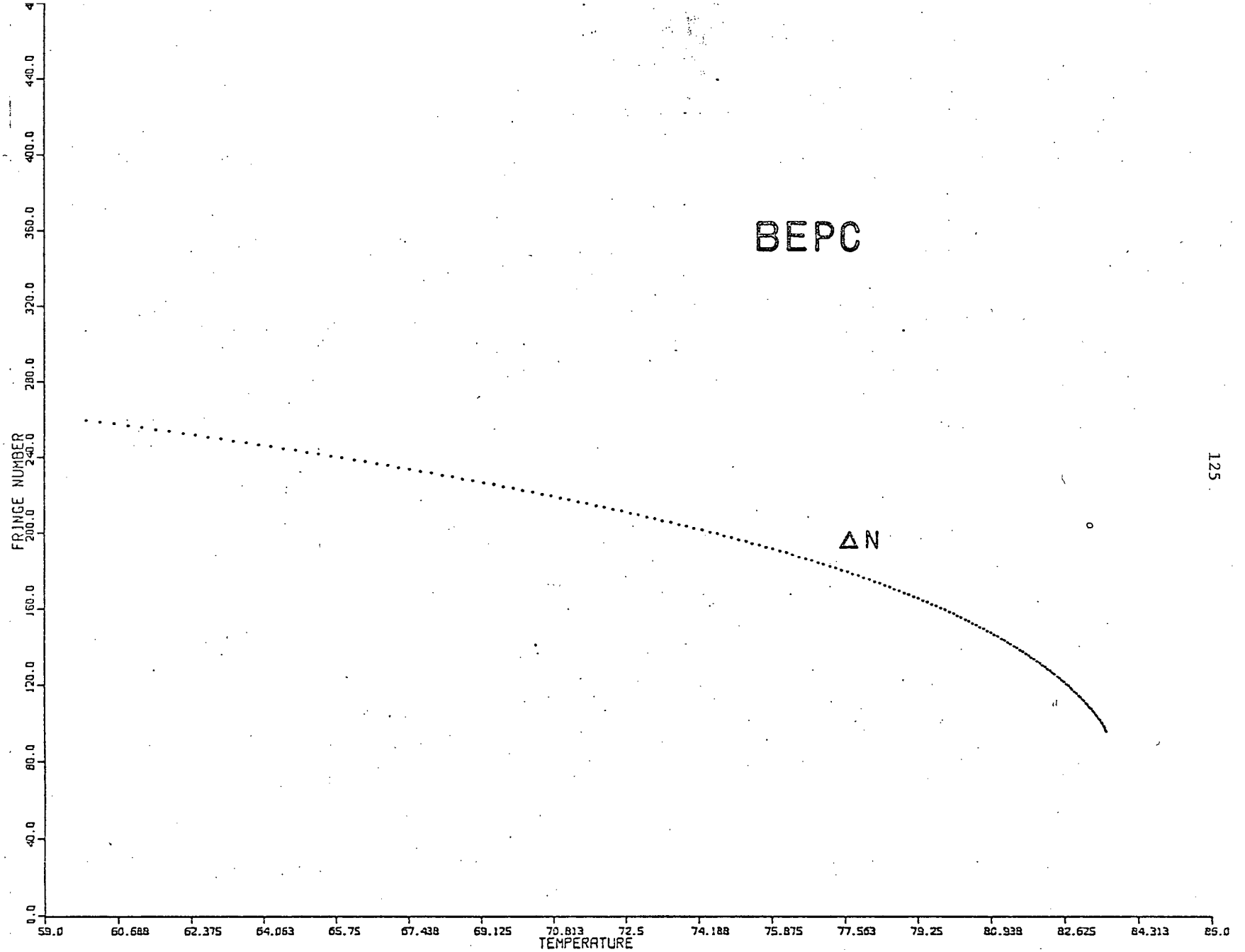
BEPC
FRINGE NUMBER
0.0
40.0
80.0
120.0
160.0
200.0
240.0
280.0
320.0
360.0
400.0
440.0
ΔN
59.0
60.688
62.375
64.063
65.75
67.438
69.125
70.813
72.5
74.188
75.875
77.563
79.25
80.938
82.625
84.313
86.0
TEMPERATURE

The absolute value of $n_{\parallel}-n_{\perp}$ can be obtained from the density of fringes in the diffraction pattern shown in Figure 31 if $n_{\perp}$ is known. The diffraction pattern was photographed approximately ten times during the course of each run. The value of the ordinary index $n_{\perp}$ was obtained from the modified Rayleigh interferometer results of the previous section for temperatures corresponding to each photograph. If θ is the angle subtended by the N^{th} fringe moving in a vertical direction from the center of the pattern, then the relation between θ, N and the refractive indices is, as shown in Appendix J,

$$(n_{\parallel}-n_{\perp})\left(1+\frac{1}{2n_{\parallel}n_{\perp}}\sin^2\theta\right) = \frac{\lambda(N+\delta)}{\ell} \tag{5.12}$$

for small angles, where $0 < \delta < 1$. Eq. (5.12) may be rewritten as

$$\sin^2\theta = mN + c \tag{5.13}$$

where $m = \dfrac{2n_{\parallel}n_{\perp}\lambda}{\ell(n_{\parallel}-n_{\perp})}$ and c is a constant. The refractive index difference then becomes, in terms of m

$$n_{\parallel}-n_{\perp} = \frac{n_{\perp}^2}{\frac{m\ell}{2\lambda} - n_{\perp}} \quad . \tag{5.14}$$

For each conoscopic photograph, N was plotted vs. $\sin^2\theta$, and m was obtained. The refractive index difference was then obtained from Eq. (5.14). The quantity $\frac{\ell}{\lambda}(n_{\parallel}-n_{\perp})$ was then subtracted from ΔN of

Eq. (5. 1) for each temperature to yield N_0. The accuracy of the measurement of the absolute value of $n_{\parallel}-n_{\perp}$ is determined by the scatter of points about N_0; for EBBA it was found to be ±0.005, whereas for BEPC it was slightly worse due to existence of fewer fringes in the diffraction pattern. This accuracy could be improved considerably by photographing the pattern more frequently and by using lenses with smaller f-number. However, the existing thermostatic cell-holder necessitates the use of lenses with focal lengths of at least 85 mm.

5.4 Refractive Indices

The refractive indices for each sample are calculated in a number of distinct steps. The absolute values of $n_\perp$ in the nematic phase is obtained from the results of cell rotation. The absolute value of $n_\parallel - n_\perp$ in the nematic phase is obtained from analysis of the conoscopic diffraction pattern, yielding $n_\parallel$ since $n_\perp$ is now known. The temperature variation of $n_\parallel$, $n_\perp$ and n_i is accurately determined from measurements using the modified Rayleigh interferometer. The consistency of the results is established by the conoscopic measurements, since the number of fringes traversing the center of the conoscopic diffraction pattern corresponds to variations in the difference between $n_\parallel$ and $n_\perp$. The refractive indices $n_\parallel$, $n_\perp$ and n_i are shown in Figures (34) and (35) for EBBA and BEPC. The meaning of the error bars is that the whole series of points can be shifted as a unit. In addition to the refractive indices, the quantity $\bar{n} = \frac{1}{3}(n_\parallel + 2n_\perp)$ is also plotted. The expected behavior of $\bar{n}$ is obtained as follows. Eq. (5.1) may be re-written as

$$\frac{n_\ell^2 - 1}{n_\ell^2 + 2} = \gamma_\ell \tag{5.15}$$

where $\gamma_\ell = \frac{4\pi}{3}\rho\alpha_\ell(1-4\pi\rho\eta_\ell\alpha_\ell)^{-1}$ and $\ell = \parallel, \perp$. Then

$$n_\ell = \left(\frac{1+2\gamma_\ell}{1-\gamma_\ell}\right)^{1/2} \simeq 1 + \frac{3}{2}\gamma_\ell + \frac{3}{8}\gamma_\ell^2 + \ldots. \tag{5.16}$$

Fig. 34 Refractive indices of EBBA.

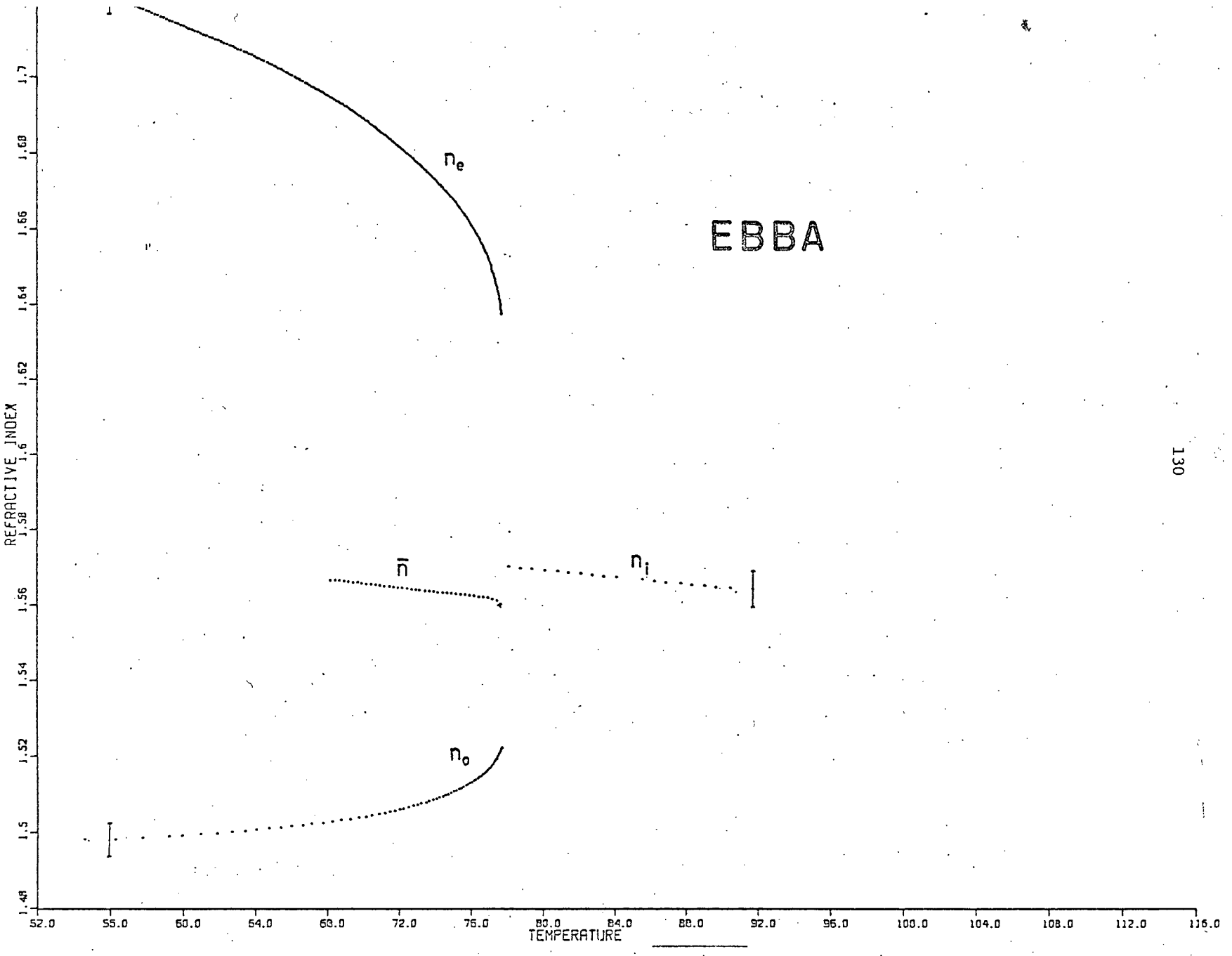
EBBA
n_e
$\bar{n}$
n_i
n_o
REFRACTIVE INDEX
1.7
1.68
1.66
1.64
1.62
1.6
1.58
1.56
1.54
1.52
1.5
1.48
52.0
55.0
60.0
64.0
68.0
72.0
76.0
80.0
84.0
88.0
92.0
96.0
100.0
104.0
108.0
112.0
116.0
TEMPERATURE

Fig. 35 Refractive indices of BEPC.

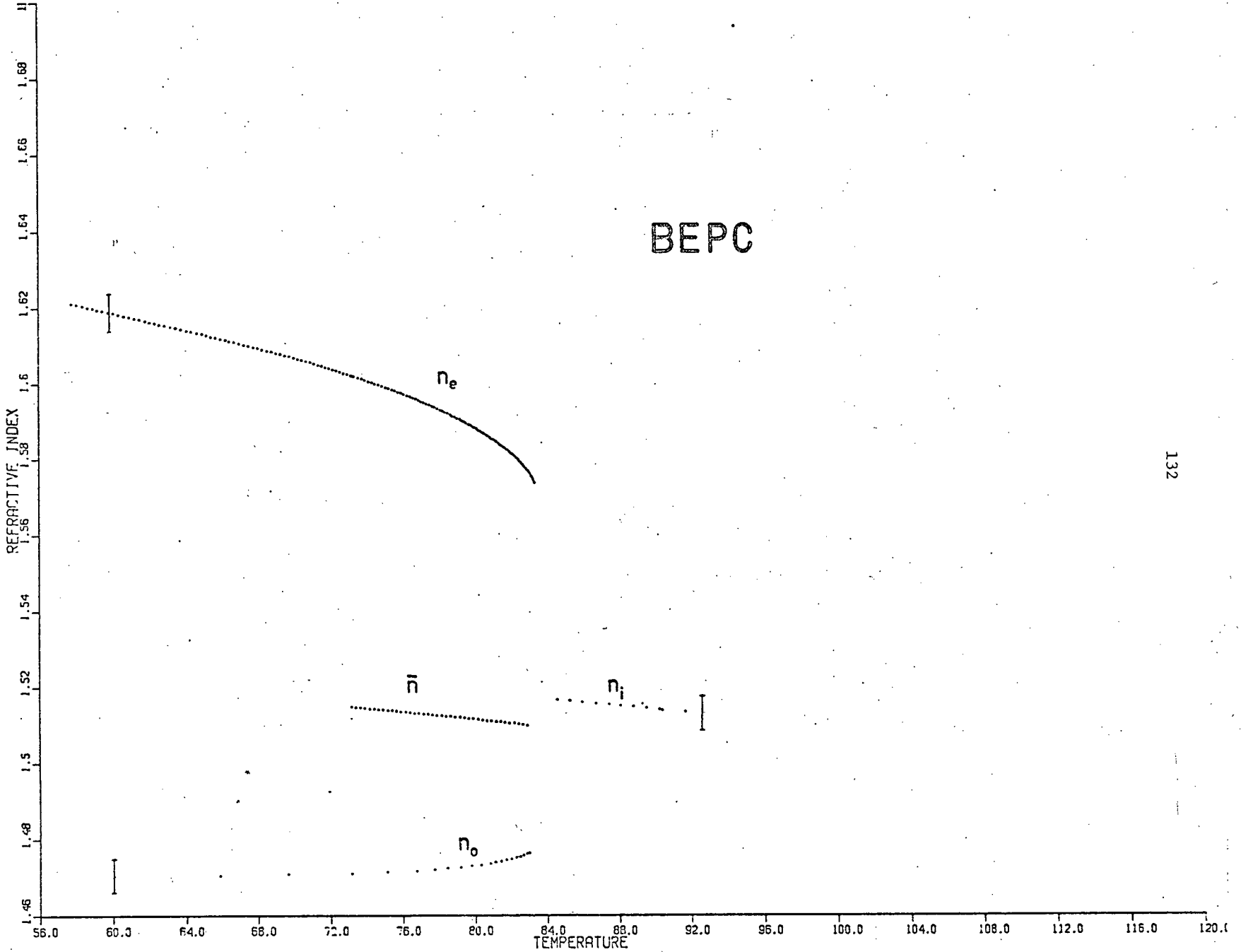
BEPC
REFRACTIVE INDEX
TEMPERATURE
n_e
$\bar{n}$
n_i
n_o
1.46
1.48
1.5
1.52
1.54
1.56
1.58
1.6
1.62
1.64
1.66
1.68
56.0
60.0
64.0
68.0
72.0
76.0
80.0
84.0
88.0
92.0
96.0
100.0
104.0
108.0
112.0
116.0
120.0

Fig. 36 Published values for the refractive indices of EBBA.

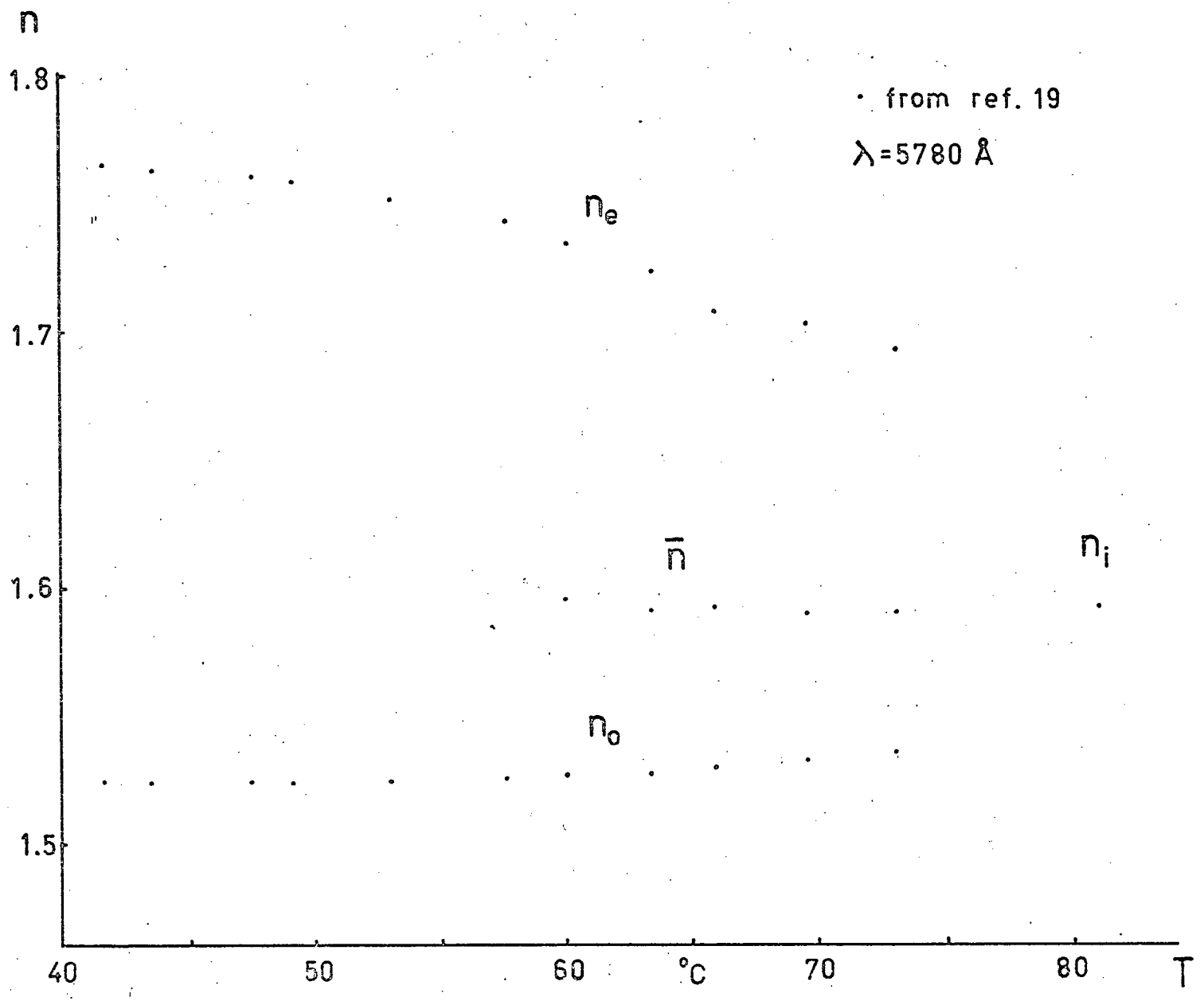
n
1.8
1.7
1.6
1.5
· from ref. 19
λ=5780 Å
n_e
$\bar{n}$
n_i
n_o
40
50
60
°C
70
80
T

since $\gamma_\ell < 1$. Since $\gamma_\ell \tilde{=} \frac{4}{3}\pi\rho\alpha_\ell$, substitution for α_ℓ yields

$$n_{\shortparallel} = 1 + 2\pi\rho(a+2\Delta S) + \ldots . \tag{5.17}$$

and

$$n_{\perp} = 1 + 2\pi\rho(a-\Delta S) + \ldots . \tag{5.18}$$

Then, to a first order

$$\bar{n} = \frac{n_{\shortparallel}+2n_{\perp}}{3} = 1 + 2\pi\rho a + \ldots . \; O(S^2) \tag{5.19}$$

and thus $\bar{n}$ varies as the density if the average molecular polarizability a is a constant. Eq. (5.19) yields for the thermal expansivity

$$\frac{1}{\rho}\frac{d\rho}{dT} = \frac{1}{\bar{n}-1}\frac{d\bar{n}}{dT} \; . \tag{5.20}$$

From Figure 28 it is clear that $\bar{n}$ decreases with temperature and that $\frac{d\bar{n}}{dT}$ is very nearly constant, giving evidence of the predicted increase of the thermal expansivity as the transition is approached from below. For EBBA at 67°C the above expression yields, since $\bar{n} = 1.599$ and $\frac{d\bar{n}}{dT} = -6.33 \times 10^{-4}/°C$ $\frac{1}{\rho}\frac{d\rho}{dT} = -1.06 \times 10^{-3}/°C$. This is in good agreement with measured results, as discussed in the next section.

The theory further predicts that

$$\frac{2(n_{\perp}^2+2)}{(n_{\perp}^2-1)} + \frac{(n_{\parallel}^2+2)}{(n_{\parallel}^2-1)} = \frac{3}{4\pi\rho}\left[\frac{1}{\alpha_{\parallel}} + \frac{2}{\alpha_{\perp}}\right] = A, \tag{5.21}$$

as given by Eq. (1.30). Expanding the polarizabilities α in terms of S yields

$$A = \frac{3}{4\pi\rho a}\left[1-2\delta S+4\delta^2S^2-8\delta^3S^3\ldots + 2 + 2\delta S + 2\delta^2S^2 + 2\delta^3S^3 + \ldots\right] \tag{5.22}$$

and

$$A \tilde{=} \frac{9}{4\pi\rho a}\left[1 + 2\delta^2S^2-2\delta^3S^3\right] \tag{5.23}$$

where $\delta = \Delta/a$. Letting $\rho = N/V$ and using Eq. (3.51) for the volume V yields

$$A = \frac{9V(0)}{4\pi Na}\,(1-3k^2S^2 + 2k^3S^3)(1+2^2\delta S^2-2\delta^3S^3) \tag{5.24}$$

where $k = \frac{\kappa-1}{\kappa+2}$, and

$$A = A(0)\left(1+(2\delta^2-3k^2)S^2-2(\delta^3-k^3)S^3+6k^2\delta^2S^4+\ldots\right). \tag{5.25}$$

For EBBA, the values of δ and k are extremely close. From recent literature (19) $a = 38.4 \times 10^{-24}$ cm^3, $\Delta = 10.5 \times 10^{-24}$ cm^3 and $\delta = 0.27$ at $\lambda = 5790$. If the hard core length to width ratio κ is assumed to be $\sim$2, then $k = 0.25$ and the coefficients of S^2 and S^3 in Eq. (5.15) are

very nearly equal to zero. The quantity A is thus expected to be nearly independent of temperature; values calculated from the refractive indices indicate that A/A(0) is constant to within ±0.0015 throughout the covered 20°C temperature range.

Fig. 37 Photograph of apparatus used in the refractive index measurements.

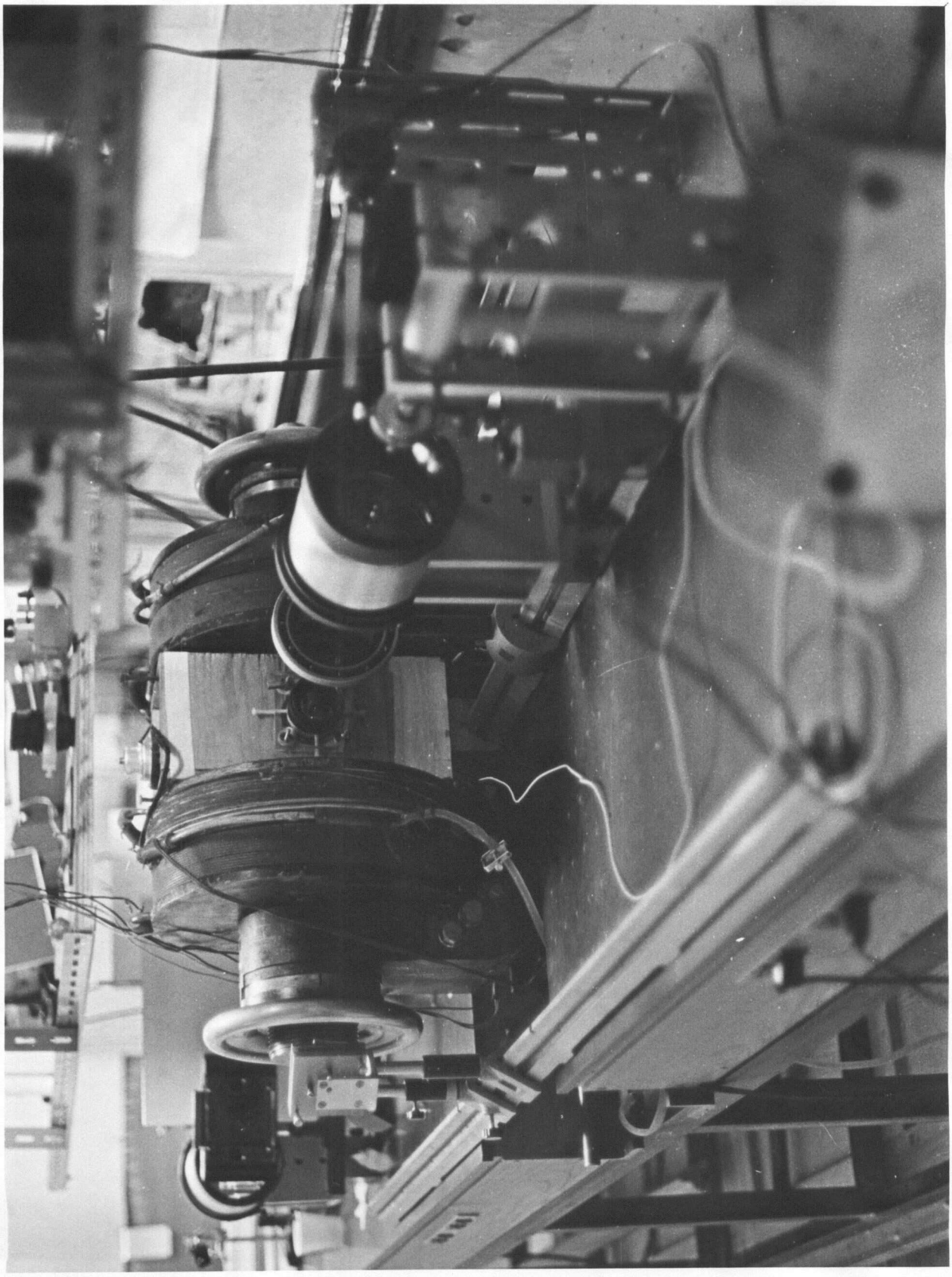

5.5 Thermal Expansivity

Experimental determination of the temperature dependence of the density is of interest because it enables comparison with theory and makes possible the calculation of the order parameter S and the local field tensor η from refractive index measurements.

The experimental method consists of filling a conventional mercury or alcohol thermometer with a liquid crystal sample and measuring the height of the meniscus in the capillary as a function of temperature. The thermometers were evacuated by the following procedure. The top sealed portion of the thermometer stem was broken off. The thermometer was then turned upside down and heated until a portion of the substance in the bulb vaporized, forcing some of the liquid out through the capillary. The thermometer was allowed to cool so that air was drawn into the bulb. The bulb was again heated and the procedure was repeated until all liquid has been expelled; a glass tube was then attached to the opened end. The cell thus formed was flushed with alcohol and was attached to a vacuum pump and pumped on for several days. Sample material was then placed in the glass tube above the thermometer stem, and the cell was re-connected via valves to the vacuum pump and to a regulated helium bottle. After pumping on the sample in the isotropic phase for one hour, repeated applications of helium at approximately 0.5 atm. forced the sample into the thermometer bulb. After further pumping the cell was sealed and placed in the temperature-controlled cell holder shown in Figure 38. The results obtained using a cell made from an alcohol thermometer (range: 40-120°F)

Fig. 38 Temperature-controlled cell holder used in thermal expansivity measurements.

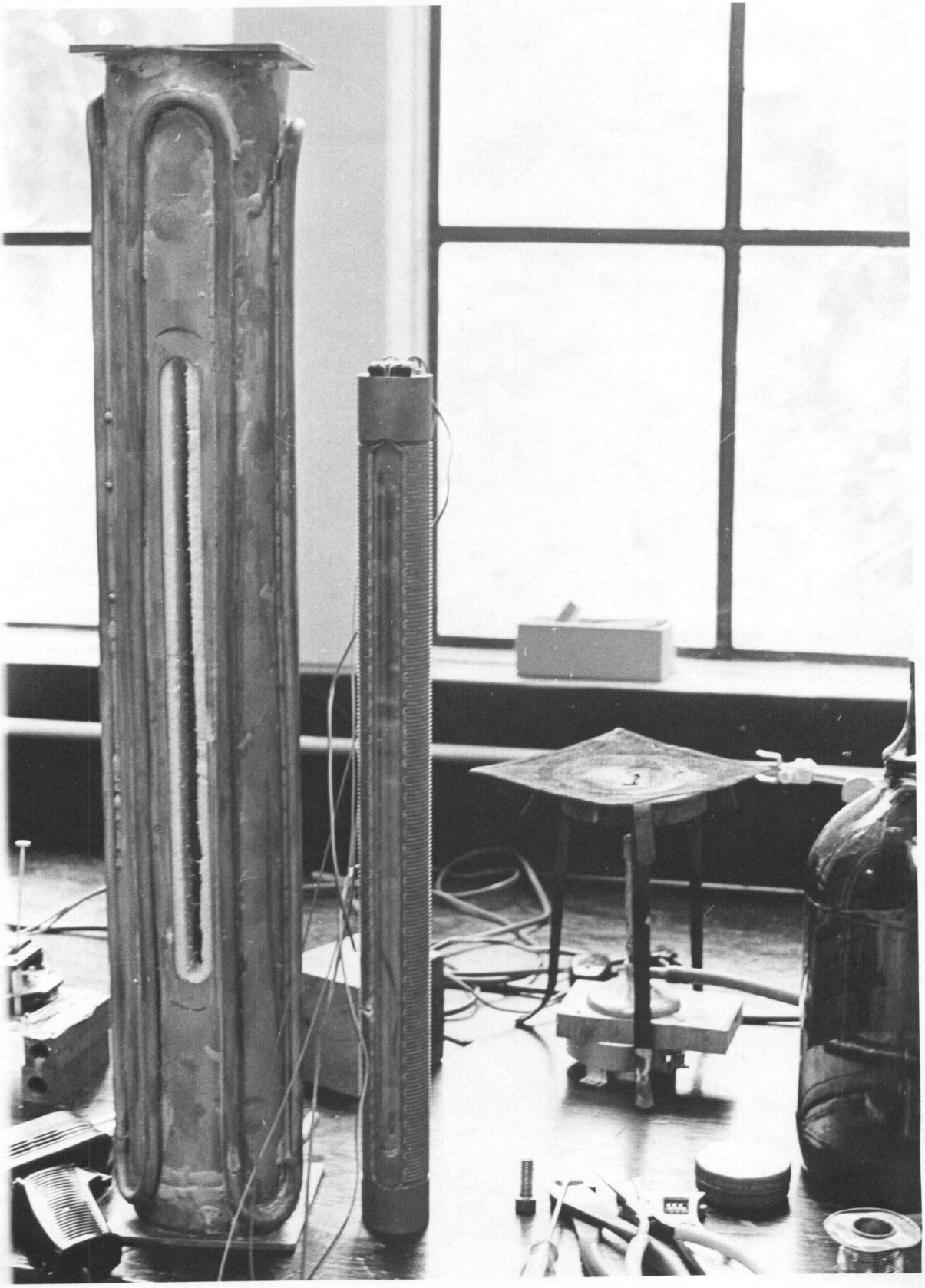

are shown in Figure 39; the points shown were obtained from three different runs. An expression of the form

$$-\frac{1}{\rho}\frac{d\rho}{dT} = \beta_0 + z(T_t - T)^{-1/2} \tag{5.26}$$

suggested by Eq. (3.53) was used to fit the data with the result that $\beta_0 = 0.81 \pm .01 \times 10^{-3}/°C$ and $z = 0.77 \pm .02 \times 10^{-3}/°C^{1/2}$. Due to the existence of an apparently stable two-phase region extending over 0.15°C, it was difficult to determine the transition temperature T_t. In this temperature interval the sample in equilibrium consisted of a nematic phase at the bottom and an isotropic phase on top separated by a well-defined meniscus. This effect was observed in both the thermometer-cells and in the quartz cells used in interferometry. If, as suggested by conoscopic measurements, $T_t = 77.75°C$, then from Eq. (5.16) the thermal expansivity $\frac{1}{\rho}\frac{d\rho}{dT}$ at 67°C is $-1.04 \times 10^{-3}/°C$ in good agreement with the result obtained in the previous section. The main problem encountered in these measurements was the segmentation of the liquid crystal filament in the capillary; this could be overcome however by using a stem with larger bore. A new cell with increased capacity utilizing an overflow trap has been made using 0.2 mm i.d. pyrex capillary; results from measurements using this cell are not yet available.

Fig. 39 Relative volume and thermal expansivity for EBBA.

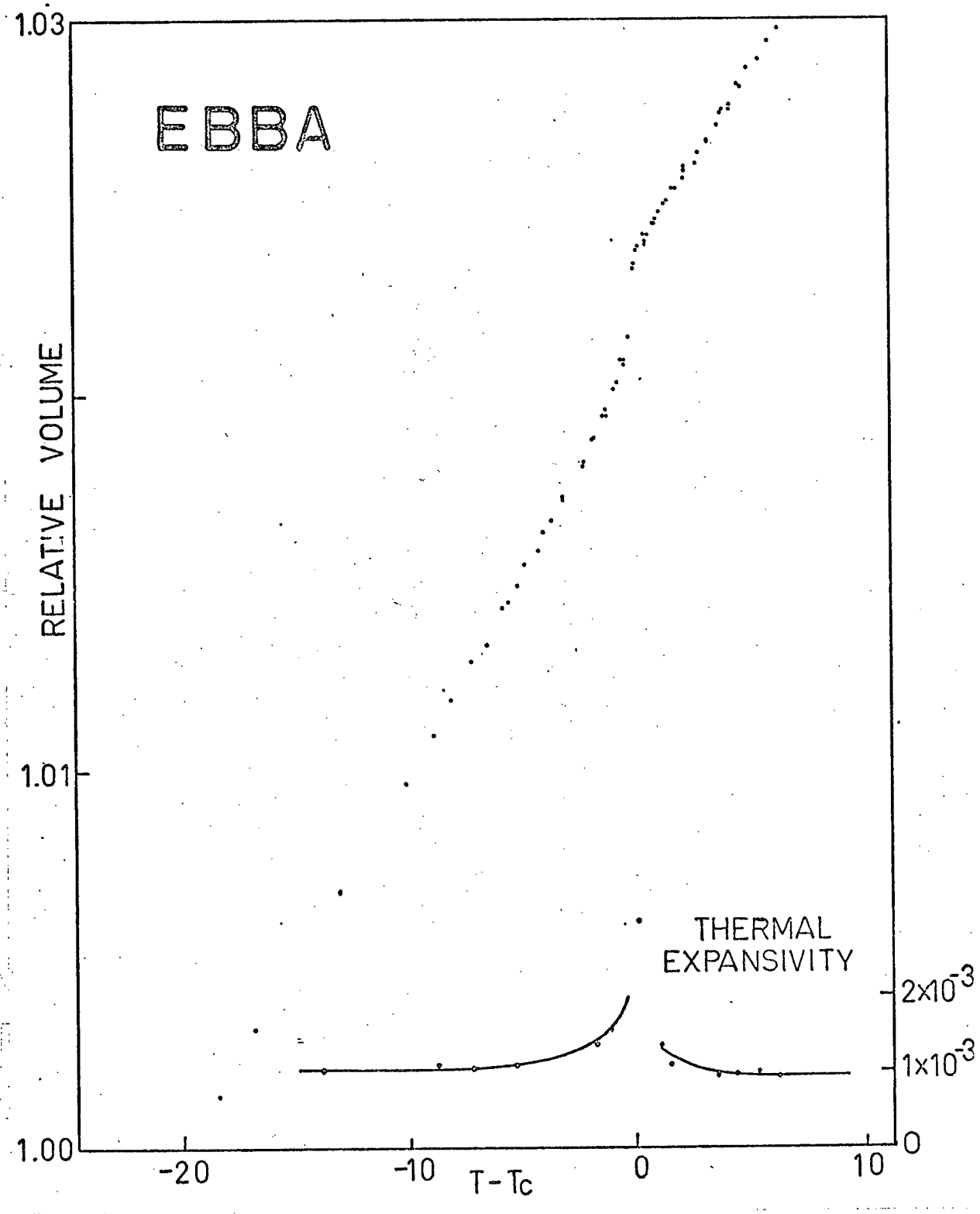
EBBA
1.03
1.01
1.00
RELATIVE VOLUME
-20
-10
T - Tc
0
10
THERMAL
EXPANSIVITY
2x10-3
1x10-3
0

5.6 The Order Parameter and the Local Field Anisotropy

The order parameter S and the local field anisotropy tensor $\eta = \eta_{zz}$ can be obtained as a function of temperature by simultaneously solving Eqs. (5.1), (5.2), (5.5) and (5.6). As shown in Appendix K, this results in

$$\alpha_{\parallel} = \frac{1}{2b}\left[3(ab-1) + \sqrt{9-30ab+9a^2b^2}\right] \tag{5.27}$$

where $a = (\alpha_{m_{\parallel}} + 2\alpha_{m_{\perp}})/3$ and

$$b = \frac{4\pi}{3}\rho\left[\frac{(n_{\parallel}^2+2)}{(n_{\parallel}^2-1)} + \frac{2(n_{\perp}^2+2)}{(n_{\perp}^2-1)}\right]. \tag{5.28}$$

S and η are then given by

$$S = \frac{\alpha_{\parallel}+\alpha_{\perp}}{\alpha_{m_{\parallel}}-\alpha_{m_{\perp}}} \tag{5.29}$$

and

$$\eta = \frac{1}{4\pi\rho\alpha_{\parallel}} - \frac{1}{3}\frac{(n_{\parallel}^2+2)}{(n_{\parallel}^2-1)} \quad . \tag{5.30}$$

In order to evaluate $\alpha_{\parallel}$, it is necessary to know $a = (\alpha_{m_{\parallel}} + 2\alpha_{m_{\perp}})/3$ and the mass density ρ_M. We have no direct way of measuring a or Δ, hence we have extrapolated published values (19) of the molecular polarizabilities of EBBA using Cauchy's formula to obtain $a = 37.1\times10^{-24}$ cm^3 and $\Delta = 9.90\times10^{-23}$ cm^3 at $\lambda = 6328$ Å. To obtain an expression for the

density consistent with our thermal expansivity measurements, we integrate Eq. (5.26) to obtain

$$\rho_M = \rho_0 \exp[\beta_0(T_t-T) + 2z(T_t-T)^{1/2}] \tag{5.31}$$

where β_0 and z are as given previously. The constant ρ_0 was determined by fitting Eq. (5.31) to published data (19) with the result that $\rho_0 = 0.977$ gm/cc; the values of ρ obtained from Eq. (5.31) were within 0.1/% to the published data over the entire 40°C temperature range. Using these values, the order parameter S and the anisotropy tensor η were calculated for EBBA as a function of temperature. The results are shown in Figures (40) and (41). Both S and η are very sensitive to density variations. In view of the poor accuracy of the available density data, we have not attempted to fit the calculated values of S to a theoretical expression. Calculated values of the local field anisotropy tensor η are in reasonable agreement with the predictions of theory; we have no explanation for the deviations from linearity.

Fig. 40. The order parameter S obtained from experimental measurements for EBBA.

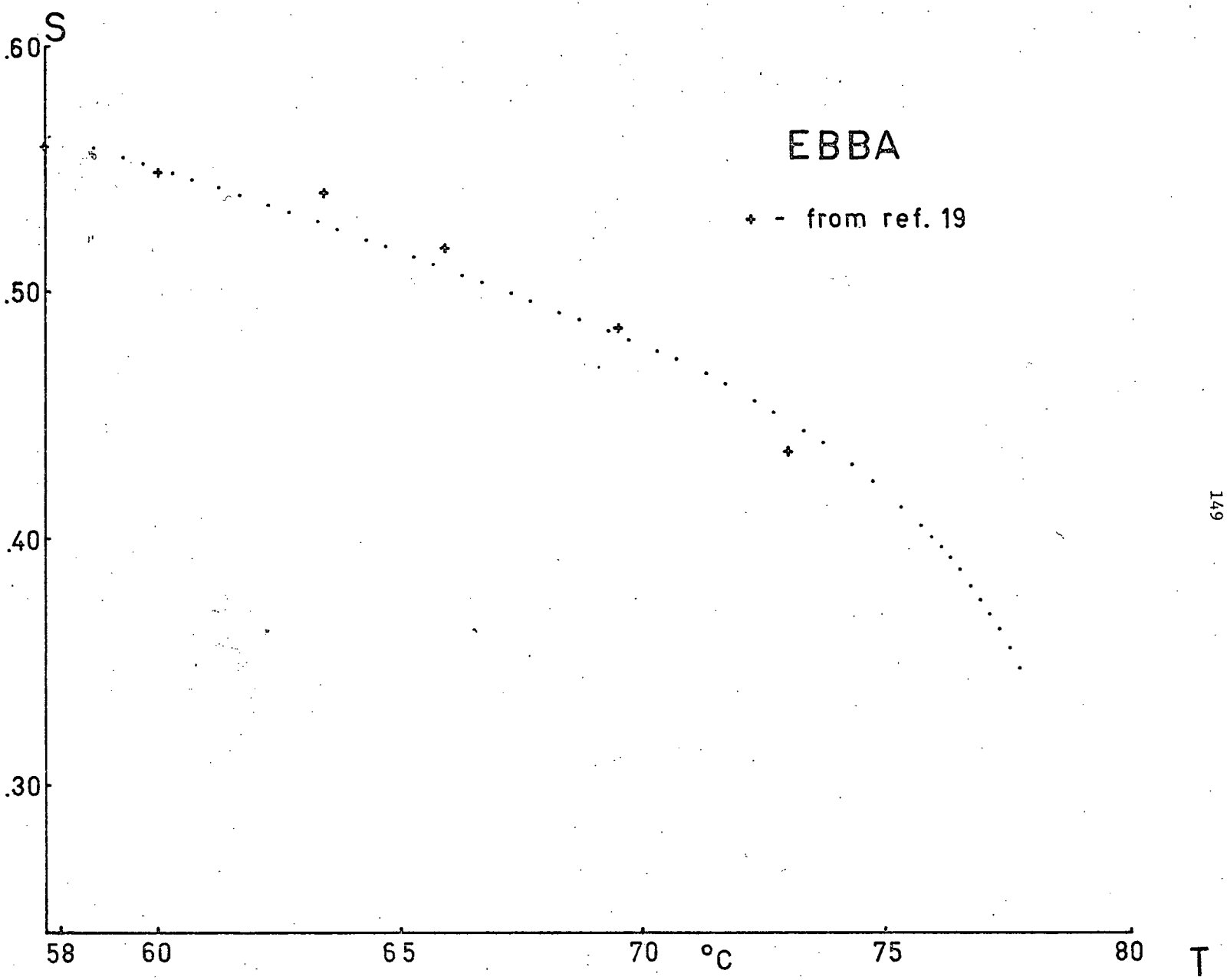
S
.60
.50
.40
.30
EBBA
+ - from ref. 19
58
60
65
70
°C
75
80
T

Fig. 41 The local field tensor η obtained from experimental measurements for EBBA.

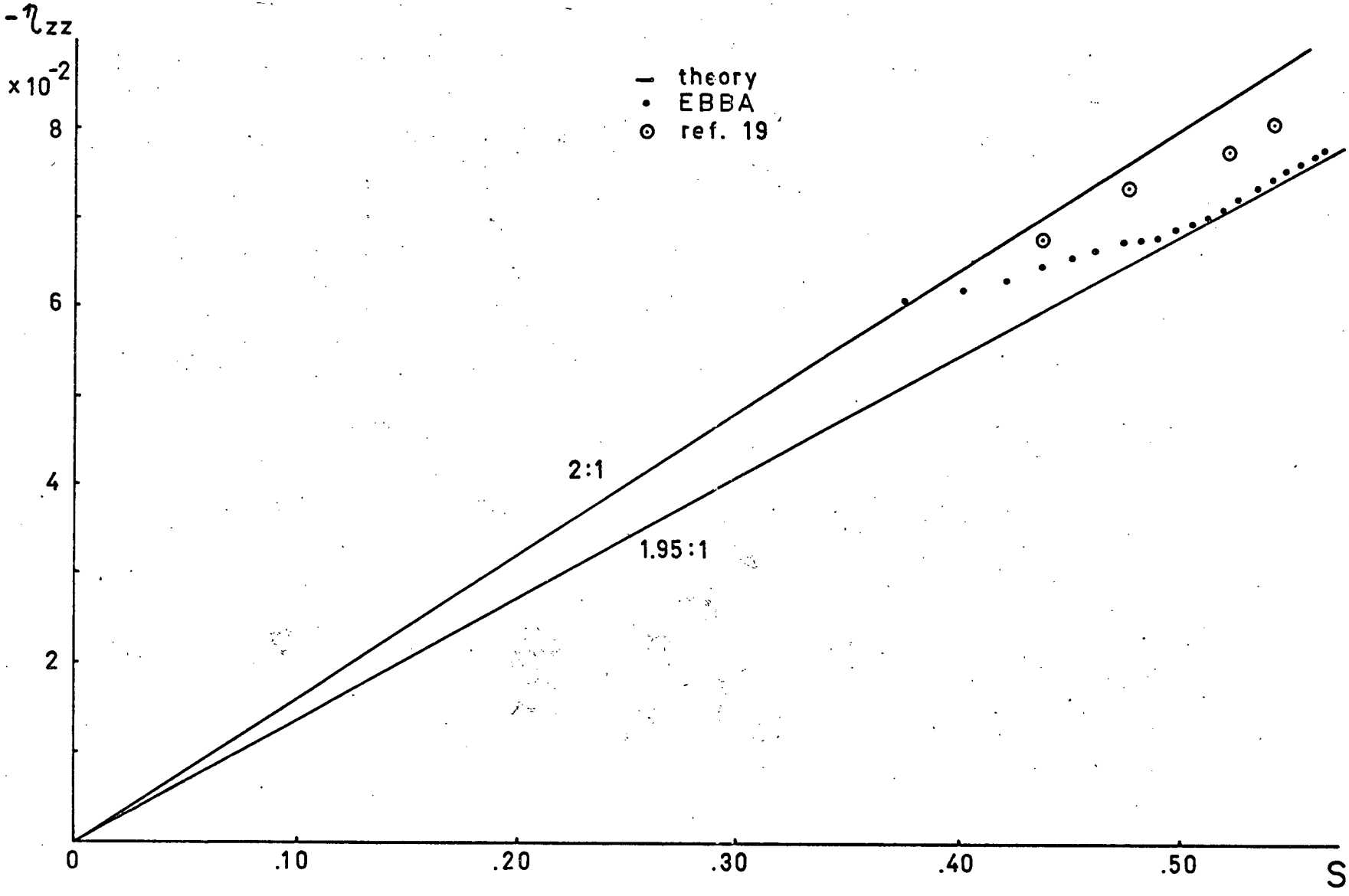
$-\eta_{zz}$
$\times 10^{-2}$
8
6
4
2
0
.10
.20
.30
.40
.50
S
theory
EBBA
ref. 19
2:1
1.95:1

CHAPTER 6

DISTORTIONS IN NEMATICS

6.1 Polarization Anomaly

The experiments described in this thesis were performed using Spindler-Hoyer Model 03-6320 polarizing filters. The 80 mm diameter filter elements were mounted on a rotatable ring with 1° divisions. Since an arrow and the letter P were inscribed at 0° on the polarizer ring; we had assumed that the electric field vector of a transmitted plane wave was co-linear with the direction of the arrow. This assumption yielded consistent results in all respects; the extraordinary (fast-decreasing) index was observed when P was along the applied $\vec{B}$-field and hence the optic axis, the ordinary (slowly increasing) index was observed when P was perpendicular to $\vec{B}$, and the conoscopic pattern of Figure 3d was observed when P was inclined at an angle of 45° to B. In addition, the conoscopic pattern was seen to disappear due to lack of contrast when P was either parallel or perpendicular to B; the polarization of the emerging wave was identical to that of the incident wave. It was felt then that the polarization and optic axis alignment were well understood. Near the completion of the experiments, however, while observing light reflected from a plane surface through a polarizer, we noticed that the electric vector $\vec{E}$ of the transmitted wave was not co-linear with P, but was instead perpendicular to it. This observation could only be reconciled with all

of the experimental results if the polarization of a wave incident on the sample was rotated an angle θ on entry, and an angle $-\theta$ on exit, where θ is the angle between the long axis of the fused quartz cell and the applied $\vec{B}$-field. Usually the angle θ was 90° since in its normal position the cell is vertical while $\vec{B}$ is horizontal, but conoscopic measurements were performed with the cell tilted in order to gain a better understanding of this effect. We concluded that there exists a transition layer in the nematic sample near the cell windows which is responsible for the rotation of polarization. The transition layer is a result of competition between field-induced alignment and strong anchoring of the nematic director $\hat{n}$ ($\hat{n} = \frac{\vec{n}}{|\vec{n}|}$) at the cell windows in the direction of the long axis of the cell. The anchoring is thought to be caused by striae on the window surfaces due to polishing during manufacture; the alignment of nematics by rubbed glass surfaces has long been known.

The effect of the twisted transition layer is clearly seen if the cell is tilted so that its long axis makes an angle θ with the $\vec{B}$-field and the conoscopic diffraction pattern is observed. The pattern does not rotate as θ is changed, since the direction $\hat{n}$ in the bulk of the sample is always along $\vec{B}$. Rotation of the crossed polarizer-analyzer pair however causes the pattern to vanish if the incident polarization is either parallel or perpendicular to the cell long axis; in this case the polarization of the emerging wave is identical to that of the incident wave. The transition region may be imagined as a set of thin uniaxial plates cut parallel to the optic axis with each plate rotated

through a small angle with respect to the preceeding one. The only significant effect of such a system is to change the polarization and phase of a wave transmitted through it; we assume therefore that all of the previously used analysis is valid if the transition layer is small compared to the bulk sample. A quantitative justification of this assumption is given in the next two sections.

6.2 Nematic Alignment

If a sample of nematic liquid crystal oriented in the direction $\hat{n}$ is placed in a uniform magnetic field $\vec{H}$, the magnetization $\vec{M}$ is given by

$$\vec{M} = \chi_{\parallel}(\vec{H}\cdot\hat{n})\hat{n} + \chi_{\perp}[\vec{H}-(\vec{H}\cdot\hat{n})\hat{n}] \tag{6.1}$$

where χ is the bulk diamagnetic susceptibility. The associated free energy per unit volume E_M is given by

$$E_M = -\int \vec{M}\cdot d\vec{H} = -\frac{1}{2}(\chi_{\parallel}-\chi_{\perp})(\vec{H}\cdot\hat{n})^2 - \frac{1}{2}\chi_{\perp}H^2 \quad . \tag{6.2}$$

Thus, if $\chi_{\parallel} > \chi_{\perp}$, E_M is minimized if $\hat{n}$ is along $\vec{H}$. Since for all known nematics the diamagnetic susceptibility is positive, the director $\hat{n}$ and hence the optic axis is expected to orient parallel to an externally applied B-field.

The free energy per unit volume associated with spatial variations of the nematic director $\hat{n}$ is given, from (23) by

$$E_D = \frac{1}{2}K_1(\nabla\cdot\hat{n})^2 + \frac{1}{2}K_2(\hat{n}\cdot(\nabla x\hat{n}))^2 + \frac{1}{2}K_3(\hat{n}x(\nabla x\hat{n}))^2 \tag{6.3}$$

where K_1, K_2 and K_3 are the elastic constants associated with the deformations splay, twist and bend respectively. Clearly E_D is a minimum if $\hat{n}$ is a constant everywhere. In the absence of external fields, then, if $\hat{n}$ is constrained to lie in a given direction at a sample boundary, surface

anchoring serves to align the bulk sample. If an external field is also present, then competition exists between the two effects; the expected alignment corresponds to spatial variations of $\hat{n}$ which minimize the total free energy. Two distinct deformations will be considered; pure twist, corresponding to the rotation of $\hat{n}$ in the plane of the cell windows from its anchored vertical direction at the cell windows to a direction parallel to B in the bulk of the sample, and a combination of bend and splay, corresponding to the rotation of $\hat{n}$ from its (nearly) vertical orientation of the liquid-vapor meniscus to a direction parallel to B in the bulk of the sample.

If $\hat{i}$, $\hat{j}$ and $\hat{k}$ are unit vectors along the x, y and z axes, then simple twist may be described by letting $\hat{n} = \cos\theta\hat{i} + \sin\theta\hat{j}$ where θ is a function of z only. Then $\hat{n}\cdot(\nabla x\hat{n}) = -\frac{\partial\theta}{\partial z}$ and contribution of twist to the free energy is

$$E_T = \frac{1}{2} K_2 \left(\frac{\partial\theta}{\partial z}\right)^2 . \qquad (6.4)$$

The combination of bend and splay may be described by letting $\hat{n} = \cos\theta\cos\phi\,\hat{i} + \cos\theta\sin\phi\hat{j} + \sin\theta\hat{k}$, where θ is a function of z only, and ϕ is a constant. Then $\nabla\cdot\hat{n} = \cos\theta\,\frac{\partial\theta}{\partial z}$ and the contribution of splay to the free energy is

$$E_S = \frac{1}{2} K_1 \cos^2\theta \left(\frac{\partial\theta}{\partial z}\right)^2 . \qquad (6.5)$$

Since $[\hat{n}x(\nabla x\hat{n})]^2 = \sin^2\theta\left(\frac{\partial\theta}{\partial z}\right)^2$, the contribution of bend to the free energy is

$$E_B = \frac{1}{2} K_2 \sin^2\theta \left(\frac{\partial\theta}{\partial z}\right)^2 . \tag{6.6}$$

In the one-constant approximation $K_1 = K_2 = K_3 = K$; formally the two distortions become identical and

$$E = \frac{1}{2} K \left(\frac{\partial\theta}{\partial z}\right)^2 . \tag{6.7}$$

To obtain $\theta(z)$ which minimizes the total energy, we consider a small slab of sample of area A and thickness t. The total energy E_F associated with the magnetization and the distortion is

$$E_F = \int_0^t A\left[-\frac{1}{2}(\chi_{\parallel}-\chi_{\perp})H^2\cos^2\theta + \frac{1}{2} K\left(\frac{\partial\theta}{\partial}\right)^2\right]dz. \tag{6.8}$$

Proceeding somewhat differently than (23), we note that the integral may be minimized by using Lagrange's equation; letting $\gamma^2 = \frac{K}{(\chi_{\parallel}-\chi_{\perp})H^2}$, θ must satisfy

$$\gamma^2 \frac{\partial^2\theta}{\partial z^2} - \sin\theta\cos\theta = 0. \tag{6.9}$$

Eq. (6.9) may be written as

$$\frac{\partial}{\partial z}\left(\frac{\gamma^2}{2}\left(\frac{\partial\theta}{\partial z}\right)^2 + \frac{1}{2}\cos^2\theta\right) = 0 \tag{6.10}$$

which yields upon integration

$$\gamma^2 \left(\frac{\partial\theta}{\partial z}\right)^2 = C_1 - \cos^2\theta \ . \tag{6.11}$$

Since $\frac{\partial\theta}{\partial z}$, $\theta \to 0$ as $z \to \infty$, $C_1 = 1$. Then

$$z = \pm\gamma \int \frac{d\theta}{\sin\theta} = \gamma \ln \tan \frac{\theta}{2} + C_2 \ . \tag{6.12}$$

Since $\theta = \frac{\pi}{2}$ if $z = 0$, $C_2 = 0$ and finally

$$\theta = 2 \tan^{-1} \exp(-z/\gamma) \tag{6.13}$$

or

$$\theta = \frac{\pi}{2} \ . \tag{6.14}$$

To determine which solution is energetically favorable for a sample of length z_0, $E_T = 0$ if $\theta = \frac{\pi}{2}$, the non-trivial solution will occur if $E_T \leq 0$, and at the Frederiksz transition

$$E_T = \int_0^{z_0} \left[\gamma^2 \left(\frac{\partial\theta}{\partial z}\right)^2 - \cos^2\theta\right] dz = 0. \tag{6.15}$$

Substitution from Eq. (6.11) gives

$$E_T = \int_0^{z_0} (1-2\cos^2\theta)dz = \int_0^{z_0} (1-2\tanh^2 z/\gamma)dz = 0 \tag{6.16}$$

and integration yields

$$\frac{z_0}{2\gamma} = \tanh \frac{z_0}{\gamma} \quad . \tag{6.17}$$

The solution of Eq. (6.17) is $z_0 = 1.915\ \gamma$. This is in good agreement with published results (23) for the case when anchoring occurs at both extremities of the twisted region; then $2z_0 = \pi\gamma$. Thus, a field greater than H_c is required to overcome surface-induced alignment in a sample of width $d = 2z_0$ where $H_c = \frac{3.83}{d}\left[\frac{K}{(\chi_{\parallel}-\chi_{\perp})}\right]^{-1/2}$. The anisotropy in the diamagnetic susceptibility is typically $\sim 10^{-7}$, while the elastic constant is $\sim 3\times10^{-7}$ dyne (23). For the d = 0.2 cm cell used in this experiment, the critical field H_c is only 33 oerstedts.

The magnetic coherence length γ for our applied 1.8 kG field is calculated to be 9.6μ. At three coherence lengths from the cell walls the director $\hat{n}$ is only at an angle of 6° from the applied field direction, thus the twisted transition region is small compared to the bulk sample width.

6.3 Propagation in a Twisted Medium

In order to determine the effect of the twisted transition region, we solve Maxwell's equations for light propagating along the twist (z) axis. (A more general derivation is given in (28)). From Eq.(1.3)

$$\frac{1}{c^2}\frac{\partial^2\vec{D}}{\partial t^2} = \nabla^2\vec{E} - \nabla(\nabla\cdot\vec{E}) \ . \tag{6.18}$$

If $\hat{i}$, $\hat{j}$ and $\hat{k}$ are unit vectors along the x, y and z axes, then the vectors

$$\hat{\eta} = \cos\theta\hat{i} + \sin\theta\hat{j} \tag{6.19}$$

$$\hat{\phi} = \sin\theta\hat{i} - \cos\theta\hat{j} \tag{6.20}$$

and $\hat{k}$ define the directions of the principal axes of the dielectric tensor; θ is a function of z. For a wave propagating along the z-axis, we let $\vec{E} = \vec{E}(z)\exp[i(\omega t-kz)]$; then $\nabla(\nabla\cdot\vec{E}) = \frac{\partial^2\vec{E}(z)}{\partial z^2}$ and Eq. (6.17) yields $D_z = E_z = 0$. We write $\vec{E}(z) = E_1\hat{\eta} + E_2\hat{\phi}$, then $\vec{D} = \varepsilon_1 E_1\hat{\eta} + \varepsilon_2 E_2\hat{\phi}$ since $\varepsilon_{\alpha\beta}$ is now diagonal. Eq. (6.17) then yields

$$\frac{1}{c^2}\frac{\partial}{\partial t^2}\left(\varepsilon_1 E_1\hat{\eta} + \varepsilon_2 E_2\hat{\phi}\right) = \frac{\partial^2}{\partial z^2}\left(E_1\hat{\eta} + E_2\hat{\phi}\right). \tag{6.21}$$

For simplicity, we assume that θ is proportional to z instead of the relation given by Eq. (6.18), that is, $\theta = \frac{2\pi z}{\lambda_h}$ where λ_h is the helix pitch. Since from Eq. (6.11) the maximum value of $\frac{d\theta}{dz} = \frac{1}{\gamma}$, a reasonable

choice of pitch is $\lambda_h = 2\pi\gamma$. Noting that $\frac{\partial}{\partial z}\hat{\eta} = -\hat{\phi}$ and $\frac{\partial}{\partial z}\hat{\phi} = \hat{\eta}$, Eq. (6.21) yields after some manipulation

$$(\varepsilon_1'-k'^2-1)E_1 = 2ikE_2 \tag{6.22}$$

and

$$(\varepsilon_2'-k'^3-1)E_2 = -2ikE_1 \tag{6.23}$$

where we have let $\varepsilon' = \varepsilon(\frac{\lambda_h}{\lambda})^2$ and $k' = \frac{k\lambda_h}{2\pi}$ where λ is the free-space wavelength of the wave. We obtain for the wave-vector k'

$$k'^2 = 1 + \varepsilon' \pm \sqrt{\delta'^2+4\varepsilon} \tag{6.24}$$

and

$$-\left(\frac{E_1}{E_2}\right)^2 = \frac{2 \mp \sqrt{\delta^2+4\varepsilon'} + \delta'}{2 \mp \sqrt{\delta^2+4\varepsilon'} - \delta'} \tag{6.25}$$

where $\varepsilon' = (\varepsilon_1'+\varepsilon_2')/2$ and $\delta' = (\varepsilon_1'-\varepsilon_2')/2$. The two solutions for $\vec{E}$ corresponding to the roots of Eq. (6.25) are

$$\vec{E}_1 = (E_{11}\hat{\eta} + E_{12}\hat{\phi})\exp[i(\omega t-k_1 z)] \tag{6.26}$$

and

$$\vec{E}_2 = (E_{21}\hat{\eta} + E_{22}\hat{\phi})\exp[i(\omega t-k_2 z)] \quad . \tag{6.27}$$

The normal modes are therefore two elliptically polarized waves, whose components are polarized along the principal axes of the dielectric tensor.

In our experiment, the magnetic coherence length γ was calculated to be $\approx$ 10μ; then $\frac{\lambda_h}{\lambda} = \frac{2\pi\gamma}{\lambda} \cong \frac{6 \times 10^{-5}m}{6.3 \times 10^{-7}m} \cong 100$. From our refractive index measurements we estimate that $\varepsilon' = 2.5 \times 10^4$ and $\delta' = 6.2 \times 10^3$. Eq. (6.23) yields for $\delta' > 2\varepsilon'$

$$k'^2 \cong 1 + \varepsilon' \pm (\delta + \frac{2\varepsilon'}{\delta}) \tag{6.28}$$

or $k_i'^2 \cong \varepsilon_i'$ within an error of 0.1%, and since $k_i = \frac{2\pi}{\lambda}\sqrt{\varepsilon_i}$, $n_i = \sqrt{\varepsilon_i}$ as before. Intensity ratios are obtained from Eq. (6.25), for $k'^2 \cong \varepsilon_1'$

$$\left|\frac{E_{11}}{E_{12}}\right|^2 \cong \frac{\delta'}{1 + \frac{\varepsilon'}{\delta'}} \cong 1000 \tag{6.29}$$

and for $k'^2 \cong \varepsilon_2'$,

$$\left|\frac{E_{21}}{E_{22}}\right|^2 \cong \frac{1 - \frac{\varepsilon'}{\delta'}}{-\delta} \cong \frac{1}{2000} \quad . \tag{6.30}$$

In our experiment therefore the normal modes are essentially plane polarized waves tracking the principal axes of the dielectric tensor with an associated refractive index n equal to $\sqrt{\varepsilon}$ to within 0.1%.

CHAPTER 7

CONCLUSIONS

7.1 Summary of Results

We have obtained a simple relation between the refractive indices, density and local field anisotropy in ordered fluids whose pair-correlation function can be made isotropic by radial scaling. Using mean field theory, we have shown that in a system of molecules with elongated hard core, the molecular distribution is anisotropic in the ordered phase. The corresponding local field anisotropy tensor is shown to be proportional to the order parameter. We have obtained an expression for the specific volume as a function of the hard-core eccentricity and the degree of orientation order. Using the order parameter obtained from the Landau theory, an expression was obtained for the density as a function of temperature.

Using a self-consistent formulation for the single particle pseudopotential, we have shown that ferroelectric order is not expected to occur for a fluid of hard rods, but may do so for a fluid of hard disks. In the latter case, the transition is expected to be of the first order. Using a single oscillator model, the London-van der Waals interaction predicts an ordered phase, but inclusion of the anisotropic hard core causes the order to vanish more abruptly than is experimentally observed.

Experimentally, we have shown that the Lorentz-Lorenz coefficient is constant to within $\pm$ 0.8% for GeH_4 and to within $\pm$ 0.5 % for SF_6 along

the coexistence curve. We have determined the critical density and temperature of GeH_4 for the first time with the result that $\rho_c = 0.504 \pm .005$ g/cc and $T_c = 38.925 \pm .05°C$.

We have measured the refractive indices of the liquid crystals EBBA and BEPC using a sensitive interferometer technique. Changes in the refractive indices were measured with an accuracy better than ±0.02%, whereas the absolute values were determined to within ±0.5%. The temperature dependence of the refractive indices was in qualitative agreement with the predictions of the theory.

We have measured the thermal expansivity of EBBA across the nematic isotropic transition, the observed behavior is in good agreement with the predictions of theory. The discontinuous volume change across the transition was ∿0.3%; the accuracy of this measurement is difficult to assess due to the existence of an apparently stable two-phase region near the transition. Using these measurements, the order parameter and local field anisotropy were calculated. Results for the order parameter are in good agreement with existing published results, while the anisotropy tensor is nearly proportional to the degree of order, as predicted by the theory.

7.2 Suggestions for Future Work

In order to exploit the sensitive refractive index measurements in the order parameter and local field tensor determination, density data of comparable accuracy is needed. To gain this end, we have constructed a special cell capable of holding 10 cc of sample; time, however, has not been available to make extensive measurements. Preliminary results using this cell indicate greatly improved accuracy. By the use of smaller f-number lenses and by photographing the diffraction pattern more frequently, the accuracy of the conoscopic measurements could be further increased. An independent scheme of measuring the cell orientation would similarly increase the accuracy of the cell rotation results, while a combination of the conoscopic and Mach-Zender interferometry could furnish additional refractive index information. We have noticed during the course of the experiments that near the transition in the nematic phase that increasing the applied B-field caused the birefringence to increase. This effect, together with the field-induced re-alignment of the nematic director merits further investigations. Exploration of the two phase region in the neighborhood of T_c may also yield information about the nature of the transition. It would be of interest to see if a relation similar to the law of corresponding states for pure fluids holds for order in nematic liquid crystals scaled to molecular eccentricity; measurements on more samples are thus required.

It is believed that the mean-field theory could be further improved if a closed-form solution for the distance of closest approach between two arbitrarily oriented elongated surfaces could be obtained.

A more realistic attractive potential consisting of coupling between two sets of three mutually orthogonal oscillators is currently being considered. Fluctuations of the nematic director have not been considered in this thesis, although known to be of considerable importance. Recently acquired photon correlation equipment is currently being set up to study light scattered from nematic materials.

APPENDIX A

Letting $x = nd_x$, $y = nd_y$ and $z = nd_z$ Eq. (1.11) may be re-written as

$$\frac{x^2}{\varepsilon_{xx}} + \frac{y^2}{\varepsilon_{yy}} + \frac{z^2}{\varepsilon_{zz}} = 1 \tag{A.1}$$

Since $\bar{D}$ is perpendicular to $\bar{k}$, $\bar{D}\cdot\bar{k} = 0$ and

$$xk_x + yk_y + zk_z = 0 \tag{A.2}$$

Furthermore, $n^2 = x^2 + y^2 + z^2$. We wish to consider extrema of n^2 subject to the constraints of Eq. (A.1) and Eq. (A.2). Using the method of Lagrange's undertermined multipliers, we wish to find the extrema of

$$F = x^2+y^2+z^2+2\lambda_1(xk_x+yk_y+zk_z) + \lambda_2\left(\frac{x^2}{\varepsilon_{xx}} + \frac{y^2}{\varepsilon_{yy}} + \frac{z^2}{\varepsilon_{zz}} - 1\right) \tag{A.3}$$

This demands that $\frac{\partial F}{\partial x} = \frac{\partial F}{\partial y} = \frac{\partial F}{\partial z} = 0$. Then

$$x + \lambda_1 k_x + \lambda_2 \frac{x}{\varepsilon_{xx}} = 0 \tag{A.4}$$

$$y + \lambda_1 k_y + \lambda_2 \frac{y}{\varepsilon_{yy}} = 0 \tag{A.5}$$

$$z + \lambda_1 k_z + \lambda_2 \frac{z}{\varepsilon_{zz}} = 0 \tag{A.6}$$

Combining Eq.'s (A.4), (A.5) and (A.6) with (A.1) and (A.2) obtains

$$n^2 + \lambda_2 = 0 \tag{A.7}$$

and

$$k^2\lambda_1 + \lambda_2\left(\frac{k_x x}{\varepsilon_{xx}} + \frac{k_y y}{\varepsilon_{yy}} + \frac{k_z z}{\varepsilon_{zz}}\right) = 0 \tag{A.8}$$

Solving for λ_1 and λ_2

$$\lambda_2 = -n^2 \tag{A.9}$$

and

$$\lambda_1 = \frac{n^2}{k^2}\left(\frac{k_x x}{\varepsilon_{xx}} + \frac{k_y y}{\varepsilon_{yy}} + \frac{k_z z}{\varepsilon_{zz}}\right) \tag{A.10}$$

Substitution into Eq. (A.4) yields

$$x\left(1 - \frac{n^2}{\varepsilon_{xx}}\right) + \frac{n^2 k_x}{k^2}\left(\frac{k_x x}{\varepsilon_{xx}} + \frac{k_y y}{\varepsilon_{yy}} + \frac{k_z z}{\varepsilon_{zz}}\right) = 0, \tag{A.11}$$

similarly for y and z. Letting $x = nd_x$, etc., in Eq. (A.11) and multiplying by D we obtain

$$D_x \left(1 - \frac{k^2 c^2}{\omega^2 \varepsilon_{xx}}\right) + \frac{c^2}{\omega^2} k_x \left(E_x k_y + E_y k_y + E_z k_z\right) = 0$$

or

$$\frac{\omega^2}{c^2} \bar{D} - k^2 \bar{E} + \bar{k}(\bar{E} \cdot \bar{k}) = 0$$

which is Eq. (1.5). Thus the permitted directions of $\bar{D}$ are those for which $n^2 = x^2+y^2+z^2$ is an extremum.

APPENDIX B

From Eq. (1.16), integration over ϕ yields

$$\eta_{zz} = \tfrac{1}{2}\int_0^{\pi} (\ln(1-e_g^2\cos^2\theta)^{\frac{1}{2}})(3\cos^2\theta-1)\sin\theta d\theta \tag{B.1}$$

If $x = \cos\theta$, integration by parts yields

$$\eta_{zz} = \tfrac{1}{2}\ln(1-e_g^2x^2)(x^3-x)\Big|_0^1 + \int_0^1 \frac{e_g^2x}{1-e_g^2x^3}\left(\frac{x^3}{3} - x\right)dx, \tag{B.2}$$

where the first term equals zero. Since $e_g^2 \leq 1$, we let $e_g x = \sin\theta$. Then

$$\eta_{zz} = \frac{1}{e_g^3}\int_0^{\sin^{-1}e} \frac{\sin^4\theta}{\cos^2\theta}\cos\theta d\theta - \frac{1}{e_g}\int_0^{\sin^{-1}e} \frac{\sin^2\theta\cos\theta d\theta}{\cos^2\theta}$$

$$= \frac{I_1}{e_g^3} - \frac{I_2}{e_g} \tag{B.3}$$

Furthermore,

$$I_1 = \int_0^{\sin^{-1}e} \frac{(1-\cos^2\theta)^2 d\theta}{\cos\theta} = \int_0^{\sin^{-1}e} \frac{d\theta}{\cos\theta} - e - \frac{e^3}{3} \tag{B.4}$$

and

$$I_2 = \int_0^{\sin^{-1}e} \frac{(1-\cos^2\theta)}{\cos\theta}\, d\theta = \int_0^{\sin^{-1}e} \frac{d\theta}{\cos\theta} - e \qquad (B.5)$$

If $y = \ln\left(\frac{1+\sin\theta}{\cos\theta}\right)$ then $dy = d\theta/\cos\theta$, and

$$\int_0^{\sin^{-1}e} \frac{d\theta}{\cos\theta} = \ln \frac{1+\sin\theta}{\cos\theta} \Bigg|_0^{\sin^{-1}e} = \ln\left(\frac{1+e_g}{\sqrt{1-e_g^2}}\right) = \ln \frac{\sqrt{1+e_g}}{\sqrt{1-e_g}}; \qquad (B.6)$$

and finally

$$\eta_{zz} = \frac{2}{3} - \frac{1}{e_g^2} - \frac{1}{2e_g}\left[1 - \frac{1}{e_g^2}\right]\ln\left[\frac{1+e_g}{1-e_g}\right] \qquad (B.7)$$

It is interesting to consider the limits of η_{zz} as $e_g \to 0$ and as $e_g \to 1$. In the first case, since

$$\tfrac{1}{2} \ln\left[\frac{1+e_g}{1-e_g}\right] = e_g + \frac{e_g^3}{3} + \frac{e_g^5}{5} + \ldots \qquad (B.8)$$

for small e_g,

$$\eta_{zz} \approx -\frac{2}{15} e_g^2 - \frac{2e_g^4}{35} \qquad (B.9)$$

and $\eta_{zz} = 0$ if $e_g = 0$. For $e_g \approx 1$, letting $x = 1-e_g$ yields

$$\eta_{zz} = \frac{2}{3} - \frac{1}{(1-x)^2} - \frac{(2-x)x}{2(1-x)} \ln\left[\frac{2-x}{x}\right] \qquad (B.10)$$

Since $\lim_{x\to 0} x\ln x = 0$, $\eta_{zz} = -\frac{1}{3}$ if $e_g = 1$. In Figure B1, η_{zz} is shown as a function of e_g.

Fig. B.1 The local field anisotropy tensor η_{zz} as function of the eccentricity e_g.

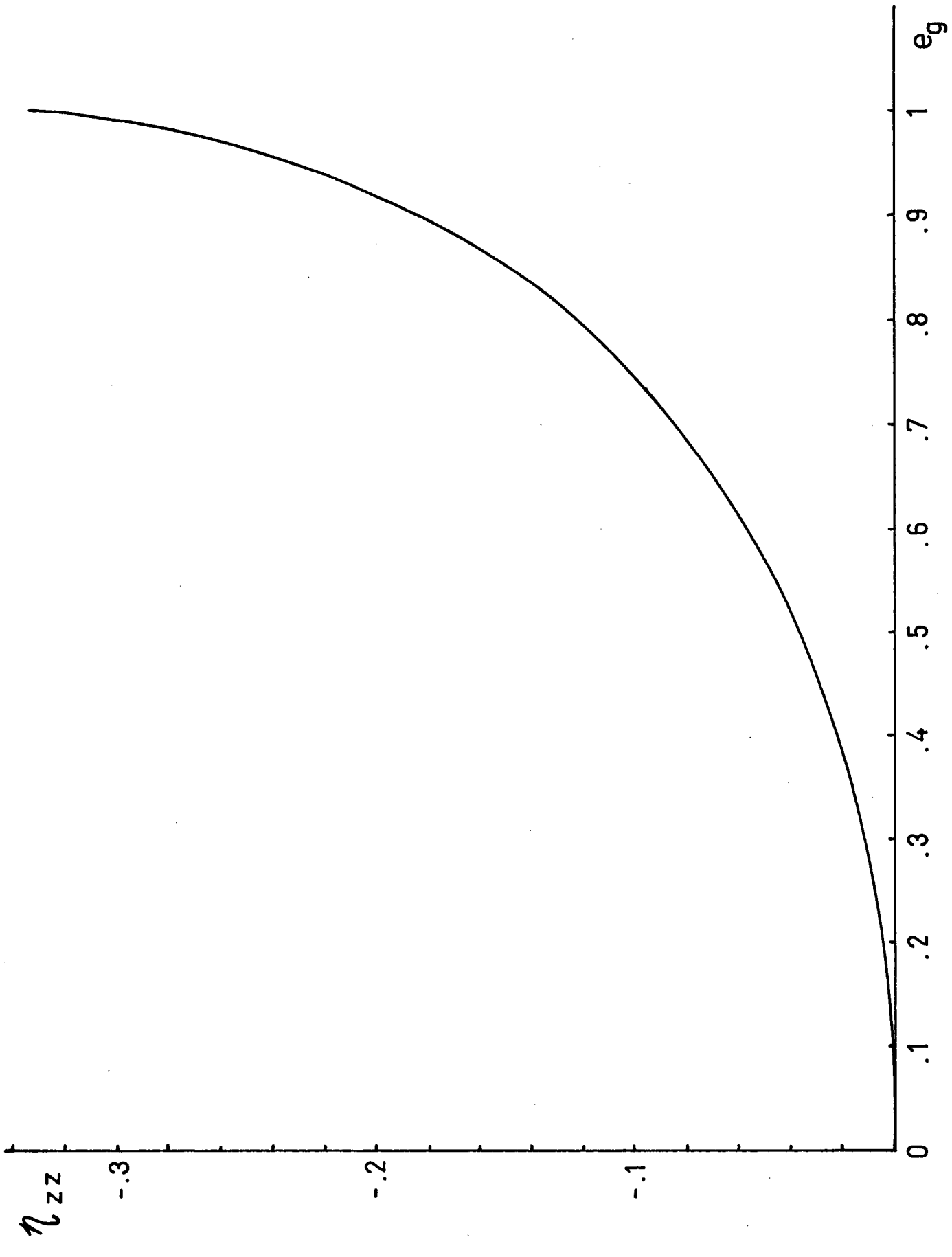
η_{zz}
-.3
-.2
-.1
0
.1
.2
.3
.4
.5
.6
.7
.8
.9
1
e_g

APPENDIX C

From Eq. (2.20)

$$\Delta F = a_2 R^2 + a_4 R^4 + a_6 R^6 \tag{C.1}$$

and the conditions that ΔF be negative and a minimum, i.e. $\Delta F \leq 0$, $\frac{\partial \Delta F}{\partial R} = 0$ and $\frac{\partial^2 \Delta F}{\partial R^2} \geq 0$ yield, respectively

$$a_2 R^2 + a_4 R^4 + a_6 R^6 \leq 0 \tag{C.2}$$

$$2a_2 R + 4a_4 R^3 + 6a_6 R^5 = 0 \tag{C.3}$$

and

$$2a_2 + 12a_4 R^2 + 30a_6 R^4 \geq 0. \tag{C.4}$$

At the transition, $\Delta F = 0$, $R = R_c$ and $T = T_c$. Eliminating a_2 between Eqs. (C.1) and (C.2) and solving for R_c yields $R_c = 0$ or $R_c^2 = \frac{-a_4}{2a_6}$. If $R_c = 0$, then R is small near the transition, and Eq. (C.3) yields $R^2 \tilde{=} \frac{-a_3}{2a_4}$. Then, if $a_4 > 0$,

$$R^2 = \frac{q}{2a_4}(T_0 - T) \quad . \tag{C.5}$$

Substitution of $R^2 = \frac{-a_2}{2a_4}$ into Eq. (C.1) yields

$$\Delta F \tilde{=} R^2 \left(a_2 + a_4\left(\frac{-a_2}{2a_4}\right)\right) = R^2 \frac{a_2}{2} \leq 0 \tag{C.6}$$

for $T \leq T_0$.

Substitution of $R^2 = \frac{-a_2}{2a_4}$ into Eq. (C.4) yields

$$\frac{\partial^2 \Delta F}{\partial R^2} \tilde{=} 2a_2 + 12a_4\left(\frac{-a_2}{2a_4}\right) = -4a_2 \geq 0 \tag{C.7}$$

for $T \leq T_0$.

If $R_c^2 = \frac{-a_4}{2a_6}$, then, solving Eq. (C.3) directly yields, if $a_4 < 0$ and $a_6 > 0$,

$$R^2 = \frac{2}{3} R_c^2 + k_1'\sqrt{T_c^+ - T} \tag{C.8}$$

where $k_1'^2 = \frac{q}{3a_6}$ and $T_c^+ = T_0 + \frac{a_4^2}{3qa_6}$. To obtain T_c, substitution of $R_c^2 = \frac{-a_6}{2a_6}$ into Eq. (C.8) yields $T_c = T_0 + \frac{a_4^2}{4qa_6}$. Straightforward substitutions show that Eq. (C.4) is satisfied for $T \leq T_c^+$, while Eq. (C.1) is satisfied for $T \leq T_c$.

From Eq. (2.23)

$$\Delta F = b_2 S^2 + b_3 S^3 + b_4 S^4 \tag{C.9}$$

and the conditions that ΔF be negative and a minimum, i.e. $\Delta F \leq 0$, $\frac{\partial \Delta F}{\partial S} = 0$ and $\frac{\partial^2 \Delta F}{\partial S^2} \geq$ yield, respectively

$$b_2 S^2 + b_3 S^3 + b_4 S^4 \leq 0 \tag{C.10}$$

$$2b_2 S + 3b_3 S^2 + 4b_4 S^3 = 0 \tag{C.11}$$

and

$$2b_2 + 6b_3S + 12b_4S^2 \geq 0 \tag{C.12}$$

At the transition, $\Delta F = 0$, $S = S_c$ and $T = T_c$. Eliminating b_2 between Eqs. (C.9) and (C.11) and solving for S_c yields $S_c = 0$ or $S_c = \frac{-b_2}{2b_4}$. If $S_c = 0$, then S is small near the transition, and Eq. (C.11) yields $S \simeq \frac{-2b_2}{3b_3}$. Then, if $b_3 > 0$,

$$S = \frac{2q}{3b_3}(T_0 - T) \tag{C.13}$$

Substitution of $S = \frac{-2b_3}{3b_3}$ into Eq. (C.9) yields

$$\Delta F \cong S^2\left(b_2 + b_3\left(\frac{-2b_2}{3b_3}\right)\right) \cdot S^2 \frac{b_2}{3} \leq 0 \tag{C.14}$$

for $T \leq T_0$. Substitution of $S = \frac{-2b_2}{3b_3}$ into Eq. (C.12) yields

$$\frac{\partial^2 \Delta F}{\partial R^2} \simeq 2b_2 + 6b_3\left(\frac{-2b_2}{3b_3}\right) = -2b_2 \geq 0 \tag{C.15}$$

for $T \leq T_0$.

The absolute minimum of ΔF is attained however if $S = -1$; then, near T_0

$$\Delta F \cong -b_3 - |b_4| \tag{C.16}$$

since $b_4 < 0$.

APPENDIX D

We wish to find the length of the normal projection of the surface

$$R^2 - e^2(\vec{R}\cdot\hat{n})^2 = R_0 \tag{D.1}$$

onto a line in direction $\hat{\ell}$ through the origin. The normal $\vec{N}$ to the surface is given by

$$\vec{N}(\vec{R}) = \vec{\nabla}[R^2-e^2(\vec{R}\cdot\hat{n})^2] = 2\vec{R}-2e^2(\vec{R}\cdot\hat{n})\hat{n} \tag{D.2}$$

The point at which $\vec{N}$ is colinear with $\hat{\ell}$ is given by $\vec{N}(\vec{R}_u) = 2u\hat{\ell}$, where u is some constant. The projection d_+ of the surface onto the line is then $d_+ = 2\vec{R}_u\cdot\hat{\ell}$. To obtain $\vec{R}_u$, consider

$$\vec{R}_u - e^2(\vec{R}_u\cdot\hat{n})\hat{n} = u\hat{\ell} \tag{D.3}$$

Multiplication by $\hat{n}$, $\hat{\ell}$ and $\vec{R}_u$ yields, respectively,

$$(1-e^2)(\vec{R}_u\cdot\hat{n}) = u(\hat{\ell}\cdot n), \tag{D.4}$$

$$\vec{R}_u\cdot\hat{\ell} - e^2(\vec{R}_u\cdot\hat{n})(\hat{n}\cdot\hat{\ell}) = u \tag{D.5}$$

and

$$R_u^2 - e^2(\vec{R}_u\cdot\hat{n})^2 = u(\vec{R}_u\cdot\hat{\ell}) = R_0^2 \tag{D.6}$$

Combining Eqs. (D.4), (D.5) and (D.6) yields

$$\vec{R}_u \cdot \hat{\ell} - \frac{e^2 R_0^2}{(1-e^2)} \frac{(\hat{\ell}\cdot\hat{u})^2}{(\vec{R}_u \cdot \hat{\ell})} = \frac{R_0^2}{(\vec{R}_u \cdot \hat{\ell})} \tag{D.7}$$

and finally

$$d_+^2 = 4(\hat{R}_4 \cdot \hat{\ell})^2 = 4R_0^2(1 + \frac{e^2}{1-e^2} (\hat{\ell}\cdot\hat{u})^2). \tag{D.8}$$

The length of the line in the $\hat{\ell}$ direction intercepted by the surface is simply given by

$$d_-^2 = 4R_0^2(1 - e^2(\hat{\ell}\cdot\hat{u})^2)^{-1}. \tag{D.9}$$

Noting that, for a random variable x, $\overline{x^m} \geq \bar{x}^m$ for all positive even m, Eq. (D.8) gives

$$\bar{d}_+ \leq 2R_0 \left(1 + \frac{e^2}{1-e^2} \overline{(\hat{\ell}\cdot\hat{n})^2}\right)^{1/2}. \tag{D.10}$$

Expanding d_-, given by Eq. (D.9), in a Taylor series in $\overline{(\hat{\ell}\cdot\hat{n})^2}$ and averaging yields

$$\bar{d}_- = 2R_0(1 + \frac{1}{2} e^2 \overline{(\hat{\ell}\cdot\hat{n})^2} + \ldots.) \geq 2R_0(1-e^2\overline{(\hat{\ell}\cdot\hat{n})^2}) \tag{D.11}$$

APPENDIX E

We wish to evaluate the integrals in Eq. (3.42)

$$R = \frac{\int_0^{\pi} \cos\theta \exp(\beta\mu H_E \cos\theta)\sin\theta d\theta}{\int_0^{\pi} \exp(\beta\mu H_E \cos\theta)\sin\theta d\theta} \quad . \tag{E.1}$$

Letting $\gamma = \beta\mu H_E$ and $x = \cos\theta$ yields

$$R = \frac{\int_{-1}^{1} x\, e^{\gamma x}\, dx}{\int_{-1}^{1} e^{\gamma x}\, dx} = \frac{e^{\gamma x}\frac{x}{\gamma} - \frac{1}{\gamma^2}\Big|_{-1}^{1}}{\frac{1}{\gamma} e^{\gamma x}\Big|_{-1}^{1}} = \frac{(e^{\gamma}+e^{-\gamma}) - \frac{1}{\gamma}(e^{\gamma}-e^{-\gamma})}{e^{\gamma}-e^{-\gamma}} \tag{E.2}$$

and

$$R = \coth\gamma - \frac{1}{\gamma} = L(\beta\mu H_E) \quad . \tag{E.3}$$

S is obtained by noting that, from Eq. (E.2) $\frac{\partial R}{\partial \gamma} = \frac{1}{3}(2S+1) - R^2$.

Then

$$S = \frac{3}{2}\left(R^2 + \frac{\partial R}{\partial \gamma}\right) - \frac{1}{2} = \frac{3}{2}\left(\coth^2\gamma - \frac{2}{\gamma}\coth\gamma + \frac{1}{\gamma^2} - \frac{1}{\sinh^2\gamma} + \frac{1}{\gamma^2}\right) - \frac{1}{2} \tag{E.4}$$

and

$$S = 1 - \frac{3}{\gamma}(\coth\gamma - \frac{1}{\gamma}) = 1 - \frac{3}{\gamma} L(\gamma) \quad .$$

APPENDIX F

Rotational symmetry about the z-axis implies that $S_{\alpha\beta}$ is diagonal and is given by Eq. (2.10), and consequently, from Eq. (3.31), $D(\hat{r})$ and $f_S(\hat{r})$ are independent of the longitude ϕ_r. Eq. (3.74) then simplifies as follows:

$$\bar{\varepsilon}_1(\Omega) = A\, n_{1\alpha} n_{1\gamma}\left[\frac{1}{3}(2S_{\beta\delta}+\delta_{\beta\delta})\right] \tag{F.1}$$

$$= \int_0^{2\pi}\int_0^{\pi} (9r_\alpha r_\beta r_\gamma r_\delta - 3r_\alpha r_\beta \delta_{\gamma\delta} - 3r_\gamma r_\delta \delta_{\alpha\beta} + \delta_{\alpha\beta}\delta_{\gamma\delta}) \frac{\sin\theta_r\, d\theta_r\, d\phi_r}{f_S^3(\cos^2\theta_r)}$$

where $A = -\dfrac{\rho\mu_S^2\alpha_n}{48R_0^3}$. Upon multiplying through, the first term I, in the integrand becomes

$$I_1 = 3n_{1\alpha}n_{1\gamma}r_\alpha r_\beta r_\gamma r_\delta(2S_{\beta\delta}+\delta_{\beta\delta}) = 3n_{1\alpha}n_{1\gamma}r_\alpha r_\gamma(2r_\beta r_\delta S_{\beta\delta}+1) \tag{F.2}$$

and since $S_{\beta\delta}$ is diagonal and $S = S_{zz} = -\frac{1}{2}S_{xx} = -\frac{1}{2}S_{yy}$

$$I_1 = 3n_{1\alpha}n_{1\gamma}r_\alpha r_\gamma(1+S(3\cos^2\theta-1)). \tag{F.3}$$

Since integration over ϕ_r eliminates all the off-diagonal elements of $r_\alpha r_\gamma$ to obtain

$$I_1 = 3n_{1\alpha}^2 r_\alpha^2(1+S(3\cos^2\theta-1)). \tag{F.4}$$

Proceeding as above, the following terms in the integrand are

$$I_2 = -n_{1\alpha}n_{1\gamma}r_\alpha r_\beta \delta_{\gamma\delta}(2S_{\beta\delta}+\delta_{\beta\delta}) = -n_{1\alpha}^2 r_\alpha^2(2S_{\alpha\alpha}+1) \tag{F.5}$$

$$I_3 = -n_{1\alpha}n_{1\gamma}r_\gamma r_\delta \delta_{\alpha\beta}(2S_{\beta\delta}+\delta_{\beta\delta}) = -n_{1\alpha}^2 r_\alpha^2(2S_{\alpha\alpha}+1) \tag{F.6}$$

$$I_4 = \frac{1}{3} n_{1\alpha}n_{1\gamma}\delta_{\alpha\beta}\delta_{\gamma\delta}(2S_{\beta\delta}+\delta_{\beta\delta}) = \frac{2}{3} n_{1\alpha}^2 S_{\alpha\alpha} + \frac{1}{3} \tag{F.7}$$

Expressing the components of $\hat{n}_1$ and $\hat{r}$ in terms of polar angles and integrating over ϕ_r yields

$$\frac{I_1}{2\pi} = S\,\frac{(3\cos^2\theta_1-1)}{2}\left[9\cos^4\theta_r-6\cos^2\theta_r+1\right] + 2S\,\frac{(3\cos^2\theta_r-1)}{2}$$

$$+ 2\,\frac{(3\cos^2\theta_1-1)}{2}\,\frac{(3\cos^2\theta_r-1)}{2} + 1 \tag{F.8}$$

$$\frac{I_2+I_3}{2\pi} = -S\,\frac{(3\cos^2\theta_1-1)}{2}\,(2\cos^2\theta_r-\frac{2}{3}) - \frac{4S}{3}\,\frac{(3\cos^2\theta_r-1)}{2}$$

$$- \frac{4}{3}\,\frac{(3\cos^2\theta_1-1)}{2}\,\frac{(3\cos^2\theta_r-1)}{2} - \frac{2}{3} \tag{F.9}$$

and

$$\frac{I_4}{2\pi} = -S\,\frac{(3\cos^2\theta_1-1)}{2}\,(\frac{2}{3}) + \frac{1}{3}\,. \tag{F.10}$$

Summing all the terms finally yields

$$\bar{\varepsilon}_1(\Omega) = 2\pi A \int_0^{\pi} \left[\frac{2}{3} + \frac{2}{3} \frac{(3\cos^2\theta_r - 1)}{2} \left(S + \frac{(3\cos^2\theta_1 - 1)}{2} \right) \right.$$

$$\left. + S \frac{(3\cos^2\theta_1 - 1)}{2} (9\cos^4\theta_r - 8\cos^2\theta_r + 1) \right] \frac{\sin\theta d\theta}{f_S^3(\hat{r})} . \qquad \text{(F.11)}$$

APPENDIX G

The self-consistent equation for S given by Eq. (3.79) becomes, on letting $x = \cos\theta$

$$S = \frac{\int_0^1 \frac{1}{2}(3x^2-1)e^{\frac{1}{2}(3x^2-1)\phi(S)\beta}\,dx}{\int_0^1 e^{\frac{1}{2}(3x^2-1)\phi(S)\beta}\,dx} \tag{G.1}$$

Letting $a_0 = \frac{3}{2}\phi(S)\beta$, and noting that $\overline{x^2} = (1+2S)/3$

$$\overline{x^2} = \frac{\int_0^1 x^2\, e^{a_0x^2}\,dx}{\int_0^1 e^{a_0x^2}\,dx} = \frac{1}{2a_0}\left[\frac{e^{a_0}}{I} - 1\right] \tag{G.2}$$

where

$$I = \int_0^1 e^{a_0x^2}\,dx = \sum_{n=0}^{\infty} \frac{a_0^n}{(2n+1)n'}. \tag{G.3}$$

It is worth noting that the series converges rapidly; since $n! \geq n^n e^{-n}$, the remainder after N terms is bounded by

$$R_N \leq \sum_{n=N}^{\infty} \left(\frac{a_0 e}{n}\right)^n. \tag{G.4}$$

Since a_0 is the order of unity, only about 10 terms are needed to get seven place accuracy, thus eliminating the need to use tabulated values of Dawson's integral. Eq. (G.2) is solved as follows. The constant a_0 may be written as

$$a_0 = \frac{A}{T}\,\phi_1(S) \tag{G.5}$$

where $\phi_1(S)$ is a polynomial in S whose coefficients are known for a given eccentricity e_g from Eq. (3.77). The constant A incorporates the oscillator strengths, hard sphere radius, packing fraction, etc.; $T' = T/A$ is regarded as a normalized temperature. An arbitrary value of a_0 is chosen to begin with, the corresponding value of S is obtained from Eq. (G.2). Once S is known, a, c and e_g can be calculated for a given molecular eccentricity e, and $\phi_1(S)$ can be evaluated. The normlized temperature corresponding to this value of S is simply $T' = \dfrac{\phi_1(S)}{a_0}$. Thus S vs. T' is obtained simply without resorting to root-finding techniques. S decreases monotonically with a_0; T' however first increases to T'_c, then decreases. Only those values of S are of interest which decrease with increasing T'. Having determined T'_c, the reduced temperature is obtained from the relation $1 - \frac{I}{T_c} = 1 - \frac{T'}{T'_c}$, .

APPENDIX H

The windows of the cell have surfaces which are nearly parallel; the first window has a wedge angle of less than 0.01° and the exit window has a wedge angle of 0.080°. If the windows had perfectly parallel surfaces, then the deviation angle for air in the cell would be zero and would be identical to the reference angle measured with the cell removed. The effect of the window wedges can be calculated and if the deviation angle measured with air in the cell is used as a zero deviation angle, the effect of the window wedge angles can be neglected.

The wedge angle of the first window is only 0.01° and is neglected in the following calculation. The geometry of the cell is shown in Figure H.1. Let the prism angle between the windows be denoted by α and the wedge angle of the second window by ϕ. The angle ϕ is of opposite sense to the prism angle α for the cell used in this experiment. Consider a ray entering the cell perpendicular to the first window. Application of Snell's law at the surfaces leads to the following equations:

$$n\sin\alpha = n_s\sin(\psi+\phi) \tag{H.1}$$

$$n_s\sin\psi = n_a\sin(\alpha-\phi+\theta) \tag{H.2}$$

where n, n_s and n_a are the refractive indices of the sample fluid, sapphire window and air. Elimination of ψ yields

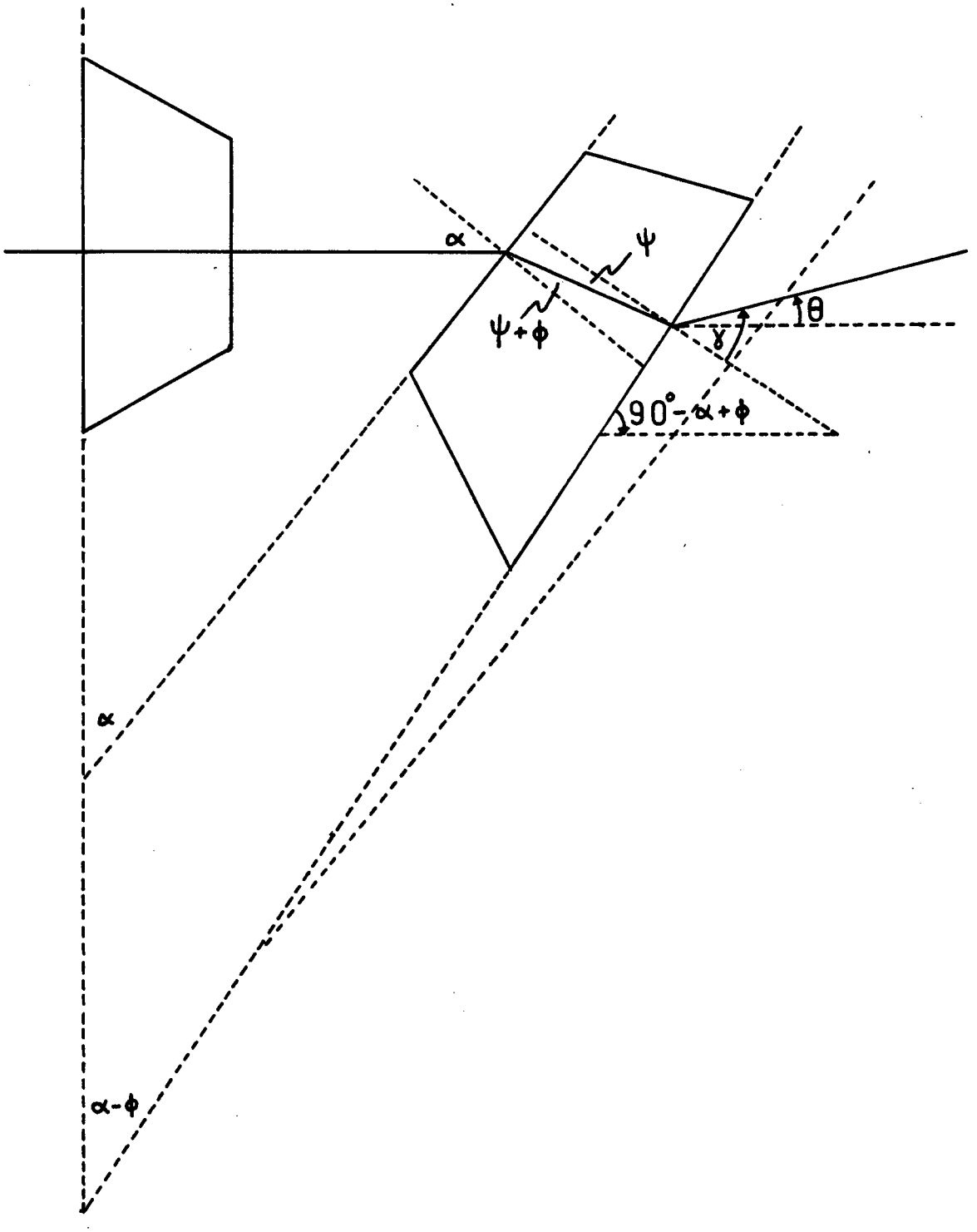

Fig. H.1 Prism cell geometry.

$$n\sin\alpha = n_a \sin(\alpha-\phi+\theta)\cos\phi+\sin\phi(n_S^2-n_a^2\sin^2(\alpha-\phi+\theta))^{1/2}. \qquad (H.3)$$

Expanding in $\sin\theta$ and retaining the first three terms gives

$$n\sin = a + b\sin\theta + c\sin^2\theta . \qquad (H.4)$$

Since the coefficients a, b and c are derivatives of $n\sin\alpha$ with respect to $\sin\theta$ evaluated at $\theta = 0$, differentiation of Eq. (H.3) with respect to $\sin(\alpha-\phi+\theta)$ and application of the chain rule yields

$$a = \sin\alpha \Big|_{\theta=0} = n_a \sin(\alpha-\phi)\cos\phi + \sin\phi(n_S^2-n_a^2\sin^2(\alpha-\phi))^{1/2} . \qquad (H.5)$$

$$b = \frac{\partial(n\sin\alpha)}{\partial\sin\theta} = -\frac{1}{2}\left[n_a^2\cos\phi - \frac{n_a\sin\phi\sin(\alpha-\phi)}{(n_S^2-n_a^2\sin^2(\alpha-\phi))^{1/2}}\right]\cos(\alpha-\phi) \qquad (H.6)$$

and

$$c = \frac{1}{2}\frac{\partial^2(n\sin\alpha)}{\partial(\sin\theta)^2}\Big|_{\theta=0} = -\frac{1}{2}\left[\frac{n_a^2 n_S^2\sin\phi\cos^2(\alpha-\phi)}{(n_S^2-n_a^2\sin^2(\alpha-\phi))^{3/2}} + n_a\cos\phi\sin(\alpha-\phi)\right.$$

$$\left. - \frac{n_a^2\sin\phi\sin^2(\alpha-\phi)}{(n_S^2-n_a^2\sin^2(\alpha-\phi))^{1/2}}\right]. \qquad (H.7)$$

If the cell is filled with air at normal density and the deviation angle θ_a is measured, Eq. (H.6) yields

$$n = \frac{1}{\sin\alpha}\left[n_a + (\sin\theta-\sin\theta_a)[b + c(\sin\theta+\sin\theta_a)]\right] . \qquad (H.8)$$

The use of θ_a rather than the angle measured with the cell removed eliminates most of the effect due to the window wedges. If the first window were also wedged, the above expression could be appropriately modified.

APPENDIX I

The geometry of the cell rotated through an angle θ is shown in Figure I.1. ℓ_N and ℓ_1 are the path lengths of rays through the evacuated position of the cell, and through that portion which is filled with the liquid crystal sample, respectively. For incident light polarized perpendicular to the optic axis, Snell's law is obeyed, and

$$\sin\theta = n \sin\theta_1 \tag{I.1}$$

where $n = n_\perp/n_A$ and $n_A = 1.00029$ is the refractive index of air. Since

$$\ell_N\cos\theta = \ell \tag{I.2}$$

$$\ell_1\cos\theta_1 = \ell \tag{I.3}$$

and

$$\ell_2 = t \sin\theta = (\ell_N\sin\theta-\ell_1\sin\theta_1)\sin\theta \ , \tag{I.4}$$

The optical path length difference L between the two rays is

$$L = n\ell_1 + \ell_2 - \ell_N$$

$$= \frac{n\ell}{\cos\theta_1} + \frac{\ell\sin^2\theta}{\cos\theta} - \frac{\ell\sin^2\theta}{n\cos\theta_1} - \frac{\ell}{\cos\theta}$$

$$= \ell\left[\sqrt{n^2-\sin^2\theta} - \cos\theta\right]. \tag{I.5}$$

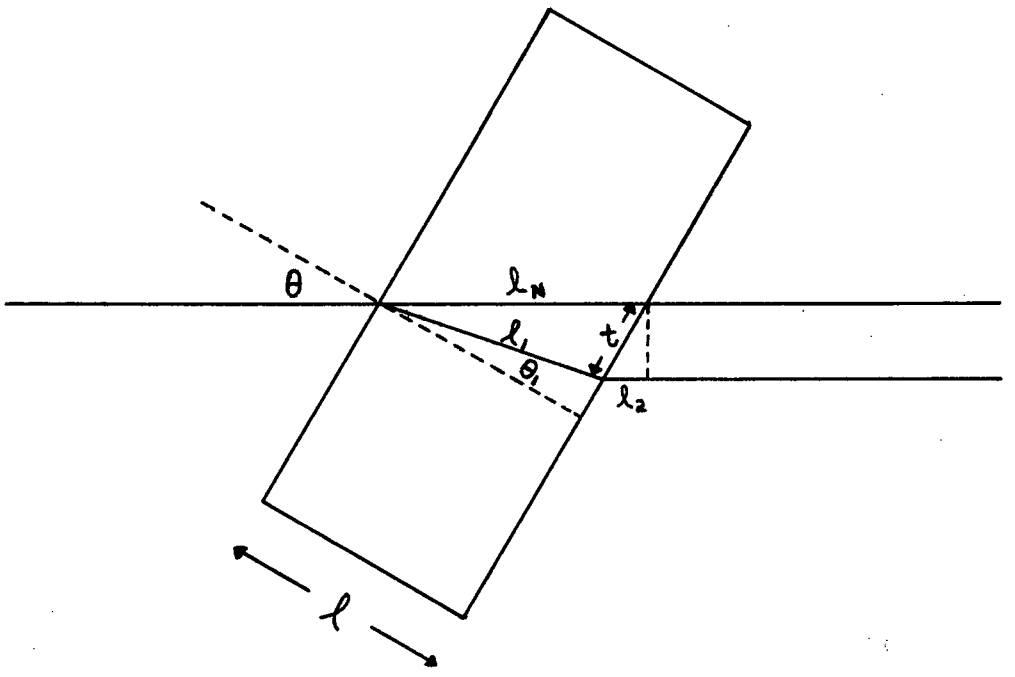

Fig. I.1 Geometry of rotated cell.

The change in the optical path length difference L if the cell is rotated from zero angle to an angle θ is

$$\Delta L = \ell\left[\sqrt{n^2-\sin^2\theta} - \cos\theta - n+1\right] . \tag{I.6}$$

Letting $\Delta L = (\Delta N+\varepsilon)\lambda$, Eq. (I.6) yields

$$\left(\frac{\Delta N\lambda}{\ell} + \cos\theta-1\right) + \frac{\varepsilon\lambda}{\ell} + n = \sqrt{n^2-\sin^2\theta} . \tag{I.7}$$

Letting

$$x = \frac{\Delta N\lambda}{\ell} + \cos\theta-1$$

$$a = -2\left(\frac{\varepsilon\lambda}{\ell} + n\right)$$

$$b = n^2 - \left(\frac{a}{2}\right)^2$$

and squaring Eq. (I.7) yields

$$x^2 + \sin^2\theta = ax + b . \tag{I.8}$$

APPENDIX J

If a plane wave of angular frequency ω and wave vector $\vec{k}_i$ is incident on a plane dielectric boundary and $\vec{k}_s$ is the wave vector of the transmitted wave, then continuity of the tangential component of the $\vec{E}$-field across the boundary demands that

$$\omega t - \vec{k}_i \cdot \vec{r} = \omega t - \vec{k}_S \cdot \vec{r} \tag{J.1}$$

everywhere on the boundary. If $\vec{r}$ is in the plane of the boundary, then

$$k_i \cos\left(\frac{\pi}{2} - \theta_i\right) = k_S \cos\left(\frac{\pi}{2} - \theta_S\right) \tag{J.2}$$

where θ_i and θ_S are the angles between $\vec{k}_i$ and $\vec{k}_S$ and the normal to the boundary. Since $k = \frac{2\pi n}{\lambda}$,

$$n_i \sin\theta_i = n_S \sin\theta_S, \tag{J.3}$$

where n_i and n_S are the refractive indices in the two media. Thus Snell's law is valid for wave-normals in anisotropic media.

The refractive indices corresponding to the two allowed polarizations for a wave propagating in the $\vec{k}$ direction is obtained from Eq. (A.1). If $n_x^2 = n_y^2 = n_\perp^2$ and $n_z^2 = n_\parallel^2$, then, letting $e^2 = 1 - \frac{n_\perp^2}{n_\parallel^2}$

$$r^2(1-e^2\cos^2\theta) = n_\perp^2 \tag{J.4}$$

where θ is the colatitude and $r^2 = n^2$. If $\vec{k}$ makes an angle α with the z-(optic) axis, then the extremal values of r^2 or n^2) are

$$n_1^2 = n_\perp^2 \tag{J.5}$$

if $\theta = \pi/2$, and

$$n_2^2 = \frac{n_\perp^2}{1-e^2\sin^2\alpha} \tag{J.6}$$

if $\theta = \pi/2-\alpha$.

The geometry for a plane wave incident on a plane slab of sample is shown in Figure J.1. From Snell's law, $n_A\sin\theta = n_1\sin\theta_1$ and $n_A\sin\theta = n_2\sin\theta_2$. The difference in the optical path lengths of the two waves is

$$\frac{\ell n_1}{\cos\theta_1} - \frac{\ell n_2}{\cos\theta_2} - d = -N\lambda \tag{J.7}$$

where we have let $n_A = 1$. Furthermore,

$$d = \sin\theta(\ell\tan\theta_1 - \ell\tan\theta_2) \tag{J.8}$$

and simple algebra yields

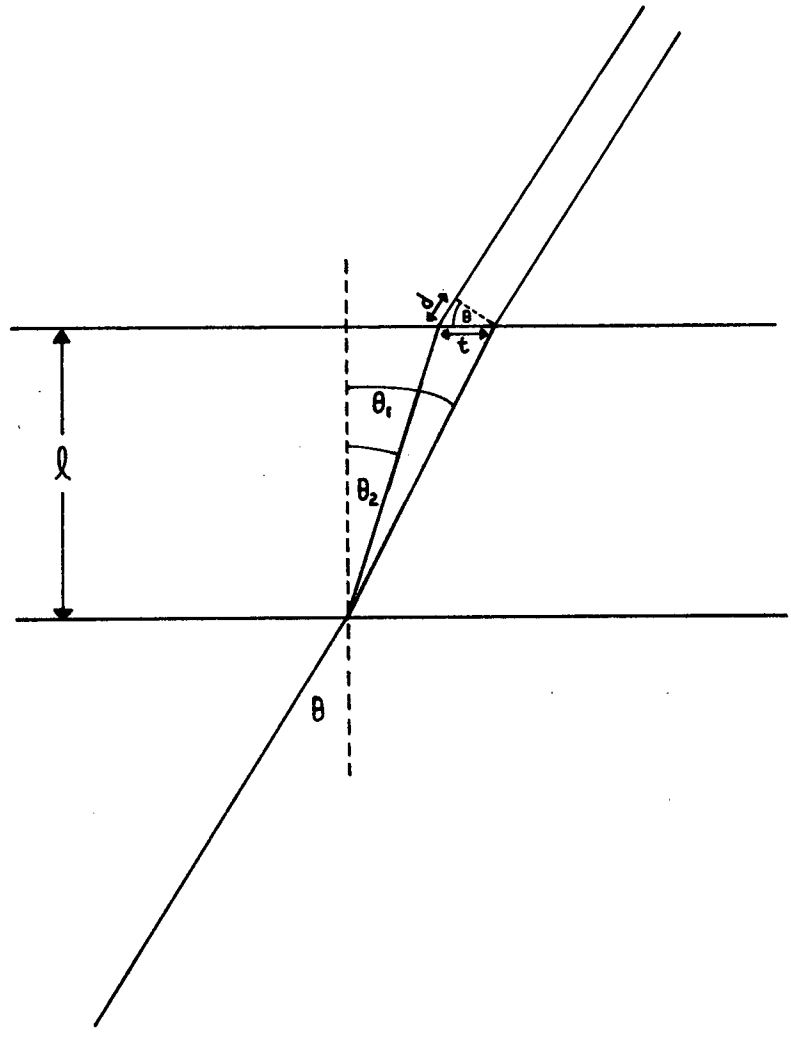

Fig. J.1 Geometry of a plane wave incident on a flat slab of sample material.

$$n_1\cos\theta_1 - n_2\cos\theta_2 = -\frac{N\lambda}{\ell} \tag{J.9}$$

If the wave vector $\vec{k}$ is perpendicular to the optic axis, corresponding to the vertical fringes in the conoscopic pattern, then $\alpha = \pi/2$ and $n_2 = n_{\parallel}$. Then

$$n_{\perp}\left(1 - \frac{1}{n_{\perp}^2}\sin^2\theta\right)^{1/2} - n_{\parallel}\left(1 - \frac{1}{n_{\parallel}^2}\sin^2\theta\right)^{1/2} = -\frac{N\lambda}{\ell} \tag{J.10}$$

and expanding in $\sin^2\theta$ yields

$$(n_{\parallel}-n_{\perp})\left[1 + \frac{1}{2n_{\perp}n_{\parallel}}\sin^2\theta\right] \cong \frac{N\lambda}{\ell} \tag{J.11}$$

If the optic axis is in the plane of incidence and is parallel to the front surface, then $\sin\alpha = \cos\theta_2$, and $n_2^2 = \frac{n_{\perp}^2}{1-e^2\cos^2\theta_2}$. Solving for $\cos^2\theta_2$ yields

$$\cos^2\theta_2 = \frac{\sin^2\theta - n_{\perp}^2}{e^2\sin^2\theta - n_{\perp}^2} \tag{J.12}$$

and

$$n_2\cos\theta_2 = n_{\parallel}\left(1 - \frac{1}{n_{\perp}^2}\sin^2\theta\right)^{1/2} \quad . \tag{J.13}$$

Eq. (J.9) gives

$$n_{\perp}\left(1 - \frac{1}{n_{\perp}^2}\sin^2\theta\right)^{1/2} - n_{\parallel}\left(1 - \frac{1}{n_{\perp}^2}\sin^2\theta\right)^{1/2} = -\frac{M\lambda}{\ell} \tag{J.14}$$

and expanding in $\sin^2\theta$ as before yields

$$(n_{\parallel}-n_{\perp})\left[1 - \frac{1}{2n_{\perp}^2}\sin^2\theta\right] = \frac{M\lambda}{\ell} . \qquad (J.15)$$

Eqs. (J.11) and (J.15) predict the experimentally observed motion of the fringes in the conoscopic pattern; as $n_{\parallel}-n_{\perp}$ decreases (with increasing temperature) the horizontal fringes more towards the center, while the vertical fringes move away from it.

A commonly occuring mistake in optics text books (see 'Optics' by Rossi for example) is the statement that the extraordinary wave surface in uniaxial crystals is an ellipsoid. From Eq. (J.6) it follows that the wave surface is given by

$$r^2 = \frac{1}{n_{\perp}^2}(1-e^2\sin^2\alpha), \qquad (J.16)$$

a fourth degree ovaloid. If the wave surface is assumed to be an ellipsoid, the angle of refraction of the extraordinary ray can be easily obtained. If the optical path length difference for the ordinary and the extraordinary wave is then calculated using this result, the resulting equation resembles Eq. (J.15), except the sign of $\sin^2\theta$ is reversed. The fact that such an equation is incorrect could easily be overlooked in situations where $n_{\parallel}-n_{\perp}$ cannot be varied continuously.

APPENDIX K

We wish to solve the following equations:

$$\frac{(n_{\parallel}^2-1)}{(n_{\parallel}^2+2)}\,(1 - 4\pi\rho\alpha_{\parallel}\eta_{\parallel}) = \frac{4\pi}{3}\,\rho\alpha_{\parallel} \tag{K.1}$$

$$\frac{(n_{\perp}^2-1)}{(n_{\perp}^2+2)}\,(1 - 4\pi\rho\alpha_{\perp}\eta_{\perp}) = \frac{4\pi}{3}\,\rho\alpha_{\perp} \tag{K.2}$$

$$\eta_{\parallel} + 2\eta_{\perp} = 0 \tag{K.3}$$

and

$$\alpha_{\parallel} + 2\alpha_{\perp} = 3a\ . \tag{K.4}$$

Letting

$$z = \frac{(n_{\parallel}^2-1)}{(n_{\parallel}^2+2)}$$

and

$$x = \frac{(n_{\perp}^2-1)}{(n_{\parallel}^2+2)}\ ,$$

elimination of η from Eqs. (K.1) and (K.2) yields

$$\frac{1}{\alpha_{\parallel}} + \frac{2}{\alpha_{\perp}} = \frac{4\pi}{3}\,\rho\left(\frac{1}{z} + \frac{2}{x}\right) = b. \tag{K.5}$$

Elimination of $\alpha_\perp$ from Eqs. (K.5) and (K.6) gives

$$b\alpha_\parallel^2 + \alpha_\parallel(3-3ab) + 3a = 0 \qquad \text{(K.6)}$$

Solution of Eq. (K.6) is

$$\alpha_\parallel = \frac{1}{2b}\left[3(ab-1) + \sqrt{9-30ab+9a^2b^2}\right., \qquad \text{(K.7)}$$

and then $\alpha_\perp = (3a-\alpha_\parallel)/2$. Since $\alpha_\parallel = a+2\Delta S$ and $\alpha_\perp = a-\Delta S$, the order parameter S is given by

$$S = \frac{\alpha_\parallel - \alpha_\perp}{3\Delta} \quad . \qquad \text{(K.8)}$$

The anisotropy tensor $\eta_\parallel$ is obtained from Eq. (K.1);

$$\eta_\parallel = \frac{1}{4\pi\rho\alpha_\parallel} - \frac{1}{3z} \qquad \text{(K.9)}$$

and $\eta_\perp = -\frac{1}{2}\eta_\parallel$. $\qquad$ (K.10)

REFERENCES

(1) Max Born and Emil Wolf, Principles of optics. (Pergamon Press, New York, 1965), 3rd ed.

(2) J.O. Hirschfelder, C.F. Curtiss and R.B. Bird, Molecular theory of gases and liquids (Wiley, New York, 1954).

(3) P.P. Ewald, Ann. Physik 64 (1921) 253.

(4) M. Born and M. Bradburn, Proc. Cambridge Phil. Soc. 39 (1934) 104.

(5) H.E.J. Neugebauer, Can. J. Phys. 32 (1954) 1.

(6) D.A. Dunmur, Mol. Phys. 23 (1972) 109.

(7) D.A. Dunmur, Chem. Phys. Letters 10 (1971) 49.

(8) L.D. Landau, Collected Papers of L.D. Landau (Gordon and Breach, New York, 1965).

(9) Y. Poggi, P. Atten and J.C. Filippini, Mol. Cryst. Liq. Cryst. 37 (1961) 1.

(10) M.J. Press and A.S. Arrott, Phys. Rev. A, 8, 3, 1973.

(11) T.W. Stinson and J.D. Litster, Phys. Rev. Lett., 25, p.503 (1970)

(12) M. Born, Ann. Physik 4 (1918) 225.

(13) S. Chandrasekhar, D. Kirshnamurti and N.V. Madhusana, Mol. Cryst. Liq. Cryst. 8 (1969) 45.

(14) A.J. van der Merwe, Z. Physik 196 (1966) 212.

(15) W. Maier and A. Saupe, Z. Naturforsch. 14A (1959) 882.

(16) D. Balzarini and K. Ohrn, Phys. Rev. Lett. 29 (1972) 840.

(17) D. Balzarini, Can. J. Phys. 50 (1972) 2194.

(18) R. Yaris and B. Kurtman, J. Chem. Phys. 37 (1962) 1775.

(19) H.S. Subramhanyam and J. Shashidhara Prasad, Mol. Cryst. Liq. Cryst., 37 (1976) 23.

(20) D. Balzarini, Phys. Rev. Lett. 25 (1970) 103.

(21) I. Haller, Prog. Sol. Stat. Chem. 10 (1975) 103.

(22) J.A. Chapman, C.P. Finnimore and B.L. Smith, Phys. Rev. Lett. 21 (1968) 1306.

(23) P.G. de Gennes, The Physics of Liquid Crystals (Clarendon Press, Oxford, 1974).

(24) P. Palffy-Muhoray, Chem. Phys. Lett. 48 (1977) 315.

(25) M.J. Freiser, Liquid Crystals 3, Part 1. ed. G.H. Brown and M.M. Labes (Gordon and Breach Science Publishers, New York, 1972) p. 281.

(26) H.S. Subramhanyam and D. Krishnamurti, Mol. Cryst. Liq. Cryst. 22, (1973) 239.

(27) D. Balzarini and P. Palffy-Muhoray, Can. J. Phys. 52 (1974) 2007.

(28) D.W. Berreman and T.J. Scheffer, Mol. Cryst. Liq. Cryst. 11, (1970) 395.